INFORMATION TO USERS

This was produced from a copy of a document sent to us for microfilming. While the most advanced technological means to photograph and reproduce this document have been used, the quality is heavily dependent upon the quality of the material submitted.

The following explanation of techniques is provided to help you understand markings or notations which may appear on this reproduction.

1. The sign or "target" for pages apparently lacking from the document photographed is "Missing Page(s)". If it was possible to obtain the missing page(s) or section, they are spliced into the film along with adjacent pages. This may have necessitated cutting through an image and duplicating adjacent pages to assure you of complete continuity.

2. When an image on the film is obliterated with a round black mark it is an indication that the film inspector noticed either blurred copy because of movement during exposure, or duplicate copy. Unless we meant to delete copyrighted materials that should not have been filmed, you will find a good image of the page in the adjacent frame.

3. When a map, drawing or chart, etc., is part of the material being photographed the photographer has followed a definite method in "sectioning" the material. It is customary to begin filming at the upper left hand corner of a large sheet and to continue from left to right in equal sections with small overlaps. If necessary, sectioning is continued again—beginning below the first row and continuing on until complete.

4. For any illustrations that cannot be reproduced satisfactorily by xerography, photographic prints can be purchased at additional cost and tipped into your xerographic copy. Requests can be made to our Dissertations Customer Services Department.

5. Some pages in any document may have indistinct print. In all cases we have filmed the best available copy.

University
Microfilms
International

300 N. ZEEB ROAD, ANN ARBOR, MI 48106
18 BEDFORD ROW, LONDON WC1R 4EJ, ENGLAND

A NUMERICAL SOLUTION TECHNIQUE FOR THREE-DIMENSIONAL MULTIPARTICLE STOKES FLOWS

by

PETER GANATOS

A dissertation submitted to the Graduate Faculty in Engineering in partial fulfillment of the requirements for the degree of Doctor of Philosophy, The City University of New York.

1978

This manuscript has been read and accepted for the Graduate Faculty in Engineering in satisfaction of the dissertation requirement for the degree of Doctor of Philosophy.

Jan. 4, 1979
date

Sheldon Weinbaum
Chairman of Examining Committee

January 5, 1979
date

Frederick E. Thau
Executive Officer

Prof. Latif M. Jiji

Prof. Robert Pfeffer

Prof. Rishi Raj

Prof. Sheldon Weinbaum, Chairman

Prof. Herbert Weinstein

Supervisory Committee

The City University of New York

Abstract

A NUMERICAL SOLUTION TECHNIQUE FOR
THREE-DIMENSIONAL MULTIPARTICLE STOKES FLOWS

by

Peter Ganatos

Adviser: Professor Sheldon Weinbaum
Co-Adviser: Professor Robert Pfeffer

This thesis contains a numerical solution technique for three-dimensional bounded or unbounded strongly interacting multiparticle low Reynolds number flows with planar symmetry. The solution technique is based on an extension of the collocation technique previously developed for treating both bounded and unbounded axisymmetric multiparticle Stokes flow problems.

The first part of the thesis examines in detail the strong hydrodynamic interaction between two or more closely spaced identical spheres in a plane. The various two-sphere configurations provide a convenient means of carefully testing the accuracy and convergence of the numerical solution technique for three dimensional flow with known exact spherical bipolar solutions.

The important difficulty encountered in applying the collocation technique to multiparticle asymmetric flows is that the selection of boundary points is rather sen-

sitive to the flow orientation. Despite this shortcoming one is able to obtain solutions for the quasi-steady particle velocities and drag for as many as 15 spheres in less than 30 sec. on an IBM 370/168 computer. The method not only gives accurate global results, but is able to predict the local fluid velocity and to resolve fine features of the flow such as the presence of separated regions of closed streamlines. Time-dependent numerical solutions are also presented for various three and four sphere assemblages falling in a vertical plane. These solutions, in which the motion of each sphere is traced for several hundred diameters, are found to be in very good agreement with experimental measurements.

In the second part of the thesis, the present collocation technique is extended to the treatment of three-dimensional bounded Stokes flow problems with planar symmetry. In particular a solution is presented for the arbitrary slow motion of a sphere in a viscous fluid bounded by two plane parallel walls. The accuracy of the new technique is tested by detailed comparison with the exact solutions for the drag and torque on a sphere moving parallel or perpendicular to a single plane wall, rotating adjacent to the wall, or in the presence of a shear field. The converged collocation solutions are in perfect agreement with exact solutions for all spacings tested. The new collocation solutions obtained in the presence of two

walls show that values for the drag on the sphere available in the literature as predicted by the method of reflections to be as much as 40 percent lower than "exact" values when the walls are spaced two sphere diameters apart and one order of magnitude lower at a spacing of 1.1 diameters. Solutions are also obtained for the motion of a neutrally buoyant sphere in two-dimensional poiseuille flow or simple shear flow between the two walls.

ACKNOWLEDGEMENTS

I wish to thank Professor Sheldon Weinbaum and Professor Robert Pfeffer for their continuous guidance and many contributions in directing this research. I also wish to thank Randall Wu and Zeev Dagan for performing the experiments presented in section I-5, Dr. Michael S. Kolansky for his help in the use of the IBM 370/168 computer system during the early part of this research and The City University of New York Computer Center for the use of their facilities.

This research was sponsored by the National Science Foundation under Grant no. GK-16506. Their support is gratefully acknowledged.

TABLE OF CONTENTS

LIST OF TABLES

LIST OF FIGURES

PART I

A NUMERICAL-SOLUTION TECHNIQUE FOR THREE-DIMENSIONAL STOKES FLOWS, WITH APPLICATION TO THE MOTION OF STRONGLY INTERACTING SPHERES IN A PLANE

I-1. Introduction

The purpose of part I of this thesis is to develop the rudiments of an efficient numerical solution technique which could be used to treat a wide variety of previously unsolved non-axisymmetric creeping-motion problems with planar symmetry where the boundaries conform to more than a single orthogonal coordinate surface. Some salient examples of such motion include the settling of three or more closely spaced spheres in a plane, the arbitrary off-axis motion of a sphere in a circular cylinder or a channel, the tumbling of a spheroid near a planar boundary, and the entrance motion of a sphere into a circular pore or a two-dimensional slit. Problems with strong hydrodynamic interaction of this nature are not easily tractable by perturbation or method-of-reflection techniques. The two principal difficulties are the slow algebraic decay of three-dimensional disturbances in Stokes flow and the slow convergence properties of an iterative solution scheme when the leading term differs greatly from the desired converged solution.

In the past few years several important advances have been made in the numerical treatment of some of the more complicated boundary-value problems in Stokes flow. These advances, with the exception of the numerical investigation of Youngren & Acrivos (1975), have been limited to axisymmetric motions. For these motions the simplification

afforded by the Stokes stream function allows one to reduce the governing equation for quasi-steady creeping motion to the compact form $D^2D^2\psi = 0$. The first highly accurate numerical solutions of this equation by collocation techniques were presented by Skalak and co-workers for several different flow problems involving an infinite array of identical particles periodically spaced along the axis of a circular cylinder. Approximate collocation procedures had previously been used by O'Brien (1968) and others with varying degrees of success. Wang & Skalak (1969), Chen & Skalak (1970) and Hyman & Skalak (1972) considered periodic coaxial arrays of spheres, spheroids and spheroidal bubbles respectively. This problem was then further generalized to an infinite periodic array of arbitrarily shaped axisymmetric particles using a finite-element approach in Skalak, Chen & Chien (1972). These studies of bounded periodic cells were largely motivated by an attempt to model the flow of red cells in the microcirculation.

For flow problems involving time-dependent multiparticle Stokes flow interactions, one needs to rapidly compute the flow field and quasi-steady drag resulting from the instantaneous interaction of a finite array of particles with arbitrary spacing and velocity. The collocation technique developed by Gluckman, Pfeffer & Weinbaum (1971) and Leichtberg, Weinbaum, Pfeffer & Gluckman (1976) is ideally suited for this purpose. The technique developed

is capable of calculating in a few seconds on an IBM 370/168 computer both the instantaneous drag and the instantaneous velocity field for as many as 100 spheres or 15 spheroids in unbounded flow with an accuracy for the drag on each particle of better than 0.1% (Gluckman et al 1971). For unbounded axisymmetric flow the selection of boundary points is not critical except for very close spacings (less than 0.1 diameters), where a judicious selection of boundary points near the axis (Leichtberg, Weinbaum, Pfeffer & Gluckman 1976) allows extension of the range of validity to less than 10^{-4} diameters with little change in computational time. The method has recently been extended to an arbitrary coaxial array of spheres in a circular cylinder (Leichtberg, Pfeffer & Weinbaum 1976), but the computational times required are about two orders of magnitude larger than for the equivalent unbounded case.

The great rapidity with which the unbounded quasi-steady solutions can be obtained for small sphere clusters (in about 10^{-2} sec for three or four spheres on an IBM 370/168) has made it possible to follow the time-dependent interaction of small coaxial groupings of spheres over hundreds of diameters and carefully document the importance of both the unsteady virtual-mass force and the Basset force (the force which arises from the time history of the $\partial V/\partial t$ term in the unsteady Stokes-flow equation) in multiparticle flows when the flow configuration is

slowly changing owing to particle interactions (Leichtberg, Weinbaum, Pfeffer & Gluckman 1976).

In another biologically related paper, Leichtberg, Weinbaum & Pfeffer (1976) studied the time-dependent multiparticle hydrodynamic interaction leading to the aggregation of identical red cells (rouleaux) in the microcapillaries by following the time-dependent motion of identical spheres along the axis of an unbounded Poiseuille profile.

The particles in all the foregoing axisymmetric investigations have been represented by a truncated series of internal singularities derived from the separable solutions of $D^2D^2\psi = 0$ in the appropriate coordinate system. For an arbitrary boundary shape one must resort to either finite-difference or finite-element solutions of the entire flow field or represent the body by a surface distribution of singularities (Gluckman, Weinbaum & Pfeffer 1972; Youngren & Acrivos 1975). In Gluckman et al (1972) the flow past an arbitrary convex body of revolution is treated using a surface distribution of spheroidal singularities of vanishing aspect ratio. The integral equation describing this surface distribution is solved using a collocation procedure equivalent to that previously developed by Gluckman, Pfeffer & Weinbaum (1971) for axisymmetric multiparticle flow. Youngren & Acrivos (1975) present the first numerical solution procedure capable of

handling the creeping flow past an arbitrary isolated three-dimensional body. The flow disturbance produced by the body is formulated as an integral equation whose kernel is the fundamental Stokeslet solution of the creeping-motion equation in three dimensions. This integral equation is solved numerically by dividing the body surface into a finite number of discrete elements in each of which the Stokeslet strength is assumed constant.

The integral-equation technique of Youngren and Acrivos is a very promising new approach for treating irregular boundary problems in creeping motion such as the flow past deforming flexible particles and bubbles. However, for a wide variety of three-dimensional problems in Stokes flow when each boundary conforms to a different orthogonal coordinate surface (such as the various examples cited at the beginning of this introduction), it is computationally more efficient to develop collocation techniques similar to those just summarized for axisymmetric flow. This approach would take advantage of the various known separable solutions of the Stokes equations in three dimensions. The basic departure from axisymmetric flow is that the fundamental solutions are given in terms of the components of the velocity field rather than a Stokes stream function. These fundamental solutions for the velocity field are

known for rectangular, cylindrical, spherical (Lamb 1945, p. 594) and spheroidal (Jeffery 1922) coordinates. In theory, the present method could be applied to bounded flow problems where the particles do not conform to natural coordinate surfaces using the extensions developed in Gluckman et al (1972) for axisymmetric flow. However, in practice computation times would be prohibitively long. The more general integral-equation approach of Youngren & Acrivos would be more practical for these problems.

A cardinal rule for the successful application of the collocation technique is that the velocity disturbance produced by each coordinate boundary may be represented by an ordered sequence of fundamental solutions appropriate to the constant orthogonal coordinate surface to be described. As demonstrated in the appendix to Gluckman et al (1972), the numerical solution can oscillate unstably as the number of collocation points is increased if an inappropriate set of fundamental solutions is used.

Many previously unsolved three-dimensional flows can be constructed from a superposition of two or more truncated series of fundamental solutions from the four basic coordinate systems mentioned in the last paragraph. Only minor modifications of the basic collocation scheme described herein for multiple spheres are required to treat spheroids instead of spheres or to combine spheres of different sizes; see Gluckman et al (1971), where the

equivalent problem is treated for axisymmetric flow. Also, as outlined in the concluding section, the important extension from unbounded to bounded flow, while very laborious because of the coordinate transformations involved, is straightforward and follows the same general procedure as has already been performed for axisymmetric flow in Leichtberg, Pfeffer & Weinbaum (1976). The exact no-slip boundary conditions are imposed along the boundaries of the system, whether they be that of a plane, channel or circular cylinder, and the problem is reduced to a collocation procedure applied along the boundaries of each particle. For all the above reasons, the logical starting point in the development of a collocation technique for three-dimensional flows is the basic interaction between two or more spheres using Lamb's (1945, p.594) spherical-harmonic series solutions for each sphere. The two-sphere problem is itself of special importance since it enables one to carefully examine the accuracy and convergence of the three-dimensional collocation technique by comparison with exact spherical bipolar solutions. This comparison is essential since the difficulty in constructing a collocation technique is not its formulation, which is conceptually simple, but the detailed development of the truncation. While there is no assurance that the treatment of boundary points for two spheres can be carried over to three or more spheres, the detailed comparison with ex-

periment (described in section I-5) and with previous multisphere axisymmetric solutions provides some confidence that this is indeed the case.

Although the primary motivation of part I is to lay the foundations for a more general numerical treatment of bounded three-dimensional creeping motions, it is worth mentioning that the current study is, to the author's knowledge, the first strong-interaction theory for the non-axisymmetric motion of three or more spheres. Many of the flow configurations described in section I-5 have been observed experimentally by Jayaweera, Mason & Slack (1964) and studied theoretically in a qualitative manner using a weak-interaction first-order reflection theory by Hocking (1964).

Section I-2 contains the mathematical formulation of the basic collocation technique for an arbitrary planar configuration of N spheres. In section I-3 solutions obtained by this method are compared with the exact solutions of Stimson & Jeffery (1926) for two equal spheres moving parallel to their line of centers and Goldman, Cox & Brenner (1966) for two equal spheres in an arbitrary orientation. Solutions for instantaneous configurations of three or more spheres are presented in section I-4. In section I-5 quasi-steady time-dependent solutions are presented for the trajectories of three or four spheres settling in a vertical plane

starting from various initial configurations. Finally, in section I-6, the extension of the collocation technique to bounded three-dimensional flows with planar symmetry is discussed. Most of the material presented in part I has appeared in Ganatos, Pfeffer & Weinbaum (1978).

I-2. Formulation for multiple spheres

In accord with the comments in the introduction, consider the slow motion of a finite number of equal spheres in an arbitrary asymmetric planar configuration. The steady-state creeping-motion governing equations are

$$\mu \nabla^2 \vec{V} = \nabla p \,, \qquad \nabla \cdot \vec{V} = 0 \,. \tag{I-2.1a,b}$$

where the symbols have their usual meaning. The fundamental solution of (I-2.1) which is capable of describing an arbitrary disturbance on the surface of a sphere of radius a is given in Happel & Brenner (1973, p. 65):

$$\vec{V} = \sum_{n=1}^{\infty} \Big[\nabla \times (\vec{r}\, \chi_{-(n+1)}) + \nabla \Phi_{-(n+1)} - \frac{(n-2)}{\mu 2n(2n-1)} r^2 \nabla P_{-(n+1)} + \frac{(n+1)}{\mu n(2n-1)} \vec{r}\, P_{-(n+1)} \Big] . \tag{I-2.2}$$

Here $\chi_{-(n+1)}$, $\Phi_{-(n+1)}$ and $P_{-(n+1)}$ are solid spherical harmonic functions of order $-(n+1)$ and $\vec{r}$ is the radial position vector, whose origin is at the center of the sphere.

For the simplest case of N spheres moving slowly in an unbounded quiescent fluid, the linear superposition of N solutions for an individual particle yields

$$\vec{V} = \sum_{j=1}^{N} \sum_{n=1}^{\infty} \left[\nabla \times (\vec{r}_j \chi_{-(n+1)}(r_j, \theta_j, \phi_j)) + \nabla \Phi_{-(n+1)}(r_j, \theta_j, \phi_j) \right.$$

$$- \frac{(n-2)}{\mu 2n(2n-1)} r_j^2 \nabla P_{-(n+1)}(r_j, \theta_j, \phi_j)$$

$$\left. + \frac{(n+1)}{\mu n(2n-1)} \vec{r}_j P_{-(n+1)}(r_j, \theta_j, \phi_j) \right], \qquad \text{(I-2.3)}$$

where r_j, θ_j and ϕ_j are spherical coordinates measured from the center of the jth sphere. Equation (I-2.3) will be generalized in section I-6 to include an incident stream and confining walls.

In general, the three solid spherical harmonic functions in (I-2.3) have the following form:

$$\begin{Bmatrix} \chi_{-(n+1)} \\ \Phi_{-(n+1)} \\ P_{-(n+1)} \end{Bmatrix} = \sum_{m=0}^{n} P_n^m(\zeta_j) \frac{1}{r_j^{n+1}} \left[\begin{Bmatrix} A_{jmn} \\ C_{jmn} \\ E_{jmn} \end{Bmatrix} \cos m\phi_j + \begin{Bmatrix} B_{jmn} \\ D_{jmn} \\ F_{jmn} \end{Bmatrix} \sin m\phi_j \right], \qquad \text{(I-2.4)}$$

where P_n^m is the associated Legendre function, $\zeta_j = \cos \theta_j$ and A_{jmn}, ..., F_{jmn} are unknown constants which are determined from boundary conditions.

If the N spheres are now restricted to fall freely under gravity in the vertical plane y = 0 as shown in figure I-1, the symmetry of the flow about this plane requires that

$$A_{jmn} = D_{jmn} = F_{jmn} = 0. \qquad \text{(I-2.5)}$$

To perform the operations indicated by (I-2.3) the r_j, θ_j and ϕ_j are expressed in terms of a single rectangular coordinate system as shown in figure I-1, i.e.

$$r_j^2 = (x-b_j)^2 + y^2 + (z-d_j)^2, \qquad \text{(I-2.6a)}$$

$$\zeta_j = \frac{z-d_j}{r_j} = \frac{z-d_j}{[(x-b_j)^2 + y^2 + (z-d_j)^2]^{1/2}}, \qquad \text{(I-2.6b)}$$

$$\tan \phi_j = \frac{y}{x-b_j}, \qquad \text{(I-2.6c)}$$

where b_j and d_j are the x and z coordinates of the jth sphere's center respectively.

If u, v and w denote the components of the fluid velocity V in the x, y and z directions respectively, the no-slip boundary conditions which must be satisfied on the surface of each sphere are

$$u\big|_{r_j=a} = U_j + a\omega_j \cos\theta_j, \qquad \text{(I-2.7a)}$$

$$v\big|_{r_j=a} = 0, \qquad \text{(I-2.7b)}$$

$$w\big|_{r_j=a} = W_j - a\omega_j \sin\theta_j \cos\phi_j, \qquad \text{(I-2.7c)}$$

where a is the radius of each sphere and U_j, W_j and ω_j represent the unknown horizontal, vertical and angular velocity of the jth sphere respectively.

The hydrodynamic force and torque exerted on the jth sphere are given by Happel & Brenner (1973, p. 67) as

$$\vec{F}_j = -4\pi \nabla (r_j^3 P_{-2}) \qquad \text{(I-2.8a)}$$

and

$$\vec{T}_j = -8\pi\mu \nabla (r_j^3 \chi_{-2}). \qquad \text{(I-2.8b)}$$

Substituting (I-2.4) - (I-2.6) into (I-2.8) gives the simple result

$$\vec{F}_j = -4\pi \left[E_{j11} \hat{i} + E_{j01} \hat{k} \right] \qquad \text{(I-2.9a)}$$

and

$$\vec{T}_j = -8\pi\mu B_{j11} \hat{j}. \qquad \text{(I-2.9b)}$$

The balance between buoyancy and Stokes drag requires

$$-4\pi \left[E_{j11} \hat{i} + E_{j01} \hat{k} \right] + \frac{4}{3}\pi a^3 (\rho_s - \rho) g \hat{k} = 0 \qquad \text{(I-2.10a)}$$

while the condition of zero torque yields

$$-8\pi\mu B_{j11} = 0. \qquad \text{(I-2.10b)}$$

Equations (I-2.10) allow 3N of the unknown constants in (I-2.4) to be determined, i.e.

$$E_{j11} = 0, \quad E_{j01} = \frac{1}{3} a^3 (\rho_s - \rho) g, \quad B_{j11} = 0$$

$$(j = 1, 2, 3, \ldots, N). \quad \text{(I-2.11)}$$

This is exactly equal to the number of unknown velocities introduced by (I-2.7).

Now, if the three no-slip boundary conditions are satisfied at M points on each of the N spheres and the inner two series in (I-2.3) are truncated to yield a total of 3M terms, then a set of $3 \times N \times M$ simultaneous linear algebraic equations results for the $3 \times N \times M$ unknown constants: B_{jmn} ($m \neq 1$ when $n = 1$), C_{jmn}, E_{jmn} ($m \neq 0, 1$ when $n = 1$), U_j, W_j and ω_j. For each point on the surface of the jth sphere at which the three no-slip boundary conditions are satisfied the following equations are obtained:

$$u\big|_{r_j = a} = \sum_{j=1}^{N} \underbrace{\sum_{n=1} \sum_{m=0}^{n}}_{M \text{ terms}} \left[B_{jmn} B'_{jmn} + C_{jmn} C'_{jmn} + E_{jmn} E'_{jmn} \right] = U_j + a \omega_j \cos\theta_j, \quad \text{(I-2.12a)}$$

$$v\big|_{r_j = a} = \sum_{j=1}^{N} \underbrace{\sum_{n=1} \sum_{m=0}^{n}}_{M \text{ terms}} \left[B_{jmn} B''_{jmn} + C_{jmn} C''_{jmn} + E_{jmn} E''_{jmn} \right] = 0, \quad \text{(I-2.12b)}$$

$$w\Big|_{r_j=a} = \sum_{j=1}^{N}\sum_{n=1}^{}\sum_{m=0}^{n}\left[B_{jmn}\,B'''_{jmn} + C_{jmn}\,C'''_{jmn} + E_{jmn}\,E'''_{jmn}\right] = W_j - a\,W_j \sin\theta_j \cos\phi_j \,. \quad \text{(I-2.12c)}$$

Equations (I-2.12) form the fundamental matrix equation of the collocation technique for planar multiple-sphere configurations. The primed coefficients of the constants B_{jmn}, C_{jmn} and E_{jmn} depend only on the geometry of the flow configuration and are given by

$$B'_{jmn} = \frac{1}{r_j^{n+1}}\left[-\sin\theta_j \sin\phi_j \frac{dP_n^m(\zeta_j)}{d\zeta_j}\sin m\phi_j + m\,\frac{\cos\phi_j}{\tan\theta_j}\,P_n^m(\zeta_j)\cos m\phi_j\right], \quad \text{(I-2.13a)}$$

$$C'_{jmn} = \frac{1}{r_j^{n+2}}\left[-\left((n+1)P_n^m(\zeta_j) + \zeta_j \frac{dP_n^m(\zeta_j)}{d\zeta_j}\right)\sin\theta_j \cos\phi_j \cos m\phi_j + m\,\frac{\sin\phi_j}{\sin\theta_j}\,P_n^m(\zeta_j)\sin m\phi_j\right], \quad \text{(I-2.13b)}$$

$$E'_{jmn} = \frac{1}{2\mu(2n-1)r_j^n}\left[\left((n+1)P_n^m(\zeta_j) + \frac{n-2}{n}\,\zeta_j \frac{dP_n^m(\zeta_j)}{d\zeta_j}\right) \times \sin\theta_j \cos\phi_j \cos m\phi_j - \frac{m(n-2)}{n}\,\frac{\sin\phi_j}{\sin\theta_j}\,P_n^m(\zeta_j)\sin m\phi_j\right], \quad \text{(I-2.13c)}$$

$$B''_{jmn} = \frac{1}{r_j^{n+1}}\left[\sin\theta_j \cos\phi_j \frac{dP_n^m(\zeta_j)}{d\zeta_j} \sin m\phi_j + m \frac{\sin\phi_j}{\tan\theta_j} P_n^m(\zeta_j) \cos m\phi_j\right], \quad \text{(I-2.13d)}$$

$$C''_{jmn} = \frac{1}{r_j^{n+2}}\left[-\left((n+1)P_n^m(\zeta_j) + \zeta_j \frac{dP_n^m(\zeta_j)}{d\zeta_j}\right)\sin\theta_j \sin\phi_j \cos m\phi_j - m \frac{\cos\phi_j}{\sin\theta_j} P_n^m(\zeta_j) \sin m\phi_j\right], \quad \text{(I-2.13e)}$$

$$E''_{jmn} = \frac{1}{2\mu(2n-1)r_j^n}\left[\left((n+1)P_n^m(\zeta_j) + \frac{n-2}{n}\zeta_j \frac{dP_n^m}{d\zeta_j}\right) \times \sin\theta_j \sin\phi_j \cos m\phi_j + \frac{m(n-2)}{n} \frac{\cos\phi_j}{\sin\theta_j} P_n^m(\zeta_j) \sin m\phi_j\right], \quad \text{(I-2.13f)}$$

$$B'''_{jmn} = -\frac{m}{r_j^{n+1}} P_n^m(\zeta_j) \cos m\phi_j, \quad \text{(I-2.13g)}$$

$$C'''_{jmn} = \frac{1}{r_j^{n+2}}(m-n-1) P_{n+1}^m(\zeta_j) \cos m\phi_j, \quad \text{(I-2.13h)}$$

$$E'''_{jmn} = \frac{1}{2\mu n(2n-1)r_j^n}\left[2(n+1)\zeta_j P_n^m(\zeta_j) + (n-2)(n-m+1) \times P_{n+1}^m(\zeta_j)\right] \cos m\phi_j \quad \text{(I-2.13i)}$$

and

$$\frac{dP_n^m(\zeta_j)}{d\zeta_j} = \frac{(n+1)\zeta_j P_n^m(\zeta_j) - (n-m+1) P_{n+1}^m(\zeta_j)}{1-\zeta_j^2}. \quad \text{(I-2.14)}$$

The system of linear equations described by (I-2.12) and (I-2.13) can be solved by any standard matrix reduction technique. It should be noted that, for m = 0,

$$B'_{jmn} = B''_{jmn} = B'''_{jmn} = 0.$$

Thus for m = 0 the B_{jmn} terms contribute nothing to the solution and should be replaced by the terms of next higher order in the series in order to conserve an equal number of equations and unknown quantities. Thus the sequence in which the terms in (I-2.12) are taken for each sphere is C_{j01}, E_{j01}, B_{j11}, C_{j11}, E_{j11}, C_{j02}, E_{j02}, B_{j12}, C_{j12}, E_{j12}, ...

In computing and presenting the results for the multiple sphere problem, it is convenient to non-dimensionalize the physical quantities involved by using the sphere radius as the basic unit length and the terminal settling velocity U_t of a single isolated sphere as the characteristic velocity:

$$U_t = \frac{2a^2(\rho_s - \rho)g}{9\mu} . \qquad \text{(I-2.15)}$$

Denoting the dimensionless variables with a tilde, the non-dimensional horizontal, vertical and angular velocities are defined as

$$\tilde{U}_j \equiv U_j/U_t, \qquad \tilde{W}_j \equiv W_j/U_t, \qquad \tilde{\omega}_j = a\omega_j/U_t \qquad \text{(I-2.16)}$$

and the dimensionless time as

$$\tilde{t} \equiv U_t\, t/a. \qquad \text{(I-2.17)}$$

The hydrodynamic force exerted on the jth sphere in the presence of all the other spheres can alternatively be expressed as

$$\vec{F}_j \equiv -6\pi\mu a\left[U_j \lambda_{Hj}\,\hat{i} + W_j \lambda_{Vj}\,\hat{k}\right], \qquad \text{(I-2.18)}$$

where λ_{Hj} and λ_{Vj} are the horizontal and vertical drag correction factors defined by (I-2.18). Comparing this equation with (I-2.19a) and using (I-2.11), (I-2.15) and (I-2.16) one finds that

$$\lambda_{Hj} = E_{j11}/1.5\mu a U_j = 0 \quad \text{when} \quad U_j = 0, \qquad \text{(I-2.19a)}$$

$$\lambda_{Vj} = E_{j01}/1.5\mu a W_j = 1/\tilde{W}_j \qquad \text{(I-2.19b)}$$

In subsequent sections λ_{Vj} will be denoted simply as λ_j since, from (I-2.19a), $\lambda_{Hj} = 0$.

I-3. Two-sphere solutions

In this section, the accuracy and convergence of the basic collocation technique described in section I-2 will be carefully examined by comparing the present results with the exact two-sphere solutions of Stimson & Jeffery (1926) and Goldman et al (1966). Also, the sensitivity of the solution to the selection of boundary points will be explored.

When specifying the points along the boundary of each sphere where conditions (I-2.7) are to be exactly satisfied, it is necessary to choose a pattern which is symmetric about both the equatorial plane $\theta_j = \pi/2$ and the meridional plane $\phi_j = \pi/2$. Owing to the symmetry about the plane $y = 0$ only the flow in the region $y \geq 0$ need be considered. Thus the range for θ_j and ϕ_j is between 0 and π and the points chosen should lie on this hemisphere.

Trials using up to twelve boundary points on each hemisphere were made for two equal spheres falling perpendicular and parallel to their line of centers at various spacings. The sphere spacing d_{12} is defined as the center-to-center distance between two equal spheres measured in sphere diameters. The only solutions found to give meaningful results were the M = 2,4 and 12 solutions. Intermediate values of M were unsuccessful owing to one or a combination of the following reasons:

(a) Locating points at $\theta_j = 0, \pi/2, \pi$ or $\phi_j = 0, \pi/2, \pi$ in many cases produces a singular matrix, so that the symmetry requirements outlined in the previous paragraph cannot be met for odd values of M.

(b) The system of equations (I-2.12) produces an ill-conditioned matrix, i.e. a near-zero determinant, for certain configurations of points.

(c) The series (I-2.12) cannot be arbitrarily truncated at any point. Apparently, when certain terms are retained in the series, they require the presence of other terms for the series to converge uniformly. Thus, in contrast to axisymmetric flow, where boundary points could simply be added in symmetric pairs, the truncation of the matrix equation (I-2.12) following the particular ordered sequence described in section I-2, and consequently the number of boundary points taken on each sphere, proceeds in jumps.

Figure I-2(a) shows the positions of the points used for two equal spheres falling parallel to their line of centers. In this case, the flow is axisymmetric and the solution is independent of the ϕ_j coordinate of the points. However, no point should be located at $\phi_j = 0, \pi/2$ or π since this produces a singular matrix. The results for the drag correction factor at various spacings are compared with the exact values in table I-1. Rapid convergence toward the exact solution is obtained as the num-

ber of points is increased. The maximum error, for the case of touching spheres with only two boundary points on each sphere is only 2.8%. This is in sharp contrast to the method of reflections, which gives an error of 26% at this spacing.

Figure I-2(b) shows the positions of the points used for two equal spheres falling perpendicular to their line of centers. The two-point solution shown was found to be independent of the θ_j coordinate of the points. The results for the vertical drag correction factor and the angular velocity at various spacings are compared with the exact values in table I-2. Examination of table I-2 shows general convergence to the exact solution as the number of boundary points is increased, except for a small deviation for the angular velocity predicted by the four-point solution at very close spacings. This deviation for close spacings is not surprising since, as observed in Leichtberg, Weinbaum, Pfeffer & Gluckman (1976), one needs more boundary points in the vicinity of contact if one is adequately to satisfy the no-slip boundary conditions in the near-collision limit. It is interesting in this regard that the error in the twelve-point solution for both λ_j and $\tilde{\omega}_j$ is only about 0.4% when the gap between the spheres is 0.0025 diameters. However, the solution fails to predict zero angular velocity when the spheres touch.

Equally accurate quasi-steady solutions for a straight

chain of two or more spheres at any orientation β (see figure I-3) may be obtained using formulas (I-4.1) - (I-4.3) in the next section, which are based on the highly accurate truncation solutions for $\tilde{\omega}_{1j}$, $\lambda_{\parallel j}$ and λ_{1j}. These formulas can obviously not be applied to the arbitrary planar motion of three or more spheres when the sphere configuration is continuously changing owing to particle interactions. For this purpose the truncation of (I-2.12) is now examined assuming that (I-4.1) - (I-4.3) cannot be used.

The solutions shown in tables I-1 and I-2 for the vertical and horizontal two-sphere configurations exhibit both rapid convergence properties as the number of boundary points is increased from 2 to 4 to 12 and insensitivity to small changes in the location of the boundary points shown in figures I-2(a) and (b). Unfortunately, this behavior does not extend to the settling of two spheres at an arbitrary orientation β if (I-4.1) - (I-4.3) are not used. The difficulty is not the selection of boundary points for a given flow orientation (the selection of boundary points is not a sensitive function of sphere spacing for a given orientation except for small gap widths) but the fact that for each angle β a different set of boundary points should be used. This feature of the collocation technique is its most important shortcoming.

To overcome this difficulty, the angle β may be divided into several different ranges between 0 and $\pi/2$, and a different set of boundary points used in each range to keep the error in the horizontal drift and angular velocities within acceptable limits. However, satisfactory results may be obtained more conveniently by finding a single optimum configuration of points which can be used for all orientations. To this end more than 6000 solutions were tested by varying the configuration of points and the orientation angle β. These tests showed that, while a given configuration of points produced good results over a certain range of β, the same set of points could produce substantial errors outside this range. The four-point solution found to give the smallest maximum percentage error at any orientation is shown in figure I-2(c). The percentage error in the drag, angular velocity and horizontal drift velocity for this positioning of the points is presented as a function of orientation for various spacings d_{12} in figure I-4. The maximum error in the vertical drag correction factor occurs in the central range of the orientation angle for all spacings. For spacings of about 1.3 or greater, the maximum error in the horizontal drift velocity and angular velocity occurs when the line of centers is nearly horizontal or vertical. At closer spacings the maximum error in angular velocity and horizontal drift velocity occurs

at orientations of roughly 20° and 45° respectively. Even though the percentage errors in the drift and angular velocities seem large for close spacings, it should be kept in mind that the magnitude of these quantities is small and, therefore, their actual deviation is small. The maximum values for the drift and angular velocities at any spacing or orientation are less than 6 and 10% respectively of the vertical velocity component (Goldman et al 1966). Nevertheless concern about the cumulative effect of small errors for long-time interactions was one of the reasons for performing the experiments presented in section I-5.

The four-point solutions shown in figure I-4 can be substantially improved over most of the range of β by going to twelve-point solutions. This increases the number of matrix equation to be solved for each sphere from 12 to 36. Thus for time-dependent multisphere interactions involving a thousand or more quasi-steady solutions this improvement is not practical and, as seen at the end of section I-5, comparison with experiment shows that such improvement is unwarranted. However, for the single, bounded, non-axisymmetric sphere calculations described in section I-6 such improvement would certainly be desired.

A natural question to ask at this point is how accurately the collocation technique can predict the local fluid velocity. Table I-3 shows values of the local fluid

velocity $\tilde{W}_f$ relative to the sphere settling velocity $\tilde{W}$ for two spheres settling axisymmetrically at a center-to-center spacing of three diameters. This configuration was chosen since the exact local velocity field can easily be computed from the Stimson & Jeffery solution. The M = 4 and 12 collocation solutions correspond to those shown in figure 2(a). Examination of table I-3 shows that the relative velocities predicted by the collocation solutions are consistently accurate to within about 1% for M = 4 and 0.01% for M = 12 except immediately adjacent to the spheres. The accuracy of the M = 12 solution near the sphere axis is very good in light of the fact that there are no boundary points in that vicinity.

Another point of interest is to determine whether the collocation technique is capable of predicting fine features of the flow such as the presence of separated regions of closed streamlines. Davis et al (1976) have used the Stimson & Jeffery solution to show that, for steady, axisymmetric, uniform flow past two equal spheres, separation of the flow from the spheres occurs for center-to-center spacings of less than 1.79 diameters. As the spacing is further decreased, the two separated flow regions adjacent to each sphere coalesce and the fluid in the region between the two spheres rotates in one or more ring vortices. To see whether the collocation technique can predict this behavior, values of the relative

local fluid velocity were obtained for two spheres settling under gravity at a spacing of 1.7 diameters for the plane midway between the two spheres ($\tilde{Z} = 0$) and along the axis (tables I-4(a,b) respectively). Results are shown for two sets of twelve-point collocations: one as in figure I-2(a) and one in which two sets of boundary points were placed near the axis, i.e. at $\theta_j = 1^o$ and 179^o for three arbitrary values of ϕ_j with the remaining six points placed at $\theta_j = 45^o$ and 135^o in a scheme similar to that used by Leichtberg, Weinbaum, Pfeffer & Gluckman (1976) to improve the accuracy of the solution in the near-collision limit. Table I-4(a) shows that both collocation schemes are in good agreement with the exact solution with a maximum local error of about 1%. Table I-4(b) shows that both collocation schemes predict the presence of the separated flow region in accord with the exact solution. However, the extremely small relative velocities adjacent to the sphere are obscured by the relatively larger slip velocity incurred by using the collocation in figure I-2(a). A substantial improvement is observed as the slip velocity is eliminated in this vicinity by placing boundary points near the axis $\tilde{R} = 0$. This modification also produces a considerable improvement in the solution in the vicinity of the other side of the sphere (i.e. for $\tilde{Z} > 2.7$). The 12-point collocations also exhibited the various vortex patterns described by Davis et al (1976) at closer spacings.

I-4. Multiple-sphere configurations

The solutions for the vertical and horizontal two-sphere configurations shown in figures I-2(a),(b) are readily extended to vertical and horizontal arrays of any number of equally spaced spheres, the only limitation being the size of the matrix (I-2.12) that the computer can handle. Although these flow configurations are transitory, they do shed important light on the order of magnitude of particle interactions in larger chains, particle shielding effects and the effect of relative spacing and orientation. The results are also the first presented for the angular velocity of three or more closely spaced spheres.

Figure I-5 shows the drag correction factor $\lambda_{\|j}$ for straight chains containing 3, 5, 7, 9, 11, 13 and 15 equally spaced spheres falling parallel to their line of centers at a spacing of 2 diameters. The central sphere is denoted by $j = 0$. Results are shown for only half of the chains since values for the other half are symmetric about $j = 0$. Solid lines connect solutions through individual spheres in a chain, which are represented by the points shown. The dashed lines connect spheres of the same number taken from the outermost sphere. The error in $\lambda_{\|j}$ for these four-point solutions is believed to be about 0.3% on the basis of the results in table I-1 and a comparison with the axisymmetric collocation theory of

Leichtberg, Weinbaum, Pfeffer & Gluckman (1976).

Figures I-6(a) and (b) show the vertical drag correction factor $\lambda_{\perp j}$ and the angular velocity $\tilde{\omega}_{\perp j}$ for the same chains falling perpendicular to their line of centers. The meaning of the dashed and solid lines is the same as in figure I-5. The estimated error for the four-point configuration used is about 0.02% for the vertical drag correction factors and 0.09% for the angular velocities; see table I-2. The three-, five- and seven-sphere chains were also run using the twelve-point collocation (figure I-2b) and confirm this estimated accuracy of the four-point solution.

Comparison of figures I-5 and I-6(a) shows that the relative difference between $\lambda_{\parallel j}$ and $\lambda_{\perp j}$ grows progressively larger as the chain length is increased. One might conjecture that the ratio of $\lambda_{\perp}$ to $\lambda_{\parallel}$ approaches the value 2 in accord with slender-body theory as the chain length becomes infinite. A marked reduction in drag per sphere as the size of the chain is increased is clearly evident in these figures. (The fifteen-sphere vertical chain falls roughly three times as fast as an isolated sphere.) Examination of figure I-6(b) shows how the angular velocity increases as one moves to the outer spheres in a horizontal chain and that for larger chains, as shown by the dashed lines, this variation in angular velocity is very small. Spheres to the left of $j = 0$ rotate clock-

wise, while spheres to the right rotate counterclockwise. The computation times required to determine the drag and velocity field varied from about 0.75 sec for a three-sphere chain to about 30 sec for the fifteen-sphere chain using an IBM 370/168 computer.

Figures I-7 and I-8(a,b) examine the effect of sphere spacing and end effects on a seven sphere horizontal and vertical chain. These solutions were obtained using the twelve-point configurations shown in figure I-2(a,b). The maximum probable error for the drag correction factor is 0.03% for the vertical chain and 0.4% for the horizontal chain. The error in the angular velocities is less than 5% at the 1.0025 spacing and less than 0.08% at a spacing of 2. These errors decrease rapidly as the spacing is increased. Comparison of figure I-7 and I-8(a) shows that at large spacings, for a given spacing, $\lambda_{\perp j}$ is equal to $\lambda_{\parallel j}$ at twice that spacing. Furthermore, at large spacings, end effects are more predominant for a chain falling vertically while at small spacings, end effects are stronger if the chain is falling horizontally. Figure I-8(b) shows that the angular velocity of each sphere in the horizontal chain increases rapidly as the spacing is decreased until a maximum angular velocity is achieved for very small gaps in the lubrication-theory limit. This maximum is observed to occur at a spacing of about 1.05 diameters for two spheres (see table I-2) and decreases as more spheres

are added to the chain.

The solution for a straight chain of spheres falling in any arbitrary orientation β may be obtained by combining the solutions for a vertical chain and a horizontal chain with the same spacing as was done for the case of two spheres by Goldman et al (1966). If the acute angle between the line of centers and the horizontal is β (see figure I-3) the horizontal drift, angular velocity and vertical drag correction factor are given by

$$\tilde{U}_j = \frac{\lambda_{\perp j} - \lambda_{\parallel j}}{2\,\lambda_{\perp j}\,\lambda_{\parallel j}} \sin 2\beta, \qquad \text{(I-4.1)}$$

$$\tilde{\omega}_j = \tilde{\omega}_{\perp j} \cos\beta, \qquad \text{(I-4.2)}$$

$$\lambda_j = \frac{2\,\lambda_{\perp j}\,\lambda_{\parallel j}}{(\lambda_{\perp j} + \lambda_{\parallel j}) - (\lambda_{\perp j} - \lambda_{\parallel j})\cos 2\beta}, \qquad \text{(I-4.3)}$$

where values of $\lambda_{\perp j}$, $\lambda_{\parallel j}$ and $\tilde{\omega}_{\perp j}$ may be obtained from figures I-5 - I-8. As mentioned previously, these formulas based on $\tilde{\omega}_{\perp j}$, $\lambda_{\perp j}$ and $\lambda_{\parallel j}$ are considerably more accurate than the more general four-point solutions shown in figures I-4(a), (b) and (c).

An interesting configuration involving three spheres in a vertical plane is shown in figure I-9. The line of centers of spheres 1 and 3 is horizontal and sphere 2 is equidistant to the other two. If $\tilde{D}/\tilde{B}$ is small, sphere 2 interacts directly with both 1 and 3 and, therefore, falls

faster. On the other hand, if $\tilde{D}/\tilde{B}$ is large, spheres 1 and 3 act as a doublet and fall faster than sphere 2. This suggests that for a given value of $\tilde{B}$, there is a critical value of $\tilde{D}/\tilde{B}$ for which the vertical velocity component of the spheres is equal. Theoretical values of this critical value were obtained using the four point configuration shown in figure I-2(c). At close spacings this critical value is a very strong function of $\tilde{B}$. At large spacings, the spheres act like point forces and $\tilde{D}/\tilde{B}$ approaches the asymptotic value 3.735. It should be observed that this configuration is unsteady since spheres 1 and 3 possess a horizontal drift velocity tending to bring them together. Due to the reversibility of Stokes flow, the same critical spacing curve shown in figure I-9 may be used if sphere 2 lies above 1 and 3. In this case, the horizontal drift velocities are reversed. However, the spheres continue to rotate in the same direction as before.

Another intriguing behavior may be observed from a study of the three sphere configuration shown in figure I-9. For a given value of $\tilde{B}$, if the critical value of $\tilde{D}/\tilde{B}$ is exceeded, the vertical distance $\tilde{D}$ decreases. However, despite this, spheres 1 and 3 continue to approach each other and to rotate in the direction shown in figure I-9. This behavior may be analyzed qualitatively by considering the individual interactions between pairs of spheres. The interaction between spheres 1 and

2 results in sphere 1 rotating clockwise and drifting to the right. In the absence of sphere 2, sphere 3 causes sphere 1 to rotate clockwise and fall vertically without drifting. Superposition of these two motions results in sphere 1 rotating and drifting to the right. The same considerations may be made for sphere 3.

An interesting four-sphere configuration is obtained by adding a fourth sphere above sphere 1 and 3 so that it is a mirror image of sphere 2 as shown in figure I-10. Due to symmetry of Stokes flow, sphere 4 cancels the horizontal drift velocity caused by sphere 2 on 1 and 3. Furthermore, the settling velocities of spheres 1 and 3 are equal as are the settling velocities of spheres 2 and 4. If $\tilde{D}/\tilde{B}$ is large, spheres 1 and 3 form a doublet and fall faster than 2 and 4. If, on the other hand, $\tilde{D}/\tilde{B}$ is small, spheres 2 and 4 form a doublet and fall faster than 1 and 3. Again, for a given value of $\tilde{B}$, there is a critical value of $\tilde{D}/\tilde{B}$ where all four spheres fall with the same velocity. This critical value of $\tilde{D}/\tilde{B}$ as a function of $\tilde{B}$ is shown in figure I-10. Similar to the three-sphere case, the critical value of $\tilde{D}/\tilde{B}$ is a very strong function of spacing. At large spacings $\tilde{D}/\tilde{B}$ approaches the asymptotic value of 2. The shaded region in figure I-10 indicates values of $\tilde{D}/\tilde{B}$ which are physically impossible since the spheres would overlap. Unlike the three-sphere configuration, none of the spheres in the diamond con-

figuration possess a horizontal drift velocity. Thus, at the critical spacing, the diamond configuration is steady. However, it will be shown in the following section that this configuration is unstable.

Another interesting behavior may be observed for the diamond configuration. If the four spheres are at or near the critical spacing and sphere 1 is displaced to the left, one at first would suspect that spheres 2 and 4 rotate clockwise since they are closer to sphere 3 than they are to 1. However, the theory shows just the opposite to be true. In fact, for large spacings, spheres 2 and 4 continue to rotate counterclockwise until sphere 1 has been displaced a distance about equal to B. The reason for this can again be qualitatively deduced by considering the interactions between pairs of isolated spheres. The solution for two spheres falling in any arbitrary orientation shows that their angular velocity is a function of both the spacing and the orientation. In the absence of spheres 1 and 3, 2 and 4 fall vertically without rotation. Sphere 3 causes 2 and 4 to rotate clockwise while sphere 1 causes them to rotate counterclockwise. Even though sphere 4 is closer to 3 than to 1 the inclination of the line of centers between spheres 3 and 4 is greater than that between spheres 4 and 1. Rotation of a pair of spheres is caused by the component of gravity perpendicular to their line of centers. This component is greater for the pair

formed by spheres 1 and 4 than by 3 and 4. Thus the counterclockwise angular velocity of sphere 4 caused by the presence of sphere 1 is greater than the clockwise angular velocity of 4 caused by 3 and the net effect is that 4 rotates clockwise. The same analysis may be applied to sphere 2.

I-5. Time-dependent settling of three or four spheres in a vertical plane

In general, a cluster of three or more spheres falling asymmetrically in a vertical plane cannot achieve a stable steady-state configuration even after the initial quasi-steady settling velocity is achieved, since the quasi-steady Stokes drag on each sphere continues to vary because of multiparticle interaction effects that continually change as a function of particle spacing and velocity. As a result, the solutions presented in the previous section are valid for those particular configurations which exist at one instant of time except for certain special cases where the velocity of all the particles is the same and the configuration does not change.

Unsteady multiparticle creeping motions are complicated by the appearance of Basset, virtual-mass and acceleration forces and by the difficulty of calculating fluid-particle interactions for three or more closely spaced particles. Leichtberg, Weinbaum, Pfeffer & Gluckman (1976) have presented a theoretical and experimental investigation exploring the importance of each of these complicating features by examining in detail the hydrodynamic interaction between three or more spheres falling under gravity along a common axis parallel to their line of centers. The results of this investigation indicated, in general, that the Basset force is the most

important unsteady force in gravitational flow at low Reynolds numbers in which the flow configuration is slowly changing owing to fluid-particle interactions. Virtual-mass and particle acceleration, on the other hand, were shown to be of negligible importance except for a short-lived initial transient period. Nevertheless, even with the complete omission of the unsteady forces, the qualitative behavior of the problem was preserved and agreement between theory and experiment was reasonable, especially for runs of short duration in which $Re \leq 0.1$.

Although a complete theoretical analysis of the settling of clusters of spheres should include all the unsteady forces present, the computations required for including these forces for non-axisymmetric flow are prohibitively time-consuming on present computers. If the unsteady forces are omitted (i.e. at each instant of time it is assumed that the quasi-steady Stokes drag balances the gravitational buoyany forces on each sphere), the numerical integration procedure used to determine the trajectory and rotation of each sphere for a typical run requires that the system of equations given by (I-2.12) and (I-2.13) be solved between 1000 and 3000 times for runs of the order of 1000 sphere diameters. To accomplish this for a three-sphere run in which the no-slip boundary conditions are satisfied at four points on the surface of each sphere requires between 10 and 30 min of IBM 370/168

accounting time.

The numerical integration procedure used in this study is basically the same as that used by Leichtberg, Weinbaum, Pfeffer & Gluckman (1976). With the omission of the unsteady forces, the spheres may not be started from rest. Instead, the initial velocities are the quasi-steady velocities obtained from (I-2.12) and (I-2.13) for the initial configuration. The trajectory of each sphere in a vertical planar cluster of spheres is determined by integrating

$$\frac{d\vec{\tilde{S}}_j}{d\tilde{t}} = \vec{\tilde{v}}_j \,, \qquad \text{(I-5.1)}$$

where $\vec{\tilde{S}}_j = \tilde{b}_j \hat{i} + \tilde{d}_j \hat{k}$ is the instantaneous distance of the center of the jth sphere from the origin of a rectangular coordinate system which is at rest and $\vec{\tilde{v}}_j = \tilde{U}_j \hat{i} + \tilde{W}_j \hat{k}$ is the translational velocity of that sphere. Its angle of rotation α_j is obtained by integrating

$$\frac{d\alpha_j}{d\tilde{t}} = \tilde{\omega}_j \qquad \text{(I-5.2)}$$

where α_j is measured in radians and is positive in the counterclockwise direction. The numerical integration is carried out as follows. If $\tilde{t}_o$ is an arbitrary time and $\Delta\tilde{t}$ is a finite but small time interval, the position

and velocity of the jth sphere at time $\tilde{t}_o + \Delta\tilde{t}$ may be obtained in terms of the solution at $\tilde{t}_o$ by a Taylor expansion about $\tilde{t}_o$.

$$\vec{\tilde{s}}_j(\tilde{t}_o+\Delta\tilde{t}) = \vec{\tilde{s}}_j(\tilde{t}_o) + \dot{\vec{\tilde{s}}}_j(\tilde{t}_o)\Delta\tilde{t} + \tfrac{1}{2}\ddot{\vec{\tilde{s}}}_j(\tilde{t}_o)(\Delta\tilde{t})^2 + \tfrac{1}{6}\dddot{\vec{\tilde{s}}}_j(\tilde{t}_o)(\Delta\tilde{t})^3 + \cdots$$

$$= \vec{\tilde{s}}_j(\tilde{t}_o) + \vec{\tilde{v}}_j(\tilde{t}_o)\Delta\tilde{t} + \tfrac{1}{2}\dot{\vec{\tilde{v}}}(\tilde{t}_o)(\Delta\tilde{t})^2 + \tfrac{1}{6}\ddot{\vec{\tilde{v}}}(\tilde{t}_o)(\Delta\tilde{t})^3 + \cdots \qquad \text{(I-5.3)}$$

$$\vec{\tilde{v}}_j(\tilde{t}_o+\Delta\tilde{t}) = \vec{\tilde{v}}_j(\tilde{t}_o) + \dot{\vec{\tilde{v}}}_j(\tilde{t}_o)\Delta\tilde{t} + \tfrac{1}{2}\ddot{\vec{\tilde{v}}}_j(\tilde{t}_o)(\Delta\tilde{t})^2 + \tfrac{1}{6}\dddot{\vec{\tilde{v}}}_j(\tilde{t}_o)(\Delta\tilde{t})^3 + \cdots \qquad \text{(I-5.4)}$$

Solving (I-5.4) for $\dot{\vec{\tilde{v}}}_j(\tilde{t}_o)$, substituting into (I-5.3) and neglecting terms of higher order than $(\Delta\tilde{t})^3$ yields

$$\vec{\tilde{s}}_j(\tilde{t}_o+\Delta\tilde{t}) = \vec{\tilde{s}}_j(\tilde{t}_o) + \tfrac{1}{2}\left[\vec{\tilde{v}}_j(\tilde{t}_o) + \vec{\tilde{v}}_j(\tilde{t}_o+\Delta\tilde{t})\right]\Delta\tilde{t} + \vec{\varepsilon}_j(\tilde{t}_o) \qquad \text{(I-5.5)}$$

where

$$\vec{\varepsilon}_j(\tilde{t}_o) = -\tfrac{1}{12}\ddot{\vec{\tilde{v}}}_j(\tilde{t}_o)(\Delta\tilde{t})^3 \qquad \text{(I-5.6)}$$

is a correction used solely to estimate the error incurred by neglecting terms of order higher than $(\Delta\tilde{t})^2$. A similar equation may be obtained for the angle of rotation

$$\alpha_j(\hat{t}_o+\Delta\hat{t}) = \alpha_j(\hat{t}_o) + \tfrac{1}{2}\left[\tilde{\omega}_j(\hat{t}_o) + \tilde{\omega}_j(\hat{t}_o+\Delta\tilde{t})\right]\Delta\tilde{t} + \varepsilon_j(\tilde{t}_o) \qquad \text{(I-5.7)}$$

where

$$\varepsilon_j(t_o) = -\frac{1}{12}\dddot{\tilde{\omega}}_j(\hat{t}_o)(\Delta\tilde{t})^3 \qquad \text{(I-5.8)}$$

The velocities $\vec{\tilde{v}}_j(\tilde{t}_o + \Delta\tilde{t})$ and $\tilde{\omega}_j(\tilde{t}_o + \Delta\tilde{t})$ are computed simultaneously by an iterative procedure which alternately solves for the positions and angles from equations (I-5.5) and (I-5.7) and for the translational and angular velocities from equations (I-2.12) and (I-2.13) using the collocation technique until convergence is achieved. Usually, only two iterations at each time step are required. Following convergence of the iteration procedure, the error for the displacement and rotation is estimated from (I-5.6) and (I-5.8) written in finite difference form. If any of these errors exceed pre-set error limits, the time interval is halved and the computations repeated. If, on the other hand, none of these errors exceed ten percent of the pre-set error limits, the time interval $\Delta\tilde{t}$

is doubled before proceeding with the next time step computations. By doing this, computer time is kept to a minimum while the desired accuracy is maintained. All of the numerical solutions to be presented in this section are based on the four-point collocation of (I-2.12) (figure I-2c).

The simplest unsteady non-axisymmetric motion of a finite number of particles is that of three equal spheres settling freely in a vertical plane. Figure I-11 shows a series of three-sphere numerical runs relative to a stationary reference frame in which the spheres begin from a horizontal-chain configuration. In all cases, the initial center-to-center distance between the two outer spheres is six diameters while the ratio

$$C = \frac{\text{center-to-center distance from central to right outer sphere}}{\text{center-to-center distance from central to left outer sphere}} = \frac{B}{A} \qquad \text{(I-5.9)}$$

is varied from 1.0 to 2.0 in increments of 0.1. These conditions were chosen since they correspond to the experimental studies of Jayaweera et al (1964). Each figure is drawn to scale and the arrows indicate the instantaneous direction of the angular velocity of each sphere. The numbers to the left of each configuration indicate the total elapsed time $\tilde{t}$ and the distance $\tilde{d}_j$ fallen by the

uppermost sphere measured in sphere radii.

Kynch (1959) discusses a special arrangement of three spheres in a vertical plane in which one sphere is midway between and above the other two, whose line of centers is horizontal. If the particles are equal, the two outer ones separate to allow the central sphere to pass between them and then close up behind it. Because of the reversibility of Stokes flow, the trajectory of the particles after they have formed a horizontal chain is a mirror image of the trajectory before. Thus it is necessary to consider only the motion of the spheres when they are released in a horizontal chain, i.e. $C = 1$ (figure I-11a). As shown in figure I-11(a), the central sphere initially falls faster as the two outer spheres approach one another. A point is reached ($\tilde{t} = 107.8$) where the three spheres fall with the same vertical speed; see figure I-9. However, because of the non-vanishing horizontal drift, the outer spheres continue moving closer together. The outer spheres now form a doublet and begin falling faster than the central sphere. When the gap between the outer spheres reaches 0.1 diameter ($\tilde{t} = 158.3$) the four-point collocation breaks down. However, qualitative results may be obtained beyond this point by artificially constraining the spheres from moving closer or rotating while allowing them to move apart and resume rotation when this is indicated. This extended solution shows that there is no tendency for the

doublet formed by the outer spheres to separate, and the vertical distance between the doublet and the central sphere closes until a spacing is reached where all three spheres fall with equal velocity, creating a steady configuration. The run was discontinued after the ratio $\tilde{D}/\tilde{B}$ (see figure I-9) was within 0.01% of the critical value. It should be noted that the critical value of $\tilde{D}/\tilde{B}$ for $\tilde{B}$ = 1.1 shown in figure I-11(a) at $\tilde{t}$ = 277.0 is 3.567. This differs from the critical value of $\tilde{D}/\tilde{B}$ = 2.715 given by figure I-9, since in the former case the two spheres forming the doublet have been artificially constrained from rotating or moving closer to each other.

A check on the overall accuracy of the numerical integration procedure may be made by running the three-sphere problem in the previous paragraph in its entirety, i.e. beginning with $\tilde{B}$ = = 1.101 for a horizontal doublet and placing a third sphere midway between and above the other two with $\tilde{D}$ = 4.787, which is the mirror image of the configuration shown in figure I-11(a) ($\tilde{t}$ = 158.3). Under these conditions the central sphere falls slower than the doublet. However, the leading pair spreads apart, allowing the central sphere to catch up such that the three spheres form a horizontal chain. If the run is carried out for a time period equal to twice the time required for the three spheres to form a horizontal chain, the final configuration should be a mirror image of the

initial configuration. It was found that the total accumulated error for $\tilde{B}$ and $\tilde{D}$ at the end of the run was 0.08% and 0.13% of the initial values respectively, while the error in the angle of rotation of the outer spheres was -0.05% of twice the value when the spheres formed a horizontal chain.

Hocking (1964) has presented qualitative results similar to those shown in figures I-11(b-i) using a single-reflection weak-interaction theory in which the rotation of the spheres is neglected in an attempt to explain the qualitative experimental observations of Jayaweera et al (1964) for several of the flow configurations shown in figure I-11. In the experiments it was concluded that, for all values of C tested, one sphere in the cluster eventually remains behind the other two. These results as well as those of the present study are presented in table I-5.* In general the agreement between the present theory and experiment is very good, especially considering the duration of some of the runs. Differences occur only for marginal values of C. The present study also shows that there are at least two narrow bands in the range of C, near C = 1.3 and 1.8, for which the final configuration obtained from the numerical integration procedure indic-

* Jayaweera et al (1964) present their results in terms of ranges of values of C. It is not known whether their experiments were carried out for the specific values indicated in table I-5.

ates that the two leading spheres are very slowly spreading apart, which may eventually allow the trailing sphere to catch up after a long time period. These cases are labelled inconclusive in table I-5. A run was made for C = 1.33 and clearly showed that sphere 2 was left behind. The run for C = 1.4 was discontinued after spheres 2 and 3 reached a gap of less than 0.1 diameter. The result shown for C = 1.4 in table I-5 is for A + B = 10 diameters.

While the qualitative agreement with experimental observation shown in table I-5 is very encouraging, a quantitative comparison between the theoretical results and experimental measurements, especially of the small horizontal drift velocity, would be very reassuring owing to the uncertainty in the accuracy of the four-point collocation solutions for this velocity component as discussed in relation to figure I-4(b). Thus, as part of a larger experimental study of multiparticle Stokes flow interactions, Randall Wu and Zeev Dagan conducted a series of careful measurements corresponding to the initial configuration depicted in figure I-11(a). The experimental apparatus and the spheres used as well as the measurement technique are described in Leichtberg, Weinbaum, Pfeffer & Gluckman (1976, pp. 600-601). Unfortunately, these commercially made nylon spheres had tiny internal bubbles with sufficient eccentricity to preclude accurate measurements of the small hydrodynamically generated angular

velocities. After many trials three spheres with virtually identical quasi-steady settling velocities were obtained.

Figure I-12 compares theory and experiment for the time-dependent variation of the relative horizontal and vertical spacings $\widetilde{B}$ and $\widetilde{D}$ as sketched in figure I-9. Two sets of theoretical curves are shown, one in which the spheres are free to rotate and one in which the spheres are artificially constrained from rotating. The latter corresponds to the self-stabilizing configuration achieved in an internally eccentric sphere when the center of gravity of the sphere lies below its center of buoyancy. These two situations bracket the experimental conditions. The small differences in angular velocity involved are observed to have a small effect on the vertical spacing $\widetilde{D}$, which grows with time, and an almost negligible effect on the horizontal spacing $\widetilde{B}$. Optical distortion resulting from the curved walls of the settling tank introduces a measurement error of about 0.2 sphere diameters. The agreement between theory and experiment is good for both the horizontal and vertical spacing for the entire duration of the experimental runs. The time scale shown is the same as that used in figure I-11, the measured runs corresponding to roughly the first 6 frames of figure I-11(a). The length of the run, approximately 150 sphere diameters, was limited by the size of the apparatus and the spheres used. As noted in figure I-12(b), there was a tendency for the vert-

ical-spacing measurements to lag the theoretically predicted curves at the larger times in the experiments. This behavior might be attributed to the omission of the Basset force in the numerical solution. In Leichtberg, Weinbaum, Pfeffer & Gluckman (1976) it is shown that these forces can cause discrepancies in vertical spacing which grow as a $Re\ \tilde{t}$ ($Re = 0.011$ for the experiments shown) with increasing time. This effect would be much smaller for the horizontal drift because of the much smaller velocities and accelerations involved.

Figure I-13 examines the stability of the four-sphere diamond shaped configuration discussed in the previous section for $\tilde{B} = 3$. In figure I-13(a) the horizontal pair was displaced outward by 0.1% while in figure I-13(b), the horizontal pair was displaced inward by the same amount. In the first case the top and bottom spheres form a vertical doublet leaving behind a horizontal doublet formed by the other two spheres. In the second case, the bottom three spheres form a cluster leaving behind the top sphere. In both cases, the run was discontinued after the gap between any two of the spheres became less than 0.1 diameter.

I-6. Some comments on the extension of the present technique to bounded flows

The multiple-sphere collocation technique described herein can be extended to a variety of bounded flow problems with both periodic and arbitrary particle spacing and planar symmetry using procedures very similar to those already developed in Wang & Skalak (1969) and Leichtberg, Pfeffer & Weinbaum (1976) respectively for axisymmetric flow. In either case one first transforms the boundary-value problem for the collocation technique to a form that is entirely equivalent to that already treated in the present study for planar multiple-sphere configurations. This procedure is briefly outlined below.

In place of (I-2.3), the fundamental equation for the velocity field for a system of N spheres lying in a plane of symmetry, with an arbitrary symmetric upstream flow and planar or cylindrical boundaries is given by the linear superposition

$$\vec{V} = \vec{V}_\infty + \sum_{j=1}^{M} \vec{V}_{wj} + \sum_{j=1}^{N} \sum_{n=1}^{\infty} \Big[\nabla \times (\vec{r}_j \chi_{-(n+1)} + \nabla \phi_{-(n+1)} - \frac{(n-2)}{2\mu n(2n-1)} r_j^2 \nabla P_{-(n+1)} + \frac{(n+1)}{\mu n(2n-1)} \vec{r}_j P_{-(n+1)} \Big], \quad \text{(I-6.1)}$$

where in view of the planar symmetry see (I-2.4) and (I-2.5)

$$\begin{Bmatrix} \chi_{-(n+1)} \\ \phi_{-(n+1)} \\ P_{-(n+1)} \end{Bmatrix} = \sum_{m=0}^{n} P_n^m(\zeta_j) \frac{1}{r_j^{n+1}} \left[\begin{Bmatrix} 0 \\ C_{jmn} \\ E_{jmn} \end{Bmatrix} \cos m\phi_j + \begin{Bmatrix} B_{jmn} \\ 0 \\ 0 \end{Bmatrix} \sin m\phi_j \right] \quad \text{(I-6.2)}$$

Here $\vec{V}_\infty$ is the specified flow at upstream infinity and $\vec{V}_{wj}$ the velocity disturbance due to each confining boundary. The latter is a Fourier series or integral of the fundamental separable solutions of the Stokes-flow equation written in rectangular or cylindrical coordinates depending on the shape of the boundary and the particle geometry.

For an infinite periodic array of spheres with arbitrary spacing aligned at any normal distance from, but parallel to, the confining walls the expression for $\vec{V}_{wj}$ is an infinite series containing three sets of unknown coefficients F_{nj}, G_{nj} and H_{nj}. The harmonic functions (I-6.2) representing the velocity disturbance due to each sphere are now written in the coordinate system corresponding to the boundary chosen and the total velocity $\vec{V}$ set equal to zero to satisfy the no-slip boundary conditions along the entire coordinate surface of each confining boundary present. These no-slip conditions provide three equations, one for each velocity component, which are to be satisfied at every point along the confining boundary. This is accomplished by multiplying each of the three boundary equations by the infinite set of appropriate orthogonal functions and integrating over the interval of periodicity. This procedure leads to an infinite ordered system of three linear algebraic equations in which sets of F_{nj}, G_{nj} and H_{nj} are related to linear matrices involving sums of the unknown sphere coefficients

B_{jmn}, C_{jmn} and E_{jmn}. The solutions for the F_{nj}, G_{nj} and H_{nj} are now substituted back into the expressions for the $\vec{V}_{wj}$ in (I-6.1) and the no-slip boundary conditions satisfied at discrete points on the surface of each sphere as described in section (I-2). The resulting set of equations is entirely equivalent to the linear matrix equation (I-2.12) for the unknown sphere coefficients B_{jmn}, C_{jmn} and E_{jmn} obtained in the present study.

The treatment of a confined system of spheres in an arbitrary planar configuration of spheres is similar in concept to that just outlined for periodic flow geometries, but mathematically more involved. The velocity disturbance $\vec{V}_{wj}$ describing each confining boundary is a Fourier integral involving a continuous distribution of unknown Fourier coefficients $F_j(t)$, $G_j(t)$ and $H_j(t)$, where t is the transform variable. The procedure for determining these coefficients in terms of the unknown sphere coefficients B_{jmn}, C_{jmn} and E_{jmn} by employing the no-slip boundary conditions along the surface of each confining boundary is the same as that just described for periodic confined flows except that one has to evaluate the Fourier integral transform of the wall disturbance. While it is possible to perform these integrations analytically for simple coordinate geometries and thus find closed-form solutions for $F_j(t)$, $G_j(t)$ and $H_j(t)$ the evaluation of the inversion integrals is very laborious and must be performed numeric-

ally. The same difficulty arises for axisymmetric flow and is described in detail in Leichtberg, Pfeffer & Weinbaum (1976). All the preceding comments apply equally well if the particles are spheroids instead of spheres except that (I-6.2) is replaced by spheroidal harmonic functions (Jeffery 1922). One interesting biological problem in this regard is the tumbling of a red cell near a planar boundary.

The collocation technique used to solve the matrix equation which replaces (I-2.12) for bounded systems is virtually identical to that described herein for unconfined spheres. In essence, the undetermined coefficients in the series solution for each sphere are used to reduce to zero, on the surface of the sphere, the velocity disturbance produced by the incident stream, and all other boundaries, whether they originate from another sphere or a confining wall. Thus the general guidelines for the selection of boundary points are not altered. The arbitrary planar motion of a single confined sphere or periodic array of spheres relative to infinite straight boundaries can be separated into motions parallel and perpendicular to the confining wall. Thus, for these cases the highly accurate truncation techniques described for the purely horizontal or vertical motion of two spheres in section I-3 can be expected to apply equally well. On the other hand, for the planar asymmetric motion of finite arrays of two or more spheres one

would expect to find equivalent truncation difficulties to those described herein for the settling of two or more spheres at an arbitrary orientation.

Part II of the thesis contains an application of the procedure outlined in this section to the arbitrary motion of a sphere between two plane parallel boundaries.

Table I-1. Comparison of the solutions obtained by the collocation technique with the exact solution for two equal spheres falling parallel to their line of centers.

Drag Correction Factor, λ_j

Spacing	Exact Solution	M = 2 points	M = 4 points	M = 12 points
10	0.93036	0.93045	0.93040	0.93036
9	0.92325	0.92336	0.92331	0.92325
8	0.91454	0.91469	0.91461	0.91454
7	0.90360	0.90381	0.90371	0.90360
6	0.88949	0.88978	0.88966	0.88949
5	0.87060	0.87103	0.87083	0.87060
4	0.84412	0.84477	0.84462	0.84412
3	0.80472	0.80559	0.80573	0.80470
2	0.74226	0.74200	0.74458	0.74216
1.8884	0.73325	0.73247	0.73580	0.73314
1.5431	0.70245	0.69854	0.70576	0.70229
1.3374	0.68205	0.67450	0.68580	0.68192
1.1276	0.65963	0.64623	0.66371	0.65963
1.0453	0.65037	0.63391	0.65443	0.65043
1.0050	0.64572	0.62758	0.64973	0.64581
1.0025	0.64543	0.62717	0.64943	0.64552
1	0.64514	0.62678	0.64914	0.64524

Table I-2. Comparison of the solutions obtained by the collocation technique with the exact solution for two equal spheres falling freely side-by-side at various spacings.

Vertical Drag Correction Factor, λ_j

Spacing	Exact Solution	M = 2 points	M = 4 points	M = 12 points
10	0.96380	0.96384	0.96380	0.96380
9	0.95992	0.95998	0.95992	0.95992
8	0.95511	0.95520	0.95511	0.95511
7	0.94899	0.94911	0.94899	0.94899
6	0.94092	0.94111	0.94092	0.94092
5	0.92981	0.93013	0.92981	0.92980
4	0.91348	0.91410	0.91349	0.91347
3	0.88709	0.88850	0.88711	0.88708
2	0.83680	0.84113	0.83694	0.83677
1.8884	0.82819	0.83324	0.82836	0.82815
1.5431	0.79454	0.80301	0.79490	0.79445
1.3374	0.76751	0.77934	0.76804	0.76739
1.1276	0.73271	0.74887	0.73288	0.73282
1.0453	0.71771	0.73470	0.71648	0.71917
1.0050	0.71255	0.72721	0.70786	0.71523
1.0025	0.71292	0.72673	0.70730	0.71513
1	0.72469	0.72626	0.70676	0.71507

Angular Velocity, Ω_j

Spacing	Exact Solution	M = 2 points	M = 4 points	M = 12 points
10	0.0018750	0.0018633	0.0018759	0.0018750
9	0.0023149	0.0022970	0.0023161	0.0023148
8	0.0029297	0.0029013	0.0029318	0.0029297
7	0.0038265	0.0037781	0.0038300	0.0038265
6	0.0052082	0.0051190	0.0052146	0.0052081
5	0.0074997	0.0073157	0.0075120	0.0074994
4	0.011717	0.011273	0.011744	0.011716
3	0.020824	0.019452	0.020886	0.020818
2	0.046696	0.040249	0.046735	0.046660
1.8884	0.052304	0.044336	0.052288	0.052262
1.5431	0.077498	0.061181	0.076940	0.077470
1.3374	0.10101	0.075186	0.099645	0.10116
1.1276	0.13141	0.093124	0.13120	0.13150
1.0453	0.13664	0.10101	0.14534	0.13119
1.0050	0.11576	0.10495	0.15220	0.11019
1.0025	0.10825	0.10520	0.15262	0.10778
1	0	0.10545	0.15303	0.10531

Table I-3a. Comparison between exact Stimson and Jeffery solution and collocation solutions for the local fluid velocity relative to the sphere settling velocity at a spacing of 3 in the plane midway between the two spheres ($\tilde{Z} = 0$).

Radial Distance $\tilde{R}$ (radii)	$\hat{W}_f - \hat{W}$ Exact Solution	$\hat{W}_f - \hat{W}$ $M = 4$	$\hat{W}_f - \hat{W}$ $M = 12$
0	0.30190	0.29854	0.30195
0.1	0.30281	0.29946	0.30286
0.2	0.30553	0.30222	0.30558
0.3	0.31002	0.30677	0.31007
0.4	0.31624	0.31306	0.31628
0.5	0.32409	0.32100	0.32414
0.6	0.33350	0.33051	0.33354
0.7	0.34434	0.34147	0.34439
0.8	0.35650	0.35375	0.35655
0.9	0.36985	0.36723	0.36989
1.0	0.38425	0.38175	0.38429
1.5	0.46712	0.46519	0.46717
2.0	0.55677	0.55519	0.55681
3.0	0.71744	0.71604	0.71747
4.0	0.83512	0.83368	0.83516
5.0	0.91648	0.91498	0.91651
6.0	0.97328	0.97175	0.97331
7.0	1.01418	1.01264	1.01422
8.0	1.04466	1.04310	1.04469
9.0	1.06809	1.06858	1.06813
10.0	1.08661	1.08505	1.08664

Table I-3b. Comparison between exact Stimson and Jeffery solution and collocation solutions for the local fluid velocity relative to the sphere settling velocity at a spacing of 3 along the axis ($\tilde{R} = 0$).

Axial Distance $\tilde{Z}$ (radii)	$\hat{W}_f - \hat{W}$ Exact Solution	$\hat{W}_f - \hat{W}$ M = 4	$\hat{W}_f - \hat{W}$ M = 12
0	0.30190	0.29854	0.30195
0.1	0.30110	0.29773	0.30115
0.2	0.29871	0.29530	0.29876
0.3	0.29470	0.29123	0.29475
0.4	0.28906	0.28549	0.28910
0.5	0.28173	0.27804	0.28178
0.6	0.27269	0.26884	0.27273
0.7	0.26186	0.25781	0.26190
0.8	0.24920	0.24490	0.24924
0.9	0.23464	0.23004	0.23468
1.0	0.21813	0.21315	0.21815
1.1	0.19960	0.19418	0.19962
1.2	0.17906	0.17309	0.17907
1.3	0.15653	0.14991	0.15653
1.4	0.13216	0.12474	0.13213
1.5	0.10624	0.09788	0.10618
1.6	0.07937	0.06990	0.07926
1.7	0.05261	0.04190	0.05244
1.8	0.02785	0.01587	0.02760
1.9	0.00839	-0.00455	0.00806
2.0	0	-0.01269	-0.00038
4.0	0	-0.01614	-0.00032
4.1	0.01359	-0.00105	0.01333
4.2	0.04443	0.03147	0.04424
4.3	0.08317	0.07178	0.08303
4.4	0.12486	0.11485	0.12477
4.5	0.16689	0.15805	0.16683
4.6	0.20786	0.20001	0.20783
4.7	0.24707	0.24005	0.24706
4.8	0.28422	0.27790	0.28422
4.9	0.31920	0.31347	0.31922
5.0	0.35204	0.34680	0.35206
6.0	0.58720	0.58436	0.58724
7.0	0.72150	0.71934	0.72154
8.0	0.80790	0.80601	0.80794
9.0	0.86842	0.86666	0.86846
10.0	0.91338	0.91169	0.91342

Table I-4a. Comparison between exact Stimson and Jeffery solution and twelve-point collocation solutions for the local fluid velocity relative to the sphere settling velocity at a spacing of 1.7 in the plane midway between the two spheres ($\tilde{Z} = 0$).

Radial Distance $\tilde{R}$ (radii)	$\hat{W}_f - \hat{W}$ Exact Solution	$\hat{W}_f - \hat{W}$ boundary points placed as in fig. I-2a.	$\hat{W}_f - \hat{W}$ boundary points placed near point of interest
0	0.01255	0.01203	0.01288
0.1	0.01456	0.01410	0.01486
0.2	0.02066	0.02034	0.02085
0.3	0.03093	0.03082	0.03093
0.4	0.04549	0.04561	0.04521
0.5	0.06437	0.06471	0.06375
0.6	0.08751	0.08802	0.08647
0.7	0.11468	0.11532	0.11318
0.8	0.14550	0.14620	0.14352
0.9	0.17945	0.18016	0.17699
1.0	0.21592	0.21659	0.21302
1.5	0.41376	0.41415	0.40950
2.0	0.59564	0.59589	0.59112
3.0	0.84764	0.84788	0.84333
4.0	0.99070	0.99097	0.98653
5.0	1.07697	1.07725	1.07284
6.0	1.13339	1.13367	1.12928
7.0	1.17286	1.17314	1.16875
8.0	1.20194	1.20222	1.19784
9.0	1.22425	1.22452	1.22014
10.0	1.24189	1.24217	1.23778

Table I-4b. Comparison between exact Stimson and Jeffery solution and twelve-point collocation solutions for the local fluid velocity relative to the sphere settling velocity at a spacing of 1.7 along the axis ($\tilde{R} = 0$).

Axial Distance $\tilde{z}$ (radii)	$\hat{w}_f - \hat{w}$ Exact Solution	$\hat{w}_f - \hat{w}$ boundary points placed as in fig.I-2a	$\hat{w}_f - \hat{w}$ boundary points placed near point of interest
0	0.01255	0.01203	0.01288
0.1	0.01181	0.01124	0.01216
0.2	0.00974	0.00898	0.01014
0.3	0.00673	0.00563	0.00717
0.4	0.00345	0.00184	0.00391
0.5	0.00818	-0.00148	0.00121
0.6	-0.000260	-0.00336	-0.000069
0.62	-0.000262	-0.00351	-0.000123
0.64	-0.000211	-0.00358	-0.000122
0.66	-0.000127	-0.00359	-0.000083
0.67	-0.000082	-0.00357	-0.000057
0.68	-0.000041	-0.00356	-0.000032
0.69	-0.000012	-0.00353	-0.000012
0.7	0	-0.00350	0.00000
2.7	0	-0.00272	0.00000
2.71	0.000188	-0.00251	0.000187
2.72	0.000736	-0.00194	0.000736
2.73	0.00162	-0.00102	0.00162
2.74	0.00281	0.00022	0.00282
2.76	0.00605	0.00355	0.00606
2.78	0.01029	0.00790	0.01030
2.8	0.01541	0.01313	0.01541
2.9	0.05035	0.04866	0.05024
3.0	0.09420	0.09302	0.09388
4.0	0.49626	0.49650	0.49359
5.0	0.71865	0.71895	0.71515
6.0	0.85104	0.85134	0.84724
7.0	0.93882	0.93911	0.93489
8.0	1.00150	1.00179	0.99751
9.0	1.04864	1.04892	1.04461
10.0	1.08545	1.08573	1.08140

Table I-5. Sphere left behind for a horizontal chain of three unequally spaced spheres settling under gravity (A + B = 6 diameters).

C=B/A	1.1	1.2	1.3	1.4	1.5	1.6	1.7	1.8	1.9	2.0	>2.0
Hocking (1964) (theoretical)	1	1			2					1	3
Jayaweera et al. (1964) (experimental)	1	2	2	1	3	2	2	2	2	2	3
Present Study	1	1	2*	1**	3	2	2	*	2	3	3

* inconclusive

** A + B = 10 diameters

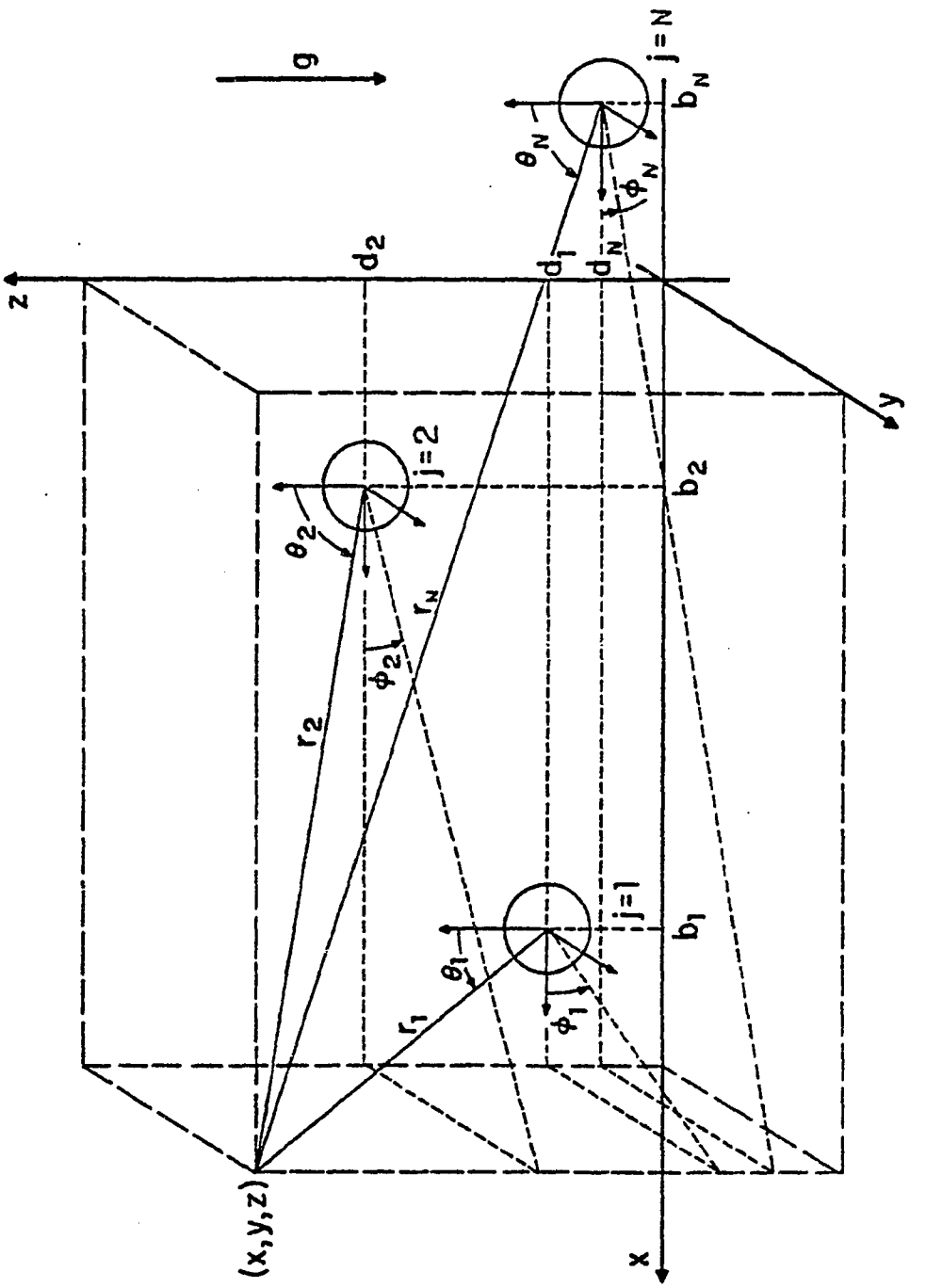

Figure I-1. Geometry for system of spheres falling freely in a vertical plane.

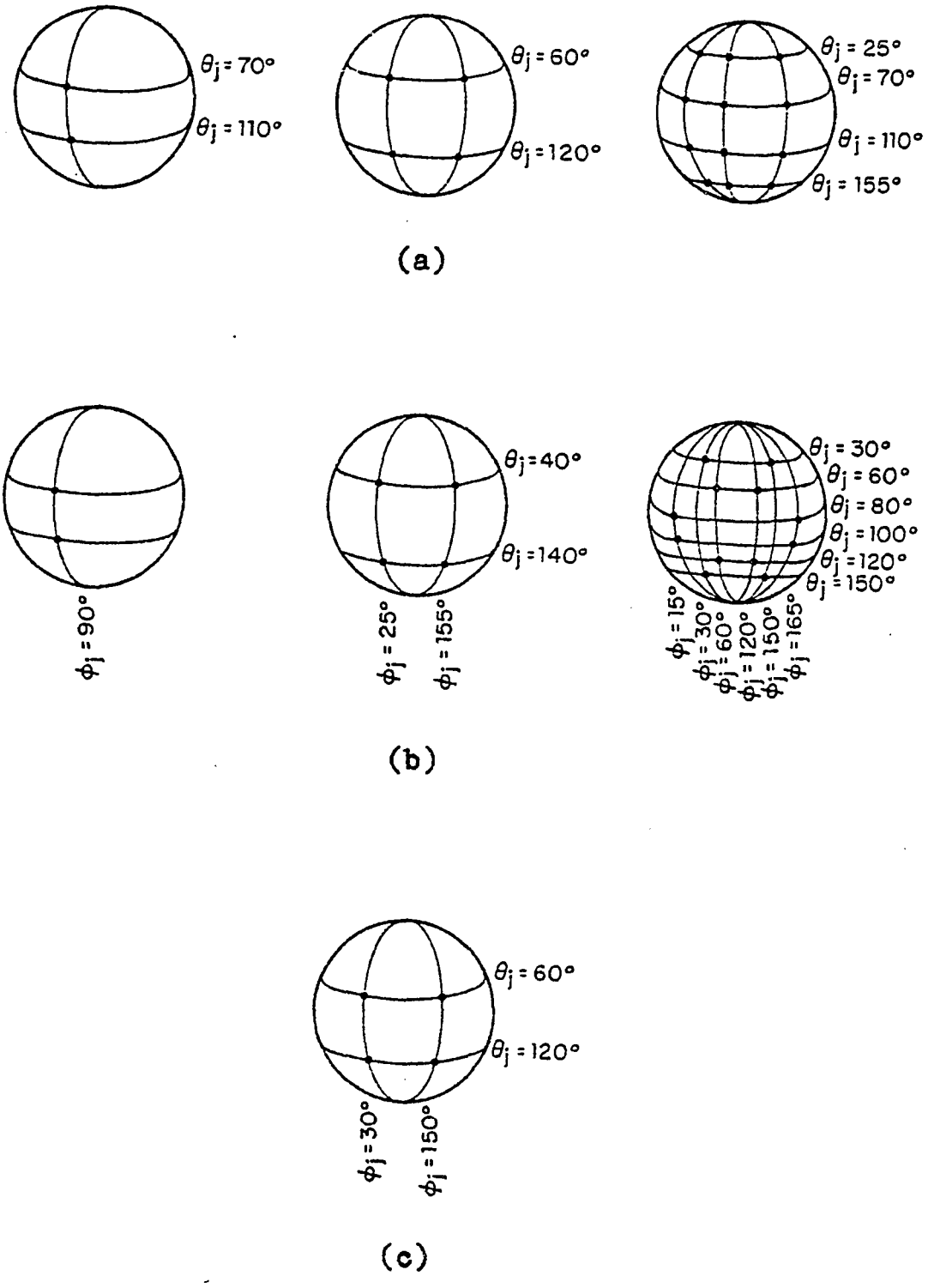

Figure I-2. Position of points for spheres falling (a) parallel to their line of centers, (b) perpendicular to their line of centers and (c) in any arbitrary orientation.

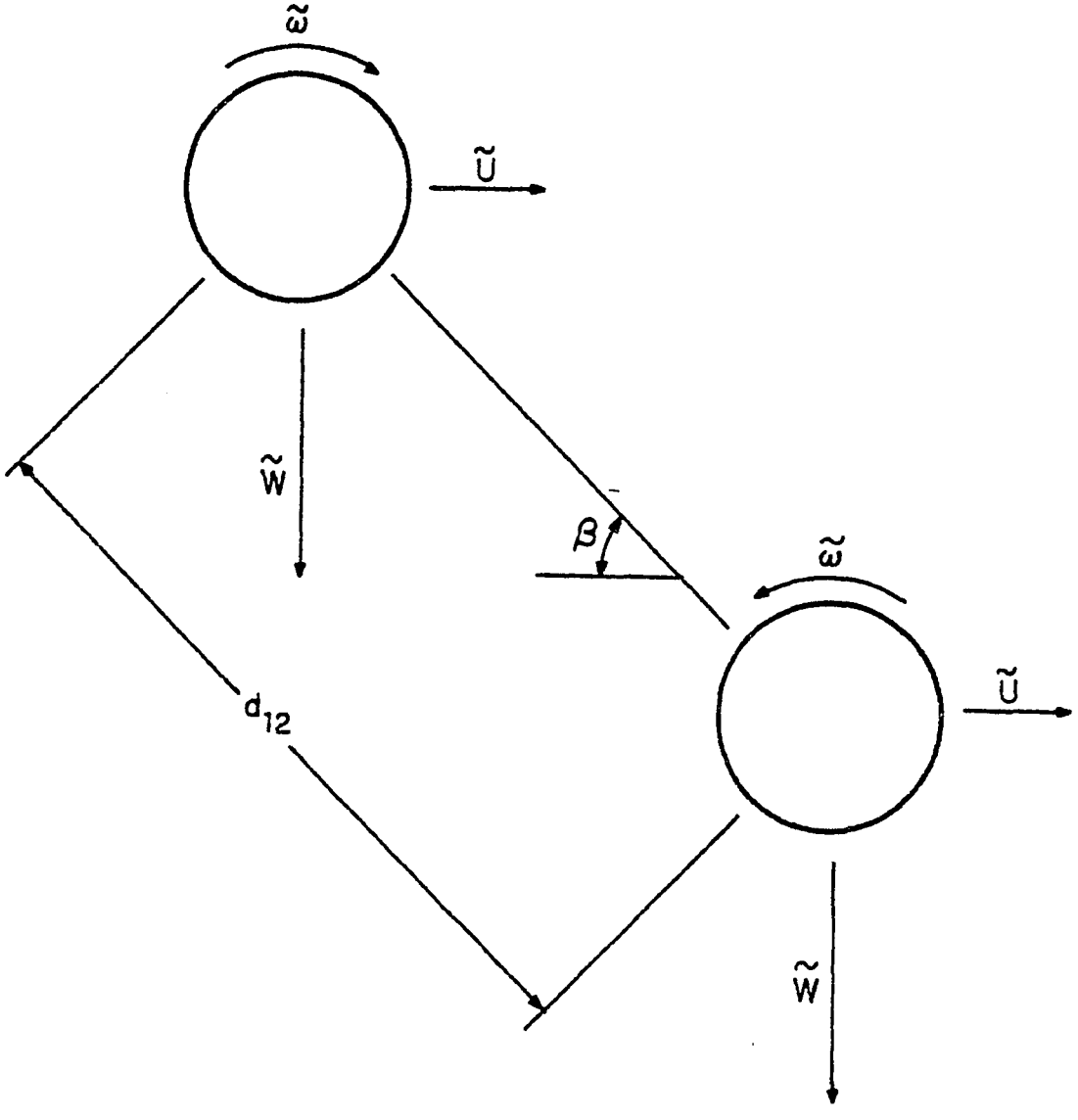

Figure I-3. Two equal spheres settling in an arbitrary orientation under gravity.

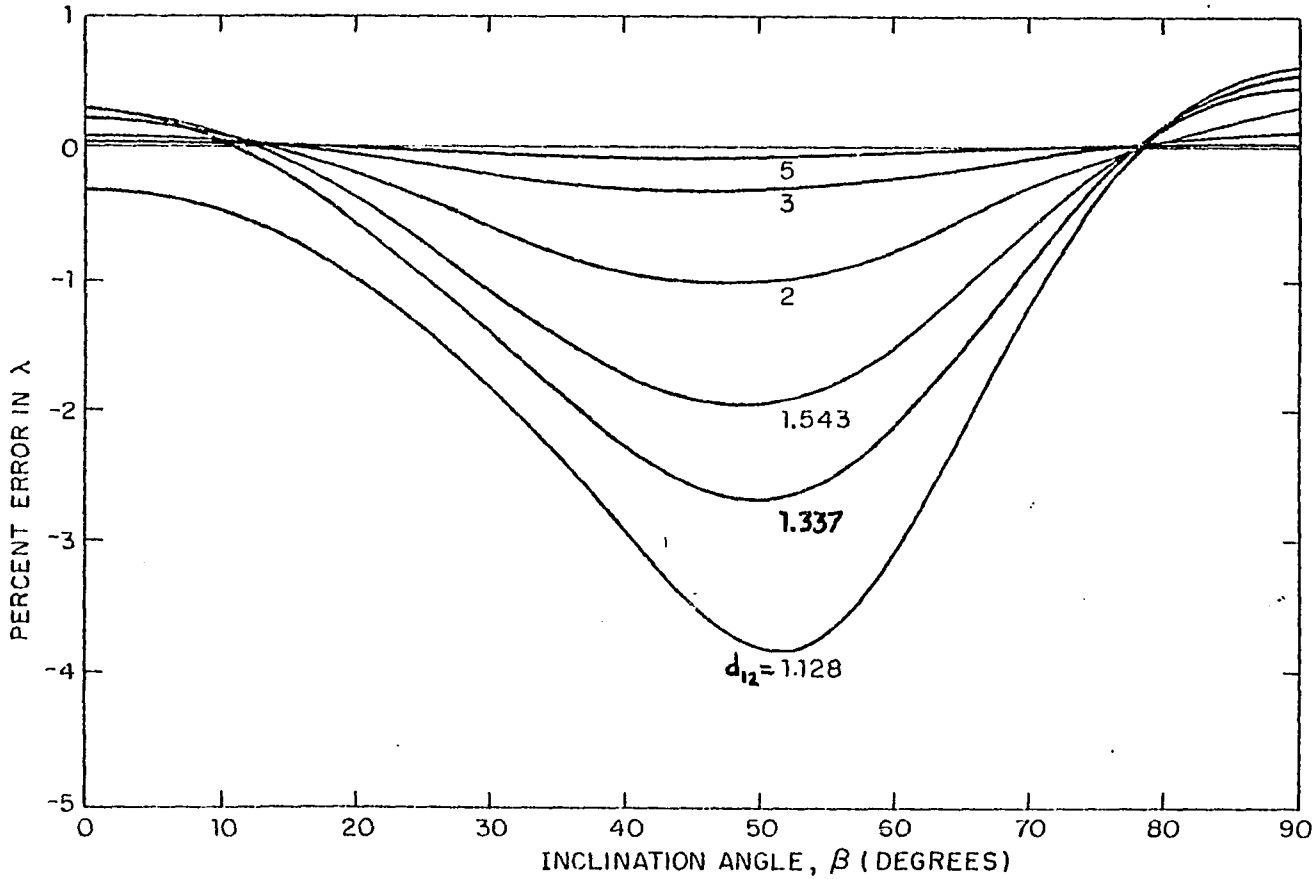

Figure I-4(a). Percentage error in vertical drag correction factor of two equal spheres as a function of orientation at various spacings.

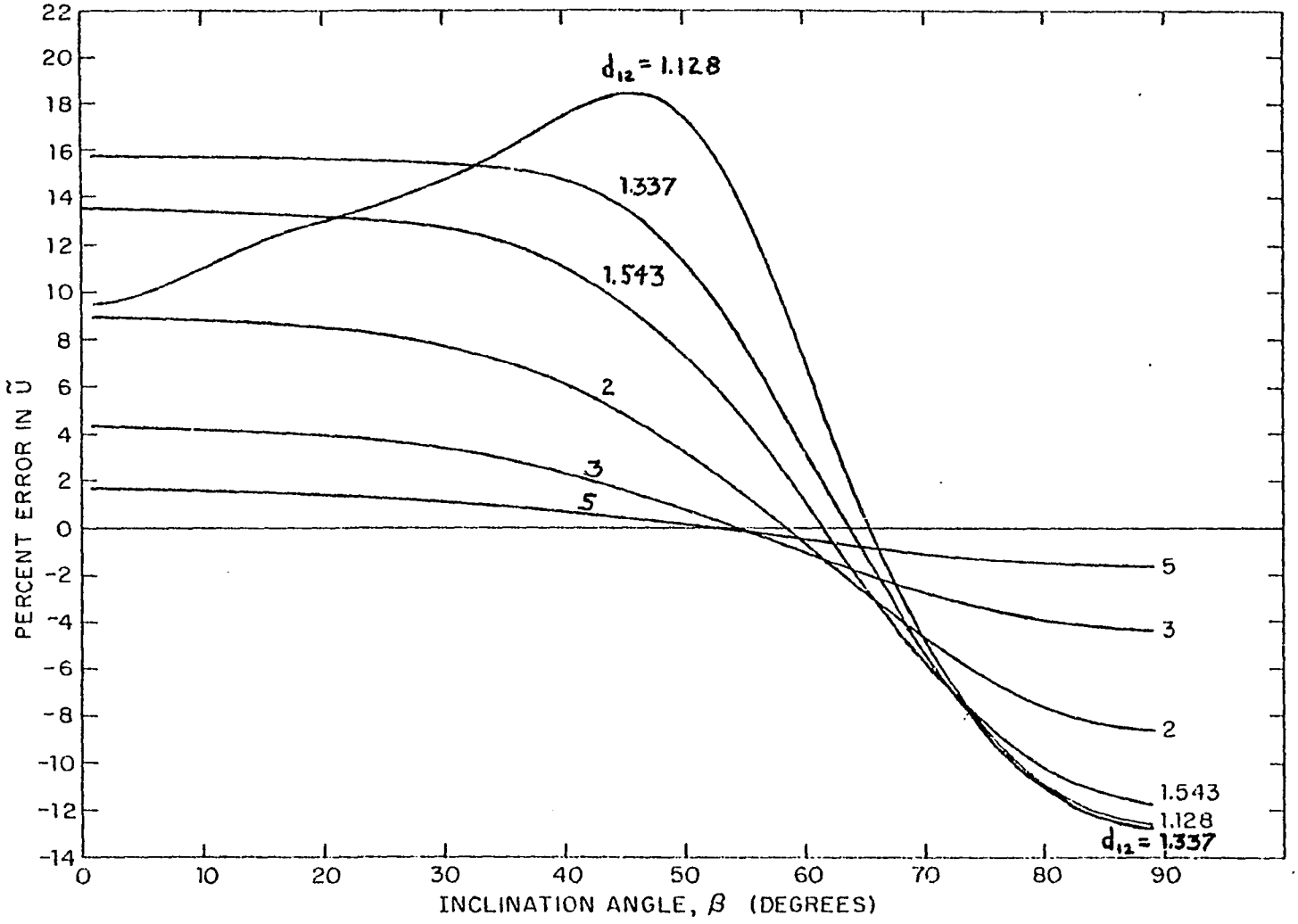

Figure I-4(b). Percentage error in horizontal drift velocity of two equal spheres as a function of orientation at various spacings.

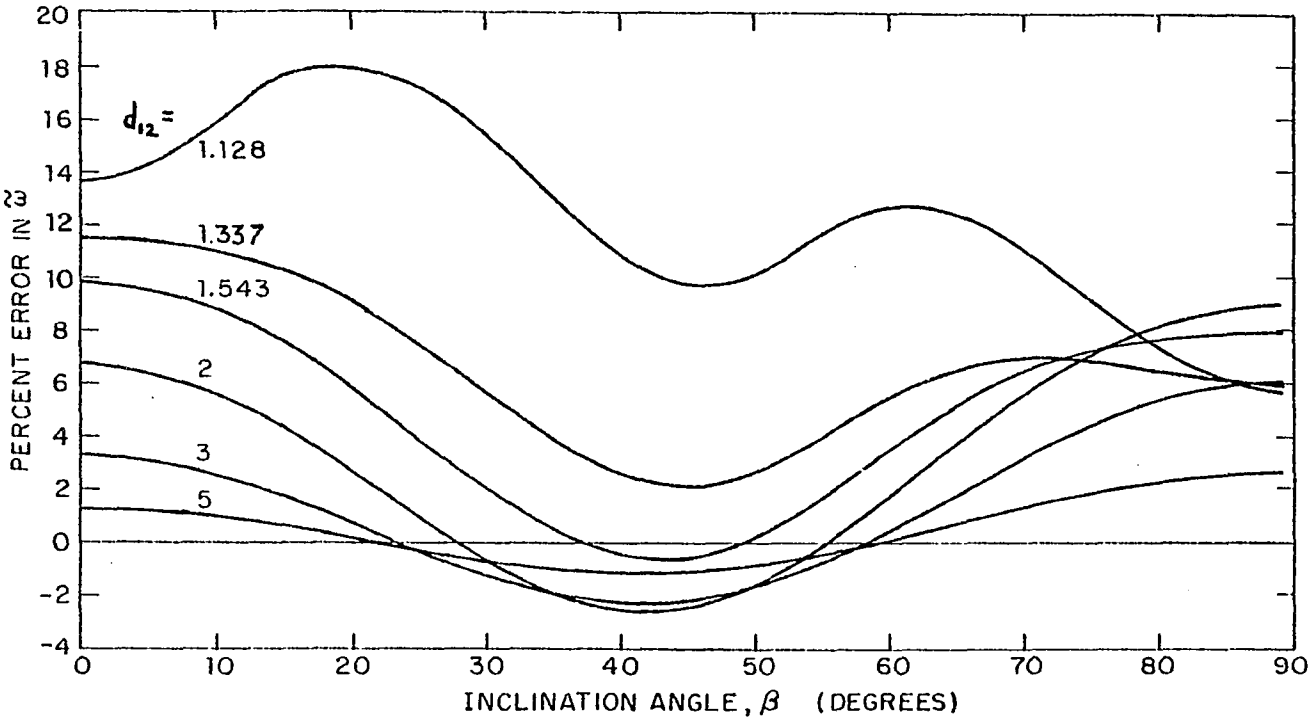

Figure I-4(c). Percentage error in angular velocity of two equal spheres as a function of orientation at various spacings.

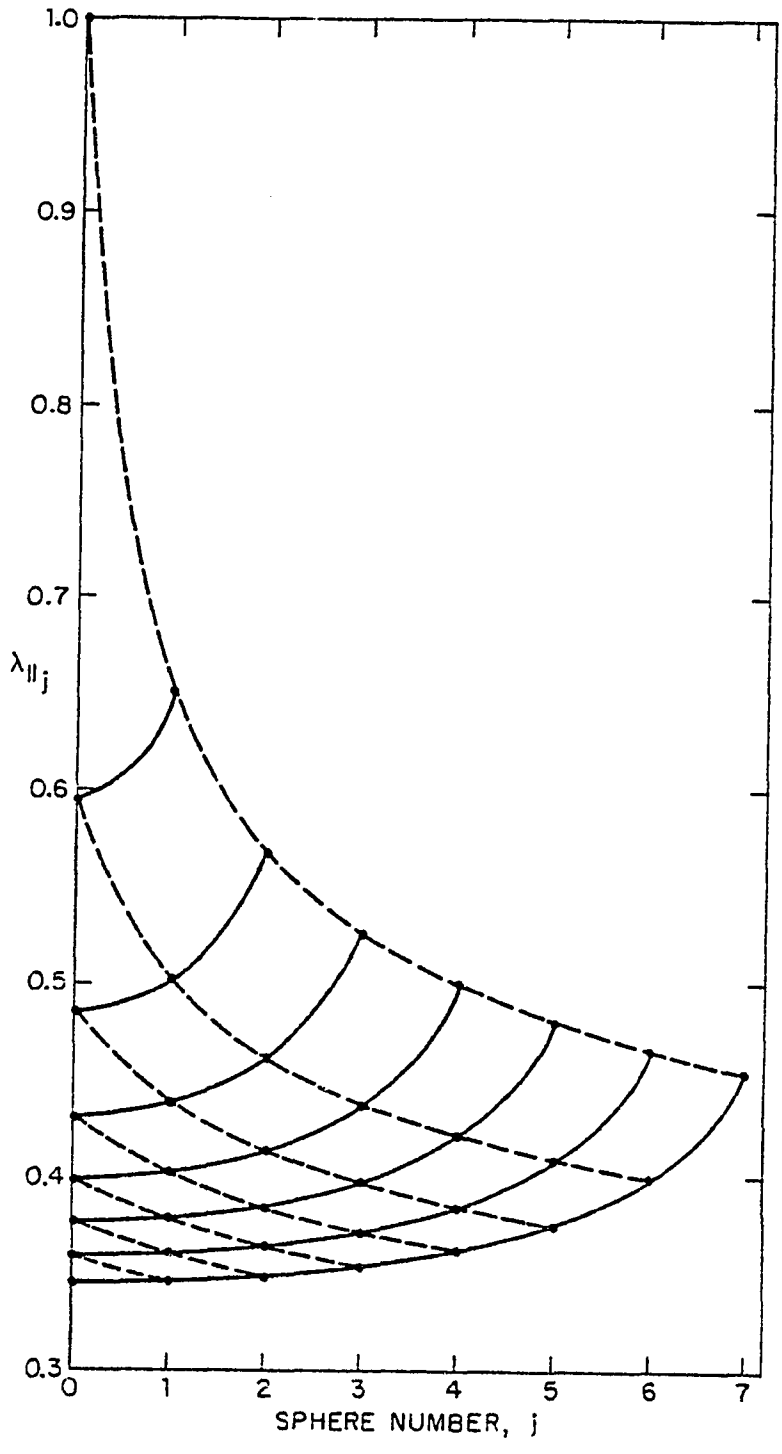

Figure I-5. Drag correction factor for vertical sphere chains at a spacing $d_{12} = 2$.

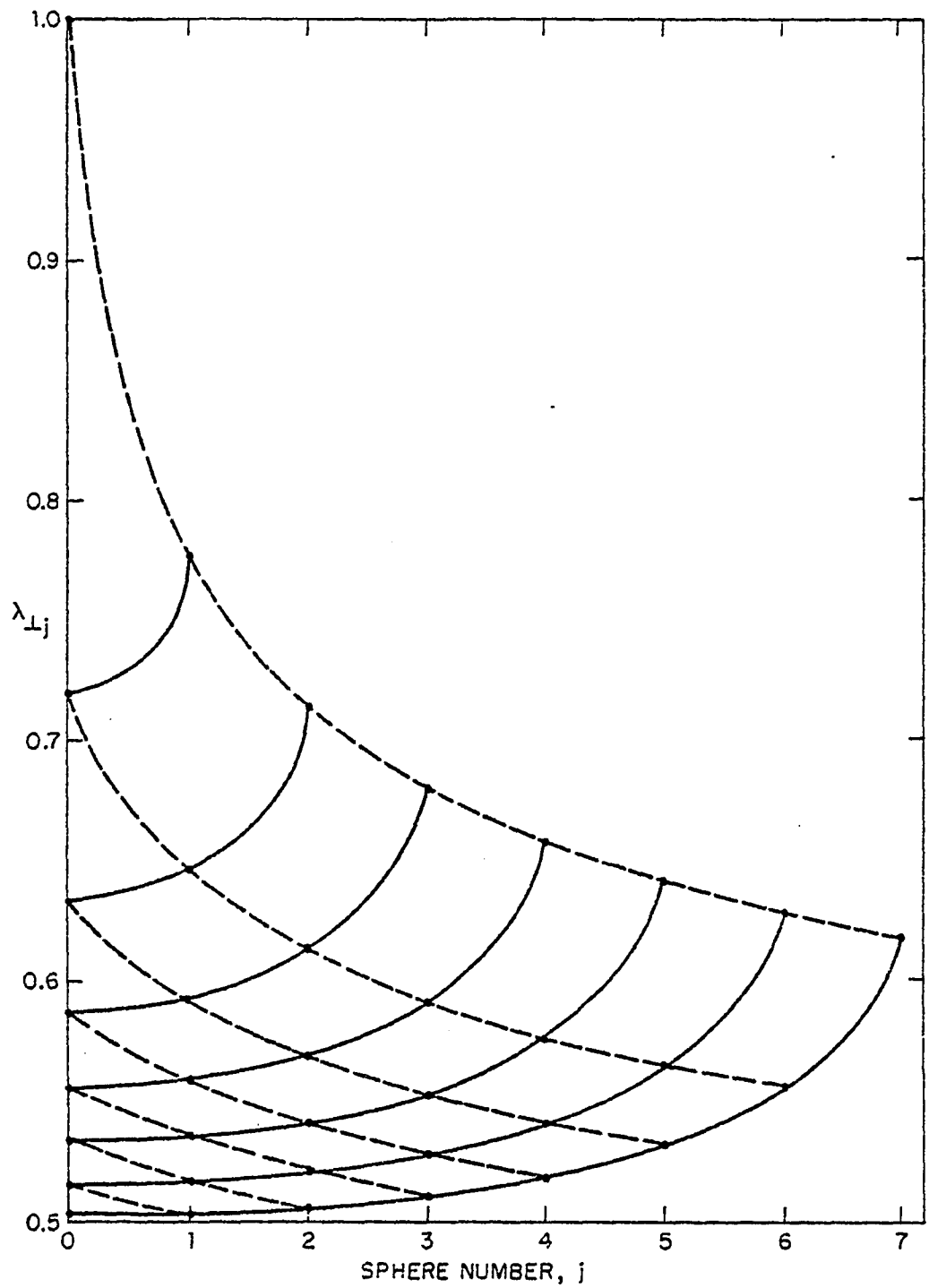

Figure I-6(a). Vertical drag correction factors for horizontal sphere chains at a spacing $d_{12} = 2$.

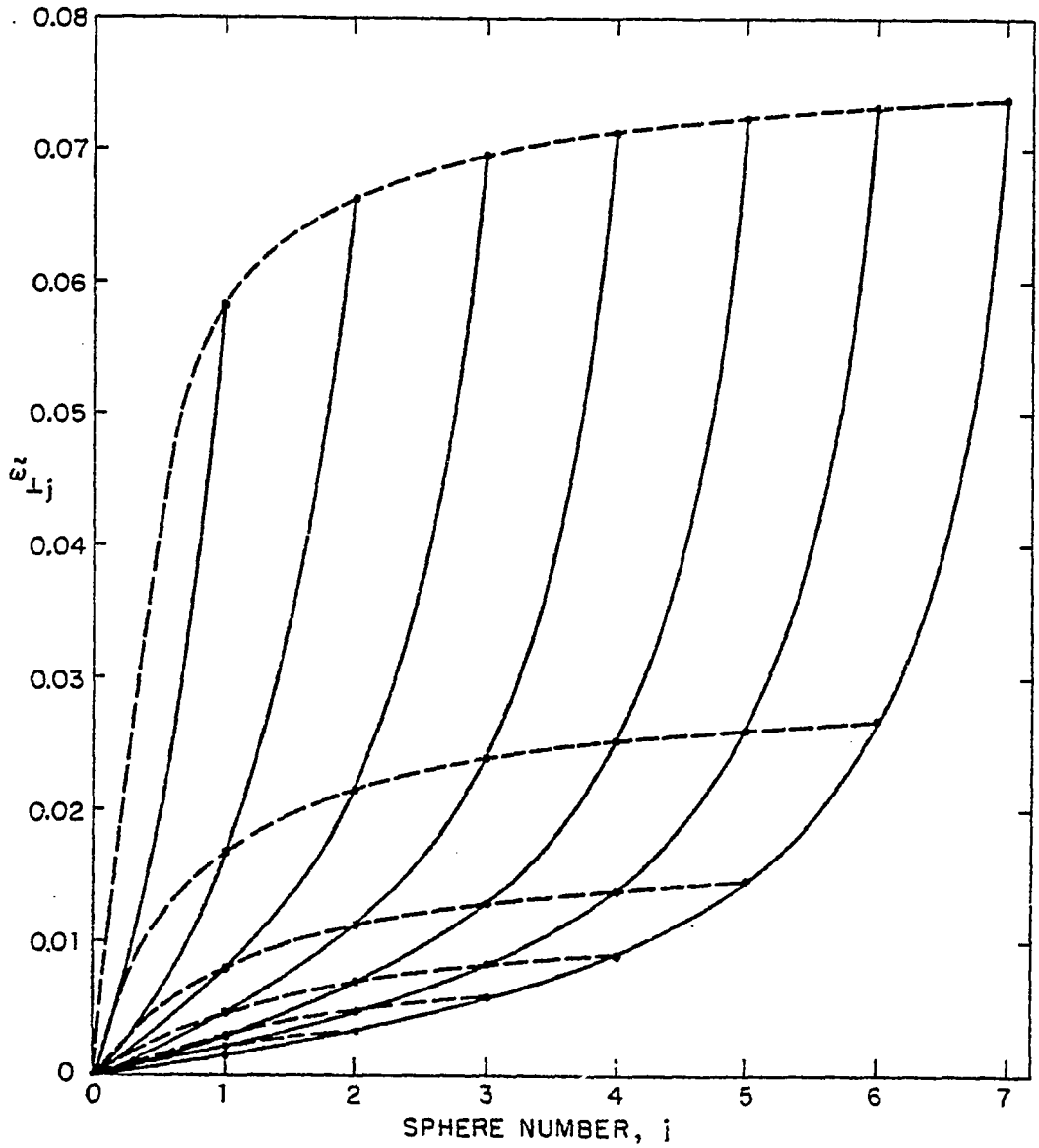

Figure I-6(b). Angular velocities for horizontal sphere chains at a spacing $d_{12} = 2$.

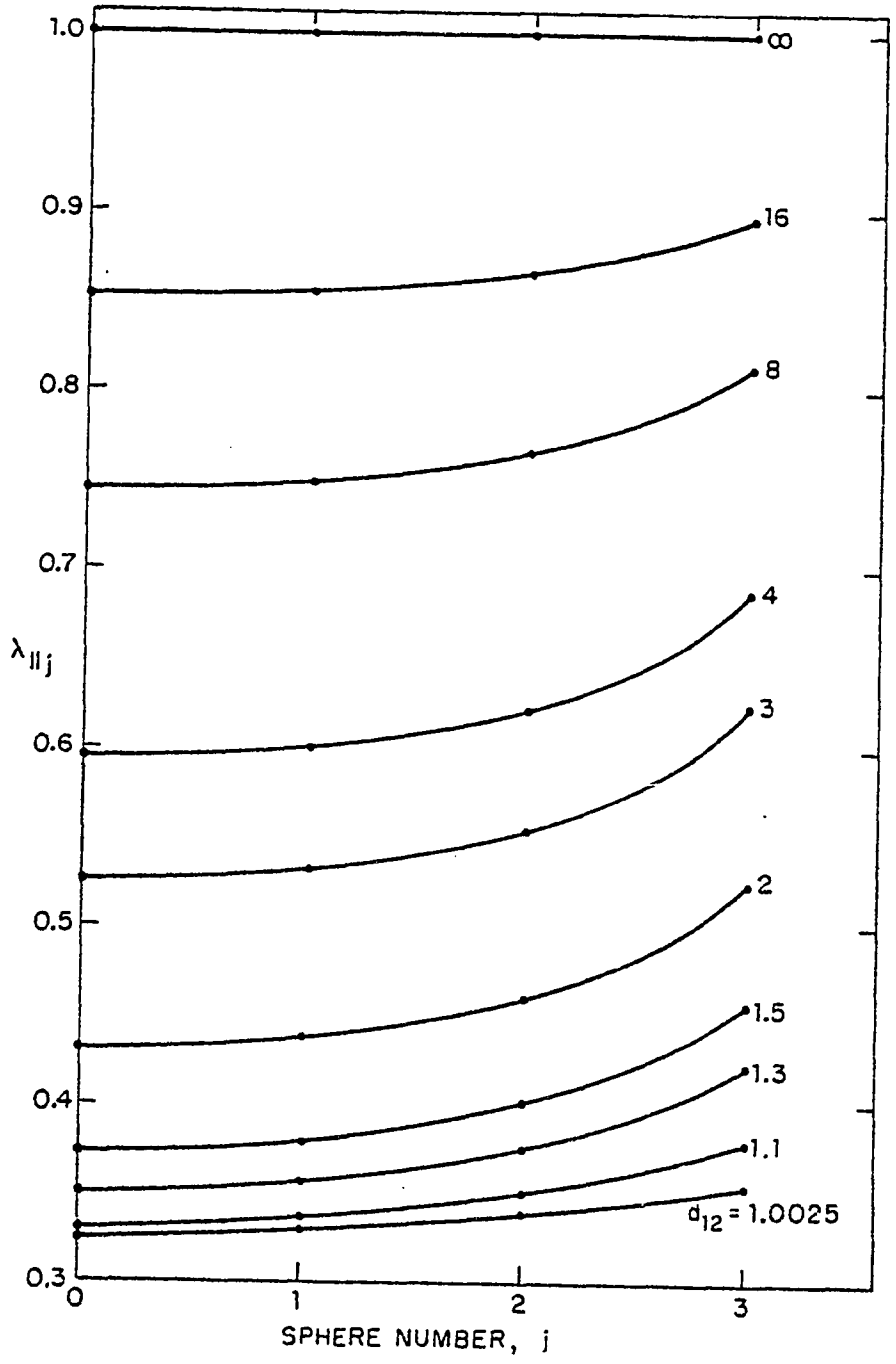

Figure I-7. Drag correction factor for a seven-sphere vertical chain at different sphere spacings.

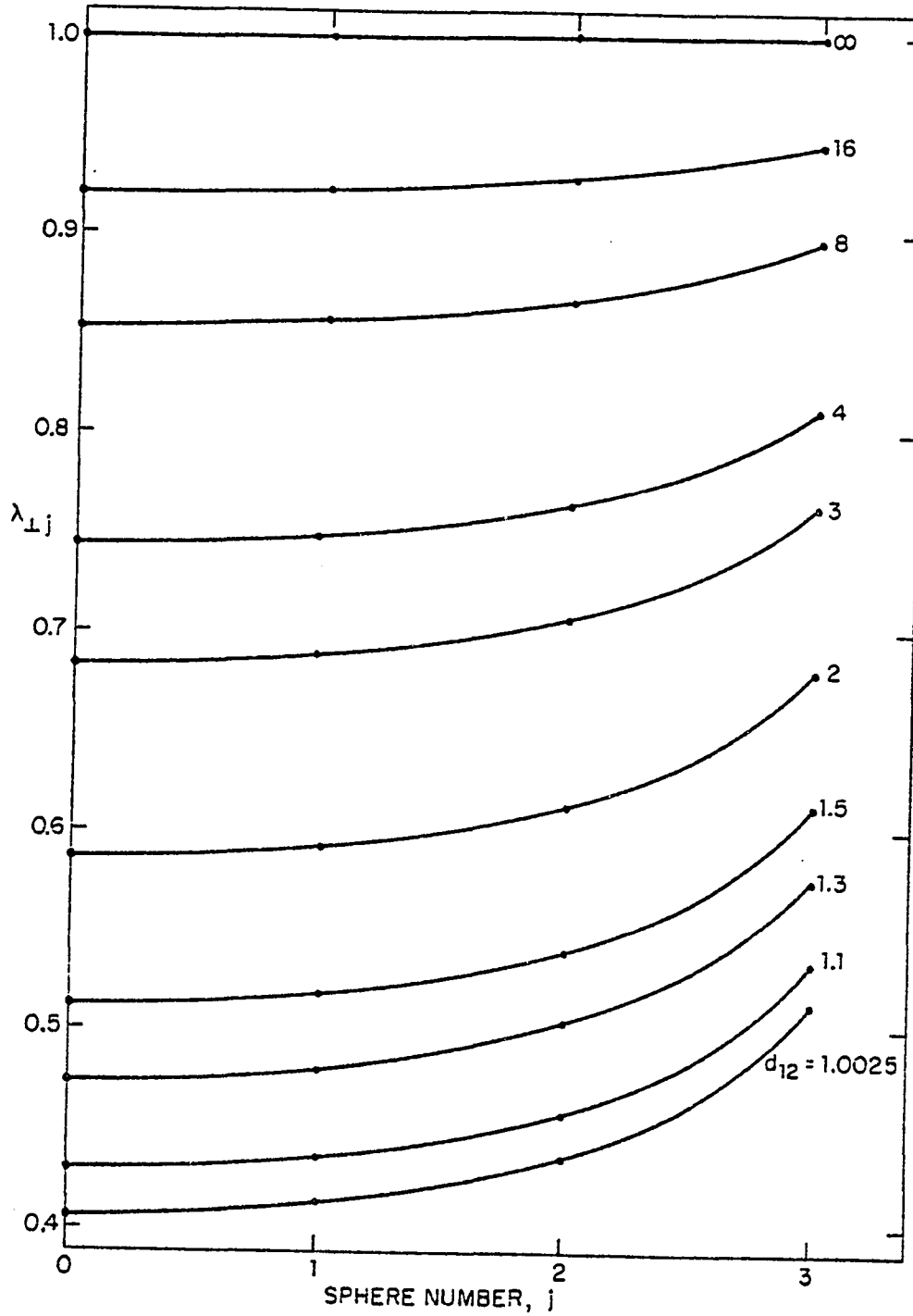

Figure I-8(a). Vertical drag correction factors for a seven-sphere horizontal chain at different sphere spacings.

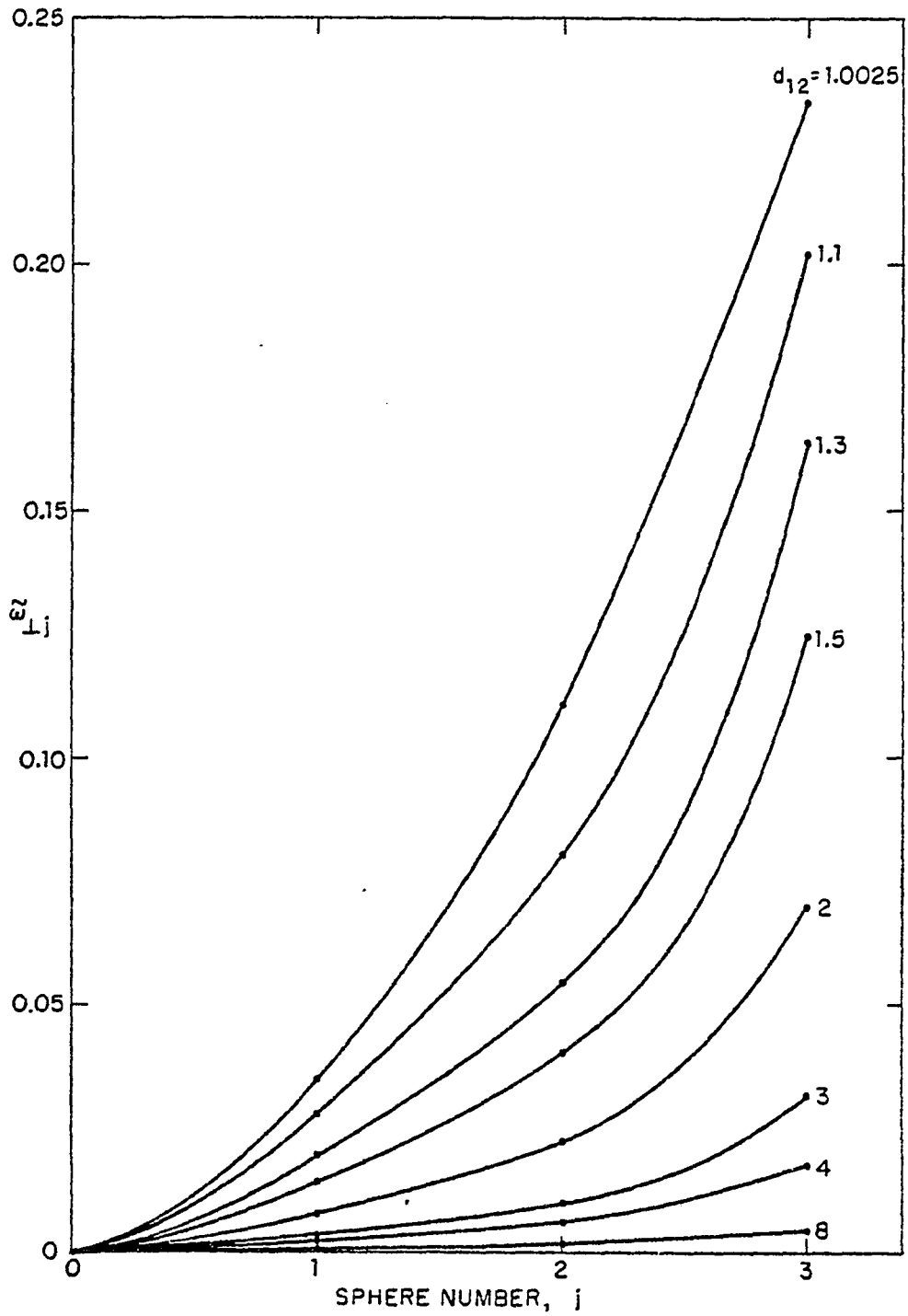

Figure I-8(b). Angular velocities for a seven-sphere horizontal chain at different sphere spacings.

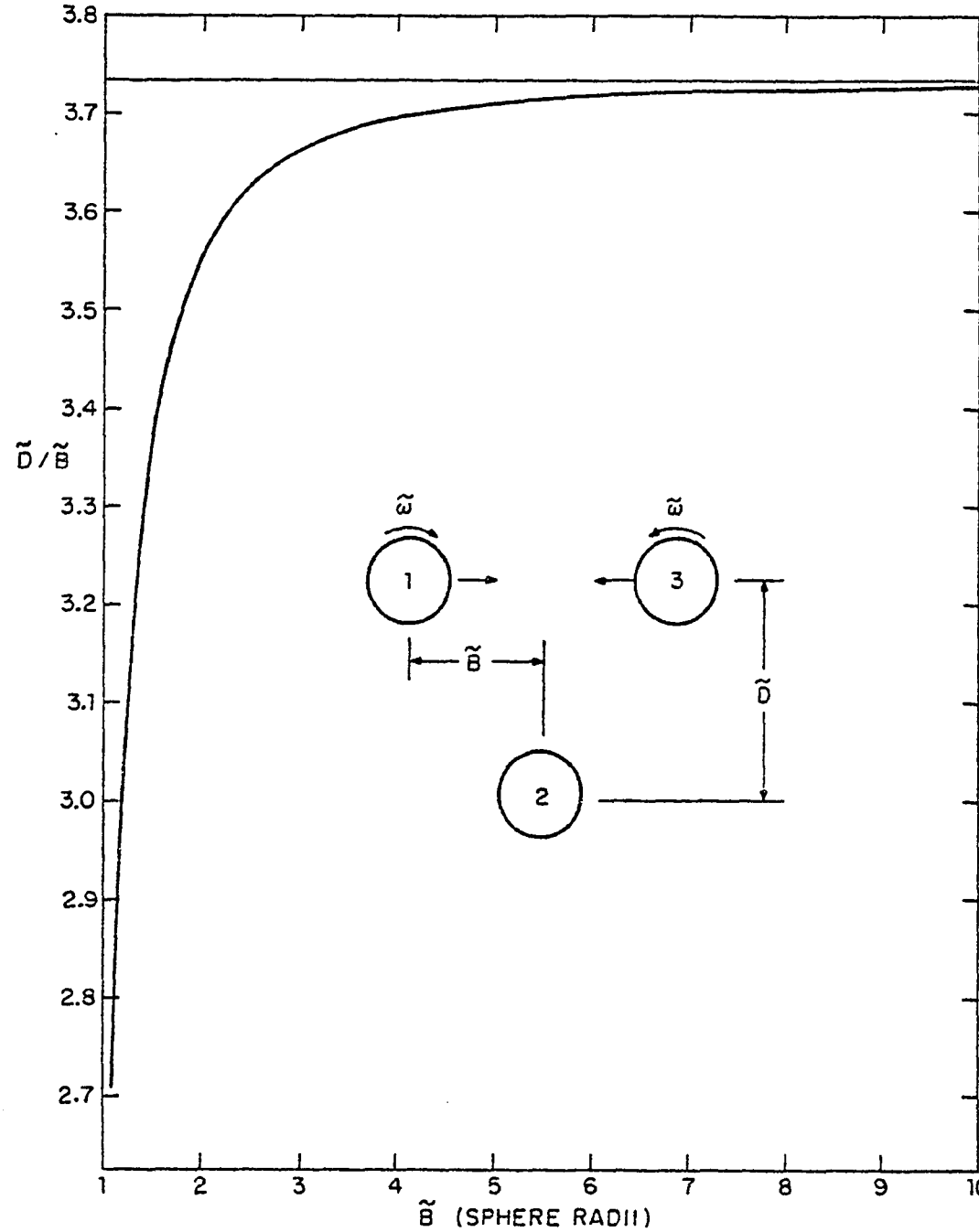

Figure I-9. Critical spacing for triangular three-sphere configuration.

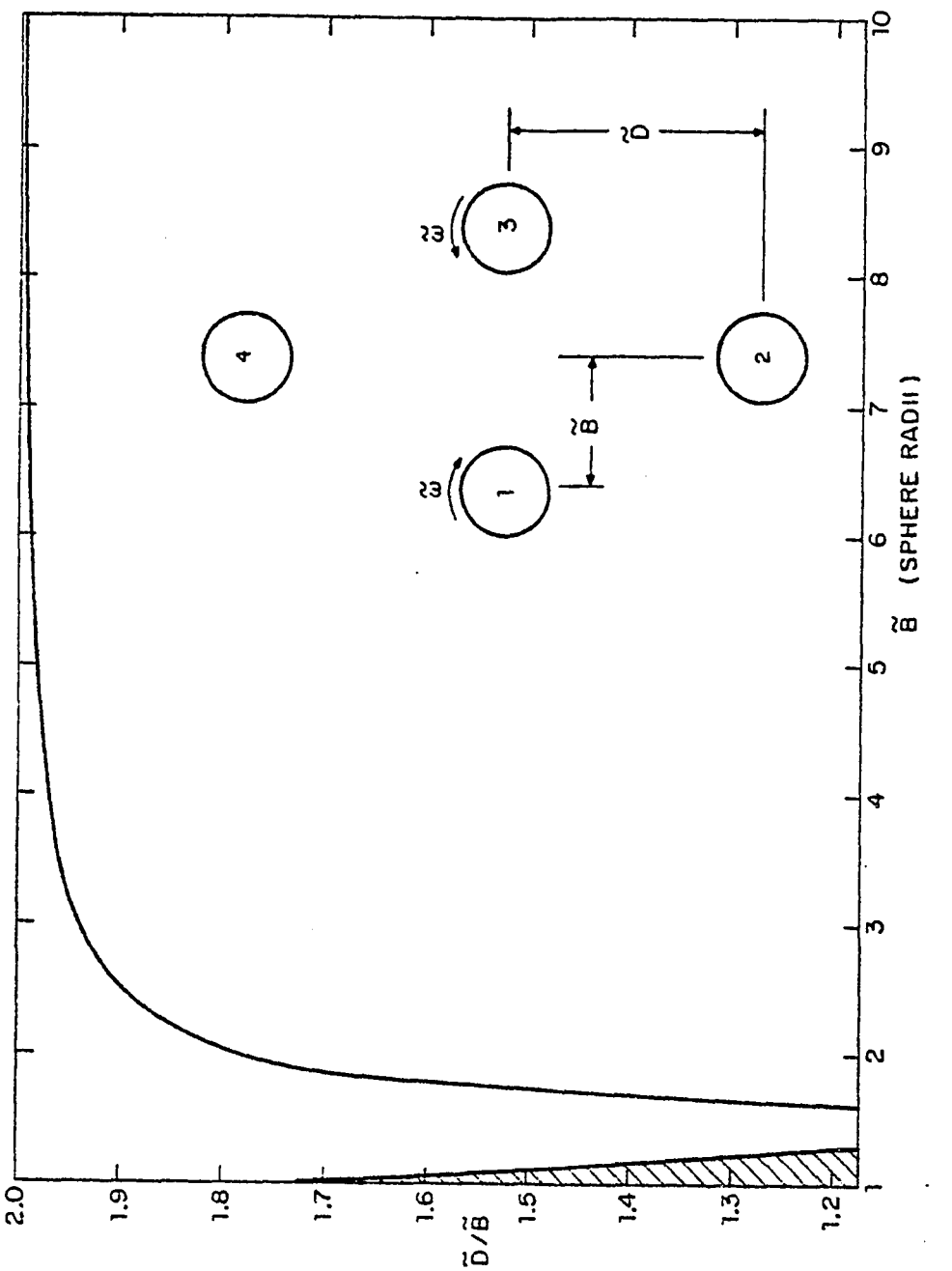

Figure I-10. Critical spacing for diamond-shaped four-sphere configuration.

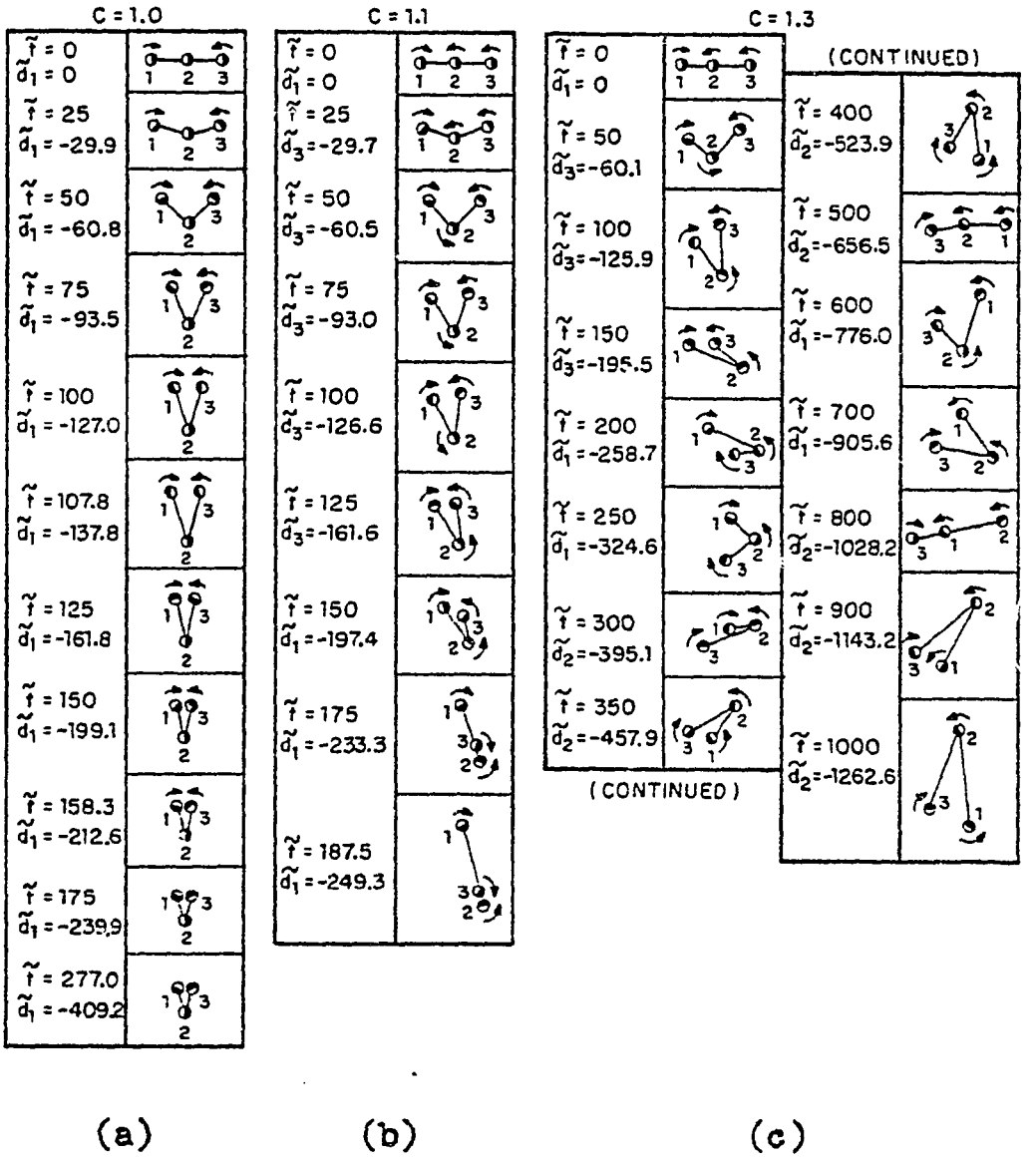

Figure I-11(a-c). Horizontal chains of three unequally spaced spheres settling freely under gravity (A + B = 6 diameters).

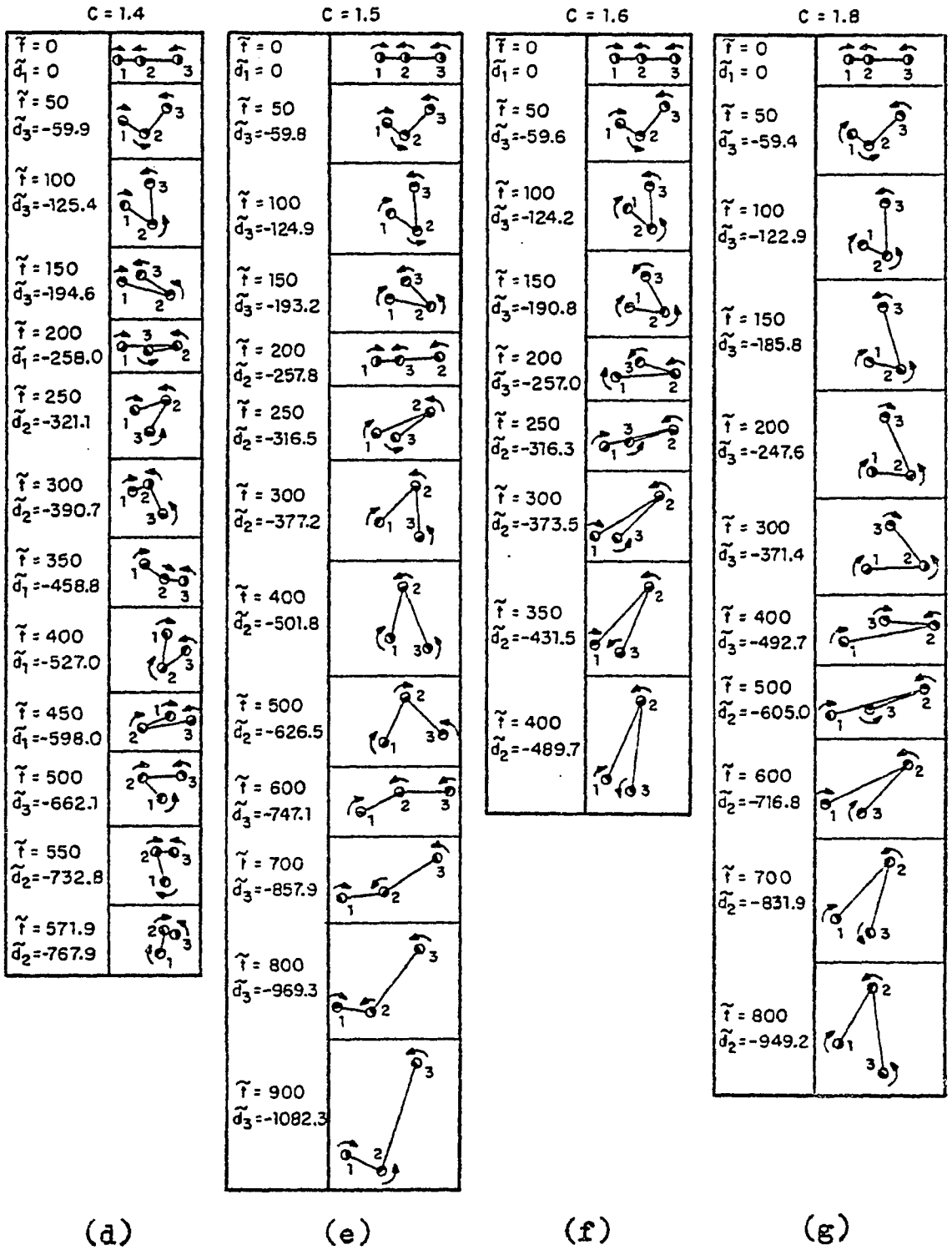

Figure I-11(d-g). Horizontal chains of three unequally spaced spheres settling freely under gravity (A + B = 6 diameters).

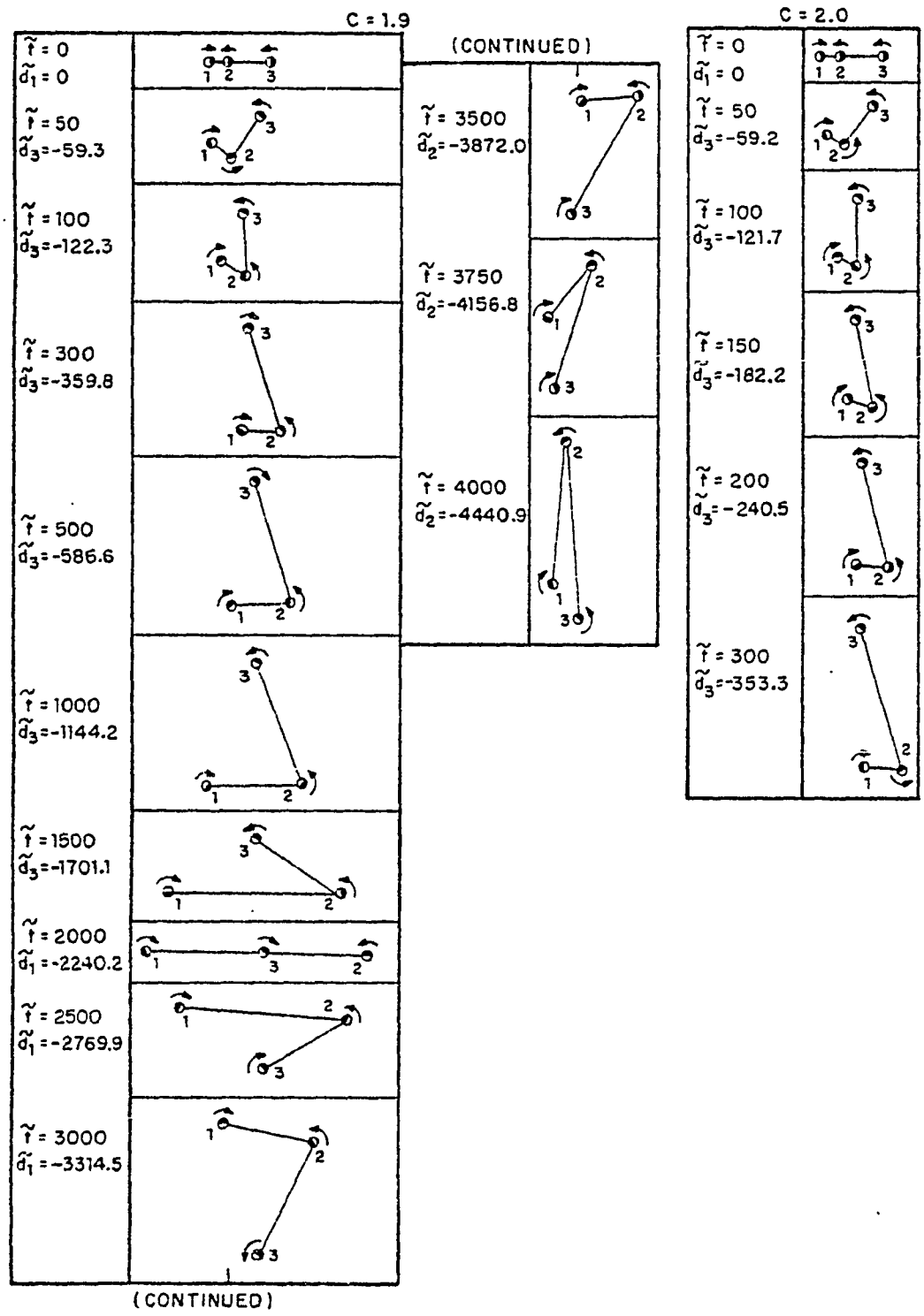

Figure I-11(h,i). Horizontal chains of three unequally spaced spheres settling freely under gravity (A + B = 6 diameters).

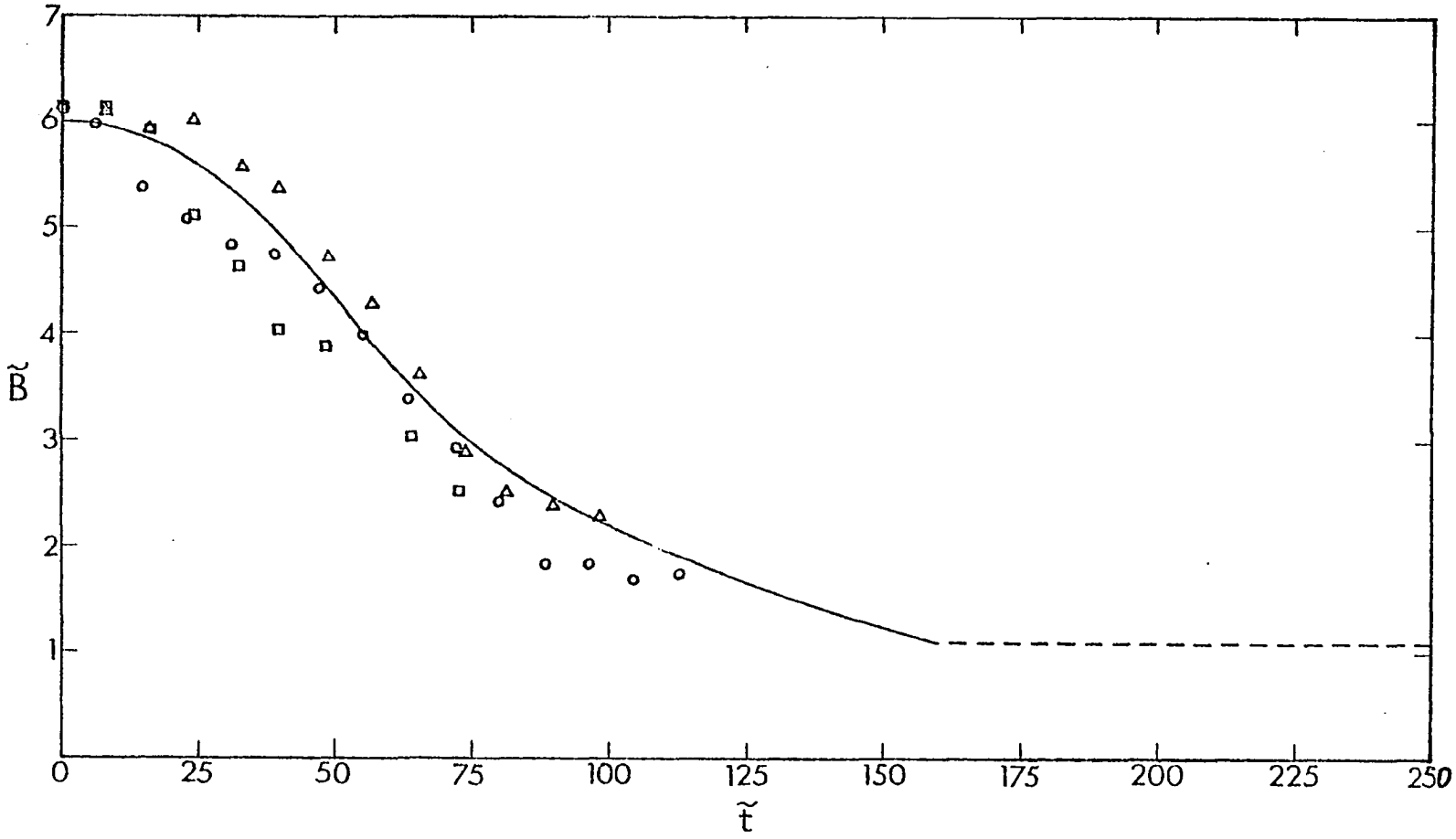

Figure I-12(a). Comparison between theory and experiment for the dimensionless horizontal sphere spacing $\tilde{B}$. Experimental Re = 0.011; □, run 1; o, run 2; Δ, run 3; ——, numerical solution; - - -, gap of doublet artificially constrained from becoming smaller than 0.1 sphere diameter in numerical solution.

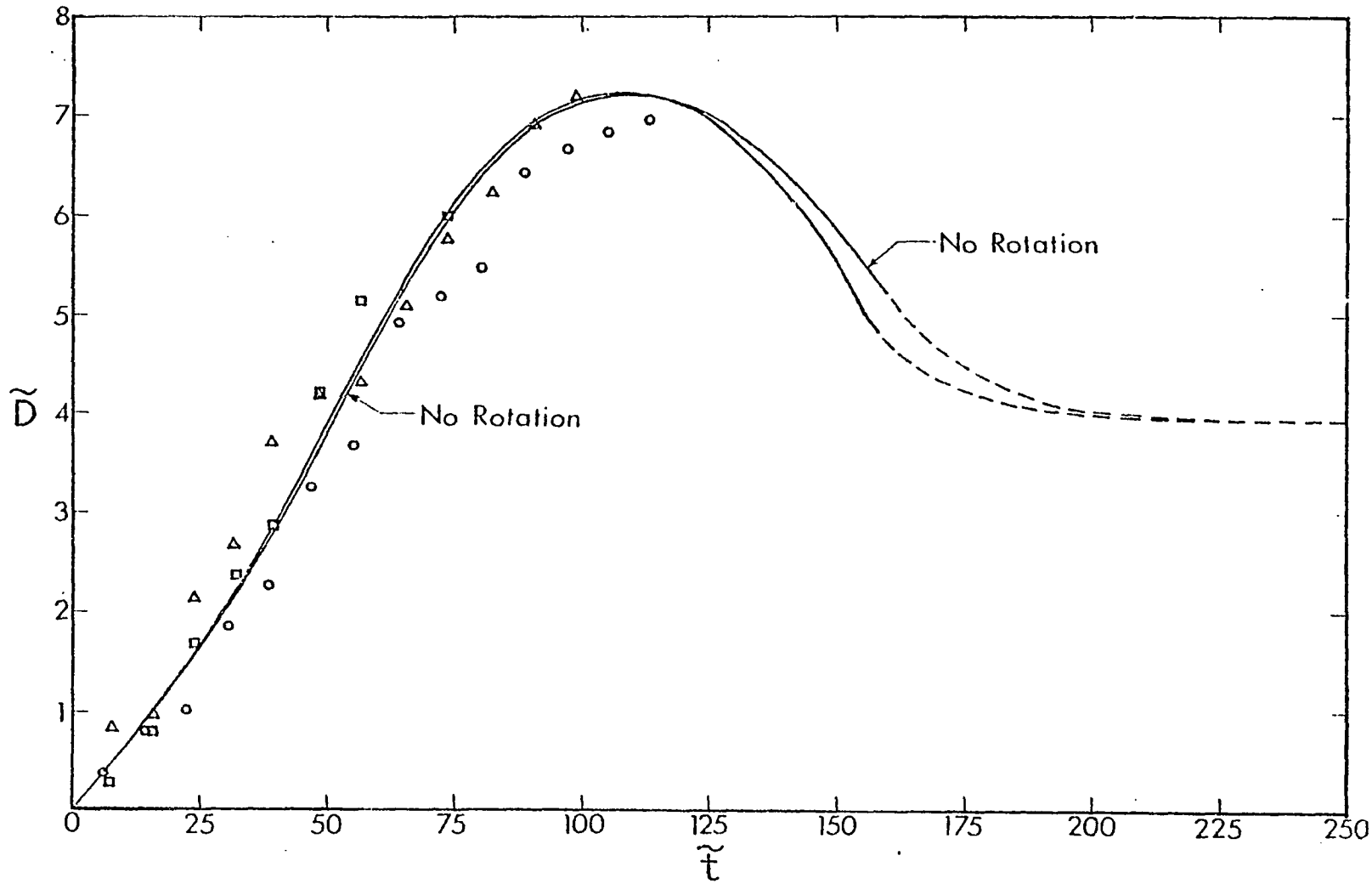

Figure I-12(b). Comparison between theory and experiment for the dimensionless vertical sphere spacing $\tilde{D}$. Experimental Re = 0.011; □, run 1; ○, run 2; △, run 3; ——, numerical solution; ---, gap of doublet artificially constrained from becoming smaller than 0.1 sphere diameter in numerical solution.

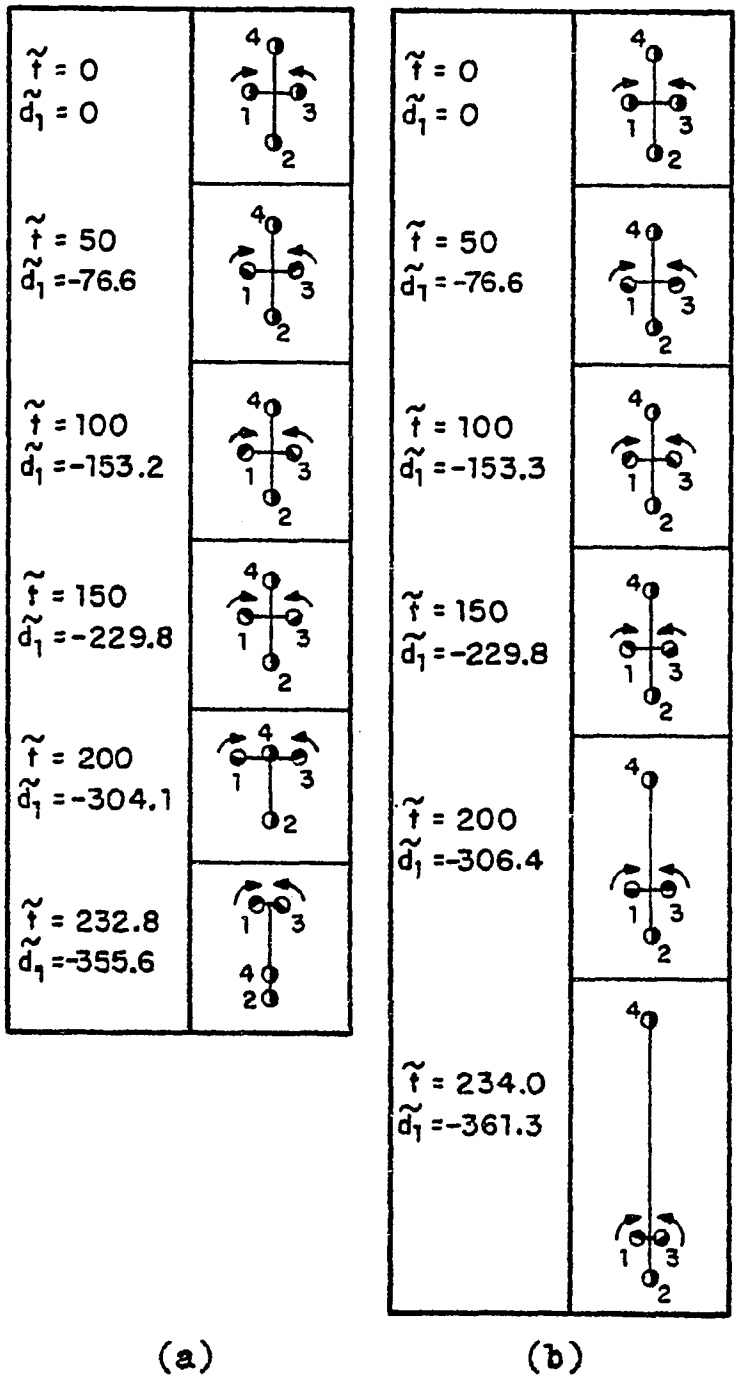

Figure I-13. Break-up of the four-sphere diamond-shaped configuration, $\tilde{B} = 3$. Spheres 1 and 3 displaced (a) outward, (b) inward by 0.1%.

PART II

THE SLOW MOTION OF A SPHERE OF ARBITRARY SIZE AND POSITION BETWEEN TWO PLANE PARALLEL WALLS

II-1. Introduction

The motion of a sphere of arbitrary size and position between two planar parallel walls has important biological and engineering applications. The theory is needed to provide the hydrodynamic interaction parameter for modelling the diffusion of plasmalemma vesicles across endothelial cells lining the artery wall (Weinbaum & Caro 1976, Arminski, Weinbaum & Pfeffer 1979). Another application is found in the diffusion of solute and small protein molecules along the interstitial channels between adjacent cells that have been observed in electron microscopic studies of endothelial and epithelial membranes. In this context the hydrodynamic resistance of the particle is a basic input into numerous existing studies of capillary permeability. This theory is also needed to provide the expressions for the filtration coefficient in Kedem-Katchalsky membrane theory (Curry 1974).

The earliest theoretical treatment of this problem was presented by Faxen (1923), details of which are given in Happel & Brenner (1973, pp. 322-327). Faxen considered the problem of a sphere translating between two plane parallel walls for the special cases where the sphere is either moving along the centerline or in a plane at 1/4 the distance between the two walls. Faxen obtained expressions for the force and torque acting on the sphere by the method of reflections using the five leading terms in the iterative series solution. This iterative method, which alternately satisfies boundary conditions on the sphere and on the walls

gives accurate results only if both walls are far removed from the surface of the sphere. At close particle-to-wall spacings, the higher order interaction effects become significant and the leading terms of the iterative series give a poor description of the particle-wall interactions. Wakiya (1956) used a similar approach to treat the problem of a neutrally buoyant sphere suspended in a simple shear flow or two-dimensional poiseuille flow bounded between two walls. The solution he presents is also only for the case where the sphere is at 1/4 of the distance between the two walls. Brenner (1961) obtained an exact solution for the motion of a sphere perpendicular to a single plane wall. Goldman, Cox & Brenner (1967a) used a solution by O'Neill (1964) to obtain exact numerical results for the translation and rotation of a sphere parallel to a single plane wall. The method used by these authors for a single wall, however, cannot be applied when two walls are present since the solution is based on the limiting case of a spherical bipolar series expansion in which one of the spheres is taken as infinitely large. Halow & Wills (1970) simply added the contribution of two individual walls in order to obtain an estimate of the force acting on a sphere at any position between the two walls. At best, this approach gives only a first-order approximation to the true drag on the sphere.

The most complete study to date of this problem is the work of Ho & Leal (1974). These authors used a perturbation method to study the lateral migration of a neutally buoyant

rigid sphere due to inertia effects when suspended in a fluid which is undergoing either simple shear flow or two-dimensional poiseuille flow between two infinite plane boundaries. Their zeroth order perturbation solution, which corresponds to the inertia-free Stokes flow solution, was obtained by the method of reflections using two reflected fields. Solutions are presented for the motion of a sphere both parallel and perpendicular to the two plane walls at an arbitrary position between them. However, since only the first two reflected fields were obtained, the accuracy of the results presented when the sphere is either close to one of the walls or of dimensions larger than about 0.1 of the spacing between the planes is limited.

The purpose of the present work is two-fold. The first objective is to determine the feasibility of extending the collocation technique presented in part I for unbounded asymmetric flows to bounded asymmetric flows. The second objective is to develop a solution for the arbitrary slow motion of a spherical particle between plane parallel boundaries which includes higher order interaction effects.

The arbitrary planar motion of a sphere relative to two parallel walls can be separated into motions parallel and perpendicular to the confining boundaries. For translation perpendicular to the walls, the fluid motion is purely axisymmetric and the problem may be treated by a collocation procedure similar to that used by Leichtberg, Pfeffer & Weinbaum (1976) for flow past a finite chain of equal spheres

at the centerline of a circular cylinder. The collocation technique outlined in section I-6 is ideally suited for non-axisymmetric motions such as translation of the sphere in a direction parallel to the walls or rotation about an axis which is parallel to the walls and perpendicular to the direction of motion.

Part II is presented in nine sections. Section II-2 contains the formulation for the motion of a sphere perpendicular to two plane parallel walls. In section II-3, the accuracy and convergence characteristics of the collocation technique are examined by detailed comparison with exact published results for the motion of a sphere perpendicular to a single plane wall. Solutions for the axisymmetric motion of a sphere between two plane parallel walls are presented in section II-4. Section II-5 contains the formulation for translation or rotation of the sphere along an axis parallel to the walls in the presence of a unidirectional flow between the walls. In section II-6, the solution obtained in section II-5 is tested against exact published results for a single wall. Solutions for the force and torque acting on the sphere in the presence of two walls are presented in section II-7. In section II-9 the solutions obtained for motion of the sphere perpendicular to the walls and parallel to the walls are combined to yield the solution for the planar arbitrary motion of a sphere between the two walls. Finally, section II-9 contains some comments about the application of the solution technique in future research.

II-2. Formulation for the motion of a sphere perpendicular to two plane parallel walls

This section contains the formulation for the slow motion of a solid sphere of radius a moving with a constant velocity W in a viscous fluid perpendicular to two infinite plane parallel rigid boundaries whose distance from the center of the sphere is b and c as shown in figure II-1. The governing equations for the fluid motion are

$$\mu \nabla^2 \vec{V} = \nabla p , \qquad \nabla \cdot \vec{V} = 0 , \qquad \text{(II-2.1a,b)}$$

where the symbols have their usual meaning. Due to the axisymmetric nature of the flow, it is convenient to introduce the stream function ψ, satisfying (II-2.1b), which is given in cylindrical coordinates by

$$v_\rho = -\frac{1}{\rho}\frac{\partial \psi}{\partial \rho} , \qquad v_z = \frac{1}{\rho}\frac{\partial \psi}{\partial \rho} \qquad \text{(II-2.2a,b)}$$

where v_ρ and v_z are the radial and axial components of the fluid velocity respectively. From (II-2.1a), the governing equation satisfied by the stream function is

$$D^2(D^2\psi) = 0, \qquad \text{(II-2.3)}$$

where D^2 is the generalized axisymmetric Stokesian operator given by

$$D^2 = \frac{\partial^2}{\partial \rho^2} - \frac{1}{\rho}\frac{\partial}{\partial \rho} + \frac{\partial^2}{\partial z^2} . \qquad \text{(II-2.4)}$$

For the geometry of the problem at hand, the stream function is linearly composed of two parts:

$$\psi = \psi_s + \psi_w \qquad \text{(II-2.5)}$$

ψ_s represents an infinite series containing all the simply separable solutions of (II-2.3) in spherical coordinates which yield a vanishing fluid velocity as $r \to \infty$ and is given by Happel and Brenner (1973, p. 136) as

$$\psi_s = \sum_{n=2}^{\infty} \left[B_n r^{-n+1} + D_n r^{-n+3} \right] I_n(\zeta) \qquad \text{(II-2.6)}$$

Here r and θ are spherical coordinates measured from the center of the sphere, (see figure II-1) $\zeta = \cos\theta$ and $I_n(\zeta)$ is the Gegenbauer function of the first kind of order n and degree -1/2. B_n and D_n are unknown constants which will be determined by satisfying the no-slip boundary conditions on the surface of the sphere in the presence of the confining walls.

ψ_w represents an integral of all the separable solutions of (II-2.3) in terms of cylindrical coordinates which produce finite velocities everywhere in the flow

field and is given by the Fourier-Bessel integral

$$\psi_w = \int_0^\infty \left[A(\alpha)\, e^{\alpha z} + B(\alpha)\, e^{-\alpha z} + C(\alpha)\, \alpha z\, e^{\alpha z} + D(\alpha)\, \alpha z\, e^{-\alpha z} \right] \rho\, J_1(\alpha \rho)\, d\alpha . \qquad \text{(II-2.7)}$$

Here $A(\alpha)$ - $D(\alpha)$ are unknown functions of the separation variable α and J_1 is the Bessel function of the first kind of order 1. The integral rather than the infinite series form of the solution in cylindrical coordinates is required due to the infinite non-periodic extent of the two planar boundaries. By proper choice of the unknown functions, the solution (II-2.7) is capable of exactly cancelling the disturbances produced by the sphere along the two confining walls.

Equation (II-2.5) is written in mixed coordinates; the cylindrical coordinate system (ρ,z) and spherical coordinate system (r,θ). In order to differentiate (II-2.6) and (II-2.7) and apply the no-slip boundary conditions along the two walls, it is necessary to relate the spherical coordinates to the cylindrical coordinate system. Using figure II-1 the coordinate transformation is given by

$$r^2 = \rho^2 + z^2, \qquad \theta = \cos^{-1}\left(\frac{z}{\sqrt{\rho^2 + z^2}}\right) . \qquad \text{(II-2.8a,b)}$$

Using (II-2.2), (II-2.5) - (II-2.8), the properties of Gegenbauer and Legendre functions and the chain rule, the radial and axial velocity components of the flow field are obtained

$$v_\rho = -\frac{1}{\rho}\frac{\partial \psi}{\partial z} = \sum_{n=2}^{\infty}\left[B_n B_n'(\rho,z) + D_n D_n'(\rho,z)\right] + \int_0^\infty E(\alpha,z)\,\alpha\, J_1(\alpha,\rho)\,d\alpha, \qquad \text{(II-2.9a)}$$

$$v_z = \frac{1}{\rho}\frac{\partial \psi}{\partial \rho} = \sum_{n=2}^{\infty}\left[B_n B_n''(\rho,z) + D_n D_n''(\rho,z)\right] + \int_0^\infty F(\alpha,z)\,\alpha\, J_0(\alpha,\rho)\,d\alpha, \qquad \text{(II-2.9b)}$$

where

$$B_n'(\rho,z) = \frac{n+1}{(\rho^2+z^2)^{n/2}}\frac{1}{\rho} I_{n+1}\left(\frac{z}{\sqrt{\rho^2+z^2}}\right), \qquad \text{(II-2.10a)}$$

$$D_n'(\rho,z) = \frac{1}{(\rho^2+z^2)^{\frac{n-2}{2}}}\frac{1}{\rho} I_{n+1}\left(\frac{z}{\sqrt{\rho^2+z^2}}\right) - \frac{2}{(\rho^2+z^2)^{\frac{n-1}{2}}}\frac{z}{\rho} I_n\left(\frac{z}{\sqrt{\rho^2+z^2}}\right), \qquad \text{(II-2.10b)}$$

$$B_n''(\rho,z) = \frac{1}{(\rho^2+z^2)^{\frac{n+1}{2}}} P_n\left(\frac{z}{\sqrt{\rho^2+z^2}}\right), \qquad \text{(II-2.10c)}$$

$$D_n''(\rho,z) = \frac{2}{(\rho^2+z^2)^{\frac{n-1}{2}}} I_n\left(\frac{z}{\sqrt{\rho^2+z^2}}\right) + \frac{1}{(\rho^2+z^2)^{\frac{n-1}{2}}} P_n\left(\frac{z}{\sqrt{\rho^2+z^2}}\right), \qquad \text{(II-2.10d)}$$

$$E(\alpha,z) = -A(\alpha)e^{\alpha z} + B(\alpha)e^{-\alpha z} - C(\alpha)(1+\alpha z)e^{\alpha z} - D(\alpha)(1-\alpha z)e^{-\alpha z} \quad \text{(II-2.11a)}$$

$$F(\alpha,z) = A(\alpha)e^{\alpha z} + B(\alpha)e^{-\alpha z} + C(\alpha)\alpha z\, e^{\alpha z} + D(\alpha)\alpha z\, e^{-\alpha z} \quad \text{(II-2.11b)}$$

and P_n are Legendre functions of order n.

Application of the boundary conditions $v_\rho = v_z = 0$ along the two walls results in

$$\int_0^\infty E(\alpha,\xi)\alpha J_1(\alpha\rho)\,d\alpha = -\sum_{n=2}^{\infty}\left[B_n B_n'(\rho,\xi) + D_n D_n'(\rho,\xi)\right]$$

$$\int_0^\infty F(\alpha,\xi)\alpha J_0(\alpha\rho)\,d\alpha = -\sum_{n=2}^{\infty}\left[B_n B_n''(\rho,\xi) + D_n D_n''(\rho,\xi)\right]$$

$$\xi = -b,\ c \quad \text{(II-2.12)}$$

where each of the above integral relation is applied at $z = \xi$ where ξ has the values -b and c corresponding to each wall. The right hand sides of (II-2.12) represent the disturbances produced by the sphere and felt on the two planar boundaries. These disturbances are functions only of the radial coordinate ρ. Inspection of (II-2.12) shows that the unknown functions E and F evaluated at the two walls are simply Hankel transforms of these disturbances. These equations may be inverted to give

$$E(\alpha,\xi) = -\int_0^\infty t\sum_{n=2}^{\infty}\left[B_n B_n'(t,\xi) + D_n D_n'(t,\xi)\right]J_1(\alpha t)\,dt$$

$$F(\alpha,\xi) = -\int_0^\infty t\sum_{n=2}^{\infty}\left[B_n B_n''(t,\xi) + D_n D_n''(t,\xi)\right]J_0(\alpha t)\,dt$$

$$\xi = -b,\ c \quad \text{(II-2.13)}$$

The integrals required in (II-2.13) are performed analytically as follows. Using the polynomial representations of the Gegenbauer and Legendre functions together with the result given by Erdelyi (1954, vol. 2, p. 24)

$$\int_0^\infty \frac{x^{\nu+\frac{1}{2}}}{(x^2+a^2)^{\mu+1}} J_\nu(xy)(xy)^{1/2}\,dx = \frac{a^{\nu-\mu} y^{\mu+\frac{1}{2}} K_{\nu-\mu}(ay)}{2^\mu \Gamma(\mu+1)} \tag{II-2.14}$$

$$\text{Re } a>0,\ y>0,\ -1<\text{Re }\nu<2\,\text{Re}\,\mu+\tfrac{3}{2},$$

where K_ν is the modified Bessel function of the second kind, one may show by induction that

$$\int_0^\infty \frac{1}{(t^2+\xi^2)^{n/2}} I_{n+1}\left(\frac{\xi}{\sqrt{t^2+\xi^2}}\right) J_1(\alpha t)\,dt = \frac{1}{(n+1)!}\left(\frac{\alpha|\xi|}{\xi}\right)^{n-1} e^{-\alpha|\xi|} \tag{II-2.15a}$$

$$\int_0^\infty \frac{1}{(t^2+\xi^2)^{\frac{n-2}{2}}} I_{n+1}\left(\frac{\xi}{\sqrt{t^2+\xi^2}}\right) J_1(\alpha t)\,dt = \frac{1}{(n+1)!}\left(\frac{\alpha|\xi|}{\xi}\right)^{n-3}\left[(2n-1)\alpha|\xi| - n(n-2)\right] e^{-\alpha|\xi|} \tag{II-2.15b}$$

$$\int_0^\infty \frac{t}{(t^2+\xi^2)^{\frac{n+1}{2}}} P_n\left(\frac{\xi}{\sqrt{t^2+\xi^2}}\right) J_0(\alpha t)\,dt = \frac{\alpha^{n-1}}{n!}\left(\frac{|\xi|}{\xi}\right)^n e^{-\alpha|\xi|} \tag{II-2.15c}$$

$$\int_0^\infty \frac{t}{(t^2+\xi^2)^{\frac{n-1}{2}}} P_n\left(\frac{\xi}{\sqrt{t^2+\xi^2}}\right) J_0(\alpha t)\, dt$$

$$= \frac{\alpha^{n-3}}{n!}\left(\frac{|\xi|}{\xi}\right)^n \left[(2n-1)\alpha|\xi| - (n-1)^2\right] e^{-\alpha|\xi|} \qquad \text{(II-2.15d)}$$

$$\int_0^\infty \frac{t}{(t^2+\xi^2)^{\frac{n-1}{2}}} I_n\left(\frac{\xi}{\sqrt{t^2+\xi^2}}\right) J_0(\alpha t)\, dt$$

$$= \frac{\alpha^{n-3}}{n!}\left(\frac{|\xi|}{\xi}\right)^n \left[(n-1) - \alpha|\xi|\right] e^{-\alpha|\xi|} \qquad \text{(II-2.15e)}$$

Direct application of these results to (II-2.13) gives

$$E(\alpha,\xi) = \sum_{n=2}^{\infty}\left[B_n \mathcal{B}_n^*(\alpha,\xi) + D_n \mathcal{D}_n^*(\alpha,\xi)\right]$$

$$F(\alpha,\xi) = \sum_{n=2}^{\infty}\left[B_n \mathcal{B}_n^{**}(\alpha,\xi) + D_n \mathcal{D}_n^{**}(\alpha,\xi)\right]$$

$$\xi = -b,\ c \qquad \text{(II-2.16)}$$

where

$$\mathcal{B}_n^*(\alpha,\xi) = -\int_0^\infty t\, B_n'(t,\xi)\, J_1(\alpha t)\, dt$$

$$= -\frac{1}{n!}\left(\frac{\alpha|\xi|}{\xi}\right)^{n-1} e^{-\alpha|\xi|} \qquad \text{(II-2.17a)}$$

$$\mathcal{D}_n^*(\alpha,\xi) = -\int_0^\infty t\, D_n'(t,\xi)\, J_1(\alpha t)\, dt$$

$$= -\frac{1}{n!}\left(\frac{\alpha|\xi|}{\xi}\right)^{n-3}\left[(2n-3)\alpha|\xi| - n(n-2)\right] e^{-\alpha|\xi|}$$

(II-2.17b)

$$\mathcal{B}_n^{**}(\alpha,\xi) = -\int_0^\infty t\, B_n''(t,\xi)\, J_0(\alpha t)\, dt$$

$$= -\frac{\alpha^{n-1}}{n!}\left(\frac{|\xi|}{\xi}\right)^n e^{-\alpha|\xi|} \qquad \text{(II-2.17c)}$$

$$\mathcal{D}_n^{**}(\alpha,\xi) = -\int_0^\infty t\, D_n''(t,\xi)\, J_0(\alpha t)\, dt$$

$$= -\frac{\alpha^{n-3}}{n!}\left(\frac{|\xi|}{\xi}\right)^n \left[(2n-3)\alpha|\xi| - (n-1)(n-3)\right] e^{-\alpha|\xi|} \qquad \text{(II-2.17d)}$$

Equations (II-2.16) and (II-2.17) give the E and F functions evaluated at the two walls in terms of the as yet unknown spherical coefficients B_n and D_n. To obtain these functions at any value of z one must determine the unknown functions $A(\alpha)$, ..., $D(\alpha)$ in (II-2.11a,b). The expressions for $E(\alpha,\xi)$ and $F(\alpha,\xi)$ obtained from (II-2.16) are substituted into (II-2.11) whose right hand sides are evaluated at the two walls $z = -b, c$. This gives rise to four linear algebraic equations which may be solved simultaneously to yield the unknown functions $A(\alpha)$, ..., $D(\alpha)$. Once these functions are obtained, they are substituted back into (II-2.11a,b) to give the E and F functions at any value of z. After a considerable amount of algebraic manipulation the result is

$$E(\alpha,z) = G_3(\sigma,\eta)\,E(\alpha,-b) - G_3(\eta,\sigma)\,E(\alpha,c)$$
$$- G_1(\sigma,\eta)\,F(\alpha,-b) + G_1(\eta,\sigma)\,F(\alpha,c) \qquad \text{(II-2.18a)}$$

$$F(\alpha,z) = -G_2(\sigma,\eta)\,E(\alpha,-b) + G_2(\eta,\sigma)\,E(\alpha,c)$$
$$+ G_4(\sigma,\eta)\,F(\alpha,-b) - G_4(\eta,\sigma)\,F(\alpha,c) \qquad \text{(II-2.18b)}$$

where

$$G_{1,2}(\mu,\nu) = 4\tau\mu\nu\left[\frac{\sinh\mu}{\mu} \pm \frac{\sinh\tau}{\tau}\,\frac{\sinh\nu}{\nu}\right]\Big/\Delta \qquad \text{(II-2.19a)}$$

$$G_{3,4}(\mu,\nu) = 4\tau\left\{\nu\left[\cosh\mu - \frac{\sinh\tau}{\tau}\,\frac{\sinh\nu}{\nu}\right]\right.$$

$$\left. \pm\,\mu\left[\frac{\sinh\mu}{\mu} - \frac{\sinh\tau}{\tau}\cosh\nu\right]\right\}\Big/\Delta \qquad \text{(II-2.19b)}$$

The subscripts 1,3 and 2,4 refer to the plus and minus sign in the right hand sides of (II-2.19) respectively, μ and ν are dummy variables,

$$\Delta = 4\left[\sinh^2\tau - \tau^2\right], \qquad \text{(II-2.20)}$$

$$\sigma = \alpha(z+b), \quad \eta = \alpha(z-c) \qquad \text{(II-2.21a,b)}$$

and

$$\tau = \alpha(b+c). \qquad \text{(II-2.21c)}$$

The expressions for $E(\alpha,z)$ and $F(\alpha,z)$, still in terms of the unknown spherical coefficients B_n and D_n, are substituted into (II-2.9) to yield the local fluid velocity at any point in the flow. After some rearranging the result is

$$v_\rho = \sum_{n=2}^{\infty}\left\{B_n\left[B_n'(\rho,z) + \mathcal{B}_n'(\rho,z)\right]\right.$$

$$\left. + D_n\left[D_n'(\rho,z) + \mathcal{D}_n'(\rho,z)\right]\right\} \qquad \text{(II-2.22a)}$$

$$v_z = \sum_{n=2}^{\infty} \left\{ B_n \left[\mathcal{B}_n''(\rho,z) + \mathcal{B}_n''(\rho,z) \right] + D_n \left[\mathcal{D}_n''(\rho,z) + \mathcal{D}_n''(\rho,z) \right] \right\} \qquad \text{(II-2.22b)}$$

where

$$\begin{bmatrix} \mathcal{B}_n'(\rho,z) \\ \mathcal{D}_n'(\rho,z) \end{bmatrix} = \int_0^{\infty} \left\{ G_3(\sigma,\eta) \begin{bmatrix} \mathcal{B}_n^*(\alpha,-b) \\ \mathcal{D}_n^*(\alpha,-b) \end{bmatrix} - G_3(\eta,\sigma) \begin{bmatrix} \mathcal{B}_n^*(\alpha,c) \\ \mathcal{D}_n^*(\alpha,c) \end{bmatrix} - G_1(\sigma,\eta) \begin{bmatrix} \mathcal{B}_n^{**}(\alpha,-b) \\ \mathcal{D}_n^{**}(\alpha,-b) \end{bmatrix} + G_1(\eta,\sigma) \begin{bmatrix} \mathcal{B}_n^{**}(\alpha,c) \\ \mathcal{D}_n^{**}(\alpha,c) \end{bmatrix} \right\} \alpha J_1(\alpha\rho)\, d\alpha \qquad \text{(II-2.23a)}$$

$$\begin{bmatrix} \mathcal{B}_n''(\rho,z) \\ \mathcal{D}_n''(\rho,z) \end{bmatrix} = \int_0^{\infty} \left\{ -G_2(\sigma,\eta) \begin{bmatrix} \mathcal{B}_n^*(\alpha,-b) \\ \mathcal{D}_n^*(\alpha,-b) \end{bmatrix} + G_2(\eta,\sigma) \begin{bmatrix} \mathcal{B}_n^*(\alpha,c) \\ \mathcal{D}_n^*(\alpha,c) \end{bmatrix} + G_4(\sigma,\eta) \begin{bmatrix} \mathcal{B}_n^{**}(\alpha,-b) \\ \mathcal{D}_n^{**}(\alpha,-b) \end{bmatrix} - G_4(\eta,\sigma) \begin{bmatrix} \mathcal{B}_n^{**}(\alpha,c) \\ \mathcal{D}_n^{**}(\alpha,c) \end{bmatrix} \right\} \alpha J_0(\alpha\rho)\, d\alpha \qquad \text{(II-2.23b)}$$

The solution (II-2.22) satisfies the no-slip boundary conditions all along the two planar boundaries for each value of the index n for any values of the coefficients B_n and D_n. The integrals indicated by (II-2.23) must be performed numerically. In this regard, it should be noted

that the expressions for the G_i functions given by (II-2.19) - (II-2.21) are prone to large roundoff errors as $\alpha \to 0$ and should be computed by their Taylor series for small values of α. Moreover, for large values of α, equations (II-2.19) - (II-2.21) produce machine overflows and their asymptotic formulas should be used.

The boundary conditions to be satisfied on the surface of the sphere, r = a, are

$$v_\rho = 0 \qquad v_z = W \qquad \text{(II-2.24a,b)}$$

where W is the velocity with which the sphere is translating perpendicular to the walls. The collocation technique presented by Gluckman, Pfeffer & Weinbaum (1971) for applying boundary conditions on the sphere surface in axisymmetric flow is ideally suited for this purpose.

To satisfy the boundary conditions (II-2.24a,b) exactly on the surface of the sphere would require the solution of the entire infinite array of unknown coefficients B_n and D_n. The collocation technique satisfies the boundary conditions at a finite number of discrete points* on the sphere's generating arc and truncates the infinite series into a finite one. The two

* Each boundary point actually represents a ring on which the no-slip boundary conditions are satisfied due to the axisymmetric nature of the problem.

unknown coefficients in each term in (II-2.22) permit one to satisfy the exact no-slip boundary at one discrete point on the sphere. If the no-slip boundary conditions are to be satisfied at M points on the generating arc of the sphere, the infinite series in (II-2.22) are truncated after the Mth term. This results in a set of 2M simultaneous linear algebraic equations for the 2M B_n and D_n unknown coefficients of the truncated solution which may be solved by any standard matrix reduction technique. Once these constants are determined, the solution for the stream function (II-2.5) and the velocity field (II-2.9) is completely known.

The force exerted by the fluid on the sphere is shown in Happel and Brenner (1973, p. 115) to be

$$F = \mu\pi \int_0^{\pi} r^3 \sin^3\theta \frac{\partial}{\partial r}\left[\frac{D^2\psi}{r^2\sin^2\theta}\right] r\,d\theta \qquad \text{(II-2.25)}$$

Performing the above integration, using (II-2.5) - (II-2.7) and the orthogonality properties of the Gegenbauer functions results in the simple relation

$$F = 4\pi\mu D_2. \qquad \text{(II-2.26)}$$

The drag force on the sphere translating perpendicular to the two confining walls can alternately be expressed using the drag correction factor λ as

$$F = 6\pi\mu a W \lambda \qquad \text{(II-2.27)}$$

where λ represents the ratio of the force that the sphere experiences in the presence of the confining walls to the force it would experience moving with the same velocity through an unbounded quiescent fluid. Equating the two expressions for the drag force yields

$$\lambda = \frac{D_2}{1.5\, a\, W} \,. \qquad \text{(II-2.28)}$$

II-3. Solutions for the motion of a sphere perpendicular to a single plane wall

In this section, the accuracy and convergence characteristics of the collocation procedure applied to (II-2.22) will be determined by comparing solutions obtained by the present method to the exact solutions of Brenner (1961) for translation of a sphere perpendicular to a single plane wall. In order to make this comparison, the influence of the second wall may be removed from the more general two-wall solution given in the previous section by taking the limit as $c \to \infty$ in (II-2.17) and (II-2.19). The functions required in the solution (II-2.23) reduce to

$$G_{1,2}(\sigma, \eta \to -\infty) = \mp \sigma e^{-\sigma}, \quad G_{1,2}(\eta \to -\infty, \sigma) = 0 \qquad \text{(II-3.1a,b)}$$

$$G_{3,4}(\sigma, \eta \to -\infty) = (1 \mp \sigma) e^{-\sigma}, \quad G_{3,4}(\eta \to -\infty, \sigma) = 0 \qquad \text{(II-3.1c,d)}$$

$$\mathcal{B}_n^*(\alpha, c \to \infty) = \mathcal{D}_n^*(\alpha, c \to \infty) = 0 \qquad \text{(II-3.2a,b)}$$

$$\mathcal{B}_n^{**}(\alpha, c \to \infty) = \mathcal{D}_n^{**}(\alpha, c \to \infty) = 0. \qquad \text{(II-3.2c,d)}$$

There are several schemes which may be used to select the boundary points on the sphere on which the no-slip boundary conditions are exactly satisfied. Two such schemes will now be examined in detail.

The most accurate lowest order truncation solution for the viscous drag force is obtained by choosing the boundary point $\theta = \pi/2$. This point is the most advantageous since it controls the projected area of the sphere normal to its direction of motion and also satisfies the no-slip boundary conditions on the largest ring (θ = constant) around the sphere. Unfortunately, an examination of the system of linear algebraic equations for the B_n and D_n coefficients shows that when the $\theta = \pi/2$ point is used, the coefficient matrix (II-2.22) becomes singular. To overcome this difficulty, the point $\theta = \pi/2$ may be replaced by two closely adjacent points $\theta = \frac{\pi}{2} \pm \delta$. The optimum value of δ is found by obtaining solutions for a single wall at various sphere-to-wall spacings with the boundary conditions being satisfied exactly at only the two points $\theta = \frac{\pi}{2} \pm \delta$ (M = 2) for a sequence of diminishing values of δ. The largest value of δ for which convergence to a desired accuracy is obtained is then chosen. The results of these runs are presented in table II-1. The bipolar coordinate parameter α in Brenner (1961) is related to the sphere spacing via $\alpha = \cosh^{-1}(b/a)$. Examination of table II-1 shows that the drag correction factor λ converges to five significant digits for all spacings when $\delta \leq 0.01^{\circ}$. Consequently, δ was taken as 0.01° in the computations which follow. Additional points were selected as mirror-image pairs about the plane $\theta = \pi/2$ in order to preserve the

geometric symmetry of the boundary about this plane.

One scheme for spacing these additional points is to divide the half-arc of the sphere into equal segments (e.g. for M = 6 use $\theta = 30^{\circ}$, 60°, 89.99°, 90.01°, 120°, 150°). This scheme, which was used by Leichtberg, Pfeffer & Weinbaum (1976) for the problem of flow past a finite length chain of spheres at the centerline of a circular cylinder, favors the larger rings on which the no-slip boundary conditions are exactly satisfied by not specifying a boundary point at $\theta = 0$ or π. Using this collocation scheme, solutions for λ were obtained for various M and α and compared with the exact solutions of Brenner (1961). These results are presented in table II-2. The table shows that the collocation solutions converge monotonically to the exact solution to five significant figures at all spacings tested. Convergence is very rapid at the larger spacings but becomes slow when the sphere is located immediately adjacent to the wall.

Another possible scheme for spacing the boundary points would be to include a boundary point at $\theta = 0$ (and π). The role of this point should be of increasing importance as the gap between the sphere and the wall is made very small. Leichtberg, Weinbaum, Pfeffer & Gluckman (1976) used this collocation scheme to obtain solutions in the near collision limit for two adjacent spheres in a chain. Unfortunately, the coefficient

matrix (II-2.22) again becomes singular if the points $\theta = 0$ or π are used. To overcome this problem a new set of trial runs were made with $\theta = \delta, \frac{\pi}{2} \pm \delta, \pi - \delta$ (M = 4) for various values of δ. The results of these runs are shown in table II-3. Again, it was found that λ converges to five significant digits for all spacings tested when $\delta \leq 0.01^{\circ}$. Additional boundary points are chosen in pairs as before (e.g. for M = 6 use $\theta = 0.01^{\circ}, 45^{\circ}, 89.99^{\circ}, 90.01^{\circ}, 135^{\circ}, 179.99^{\circ}$). The results of this collocation scheme for various M are compared to the exact single wall solutions at various spacings in table II-4. Examination of table II-4 reveals oscillatory convergence of λ to the exact solution to five significant digits for all spacings tested. Comparison between tables II-2 and II-4 shows that convergence of the latter collocation scheme is as rapid or more rapid than the previous one at all spacings. Even at $\alpha = 0.5$ (b/a = 1.12) only fourteen points are required to obtain the drag to an accuracy of 0.005%. At larger spacings, convergence is even more rapid. Accuracy to four significant figures is achieved with only eight points at $\alpha = 1$ (b/a = 1.54) and four points at $\alpha = 2$ (b/a = 3.76).

In light of the above numerical tests, it appears that the second collocation scheme is the more efficient one and consequently will be used for the two-wall solutions to be presented in the next section.

II-4. Solutions for the motion of a sphere perpendicular to two plane parallel walls

In the previous section, solutions for the motion of a sphere perpendicular to a single plane wall were presented, tested for convergence and compared to exact published results. In this section, solutions will be presented for the motion of a sphere perpendicular to two plane parallel walls. To the best of the author's knowledge, the only solutions currently available for this problem are those obtained by the approximate method of reflections technique (Ho and Leal 1974).

A study will now be presented to determine how the rate of convergence is affected by the introduction of the second planar boundary. The spherical solution (II-2.6) is now required to cancel the disturbances simultaneously produced by the presence of both walls on the surface of the sphere. It is therefore expected that more terms in the series (II-2.6) will be required to accomplish this especially at close spacings where the disturbances are strongest. Table II-5 shows the rate of convergence as a function of sphere-to-wall spacing b/a and sphere position $s = b/(b + c)$. $s = 0$ corresponds to the single-wall solution while $s = 0.5$ corresponds to the sphere being located midway between the two walls. Each configuration is solved a number of times with increasing M until convergence is achieved to four significant figures.

The starting value of M for a given case in table II-5 is the minimum value of M in table II-4 which gives convergence to four significant figures. Examination of table II-5 shows that introduction of the second wall has a surprisingly small adverse effect on the rate of convergence. The slowest rate of convergence is found at s = 0.5, b/a = 1.1 where the second wall is closest to the sphere and only four additional points are required on the sphere to achieve four digit accuracy for λ. For b/a $\geq$ 2, no additional points are required.

Table II-6 examines the effect of the position of the second wall for various sphere-to-wall spacings b/a. The solutions for λ shown are converged to four significant figures. Examination of table II-6 shows a dramatic rise in the drag force on the sphere at very close spacings. For the purpose of comparison, the results for s = 0 and s = 0.5 are also plotted in figure II-2 together with the exact results of Brenner (1961) for a single wall (s = 0) and the approximate method of reflections results of Ho and Leal (1974) for two walls (s = 0.5). Also shown is the method of reflections result obtained by Lorentz (1907) for the motion of a sphere perpendicular to a single plane wall, i.e.

$$\lambda = 1 + \frac{9}{8}\frac{a}{b} \qquad \text{(II-4.1)}$$

Examination of figure II-2 shows agreement among all theories to be fairly good at large spacings with a discrepency of about 2% at a spacing b/a = 10. At closer spacings, the results of the present study are consistent with the exact results of Brenner (1961) for s = 0. Results for λ obtained by the method of reflections are found to be up to 40% below the converged collocation solutions at a spacing b/a = 2 and up to a full order of magnitude lower for b/a = 1.1.

For the sake of completeness, converged values of λ are presented in table II-7 for various wall-to-wall spacings d/a = (b+c)/a and sphere positions s.

The calculations for the results presented in this section were performed on an AMDAHL 470/V6 computer. The bulk of the computation time was used in the evaluation of the integrals (II-2.23). Actual running times for the solution of one problem were found to be $\frac{1}{2} M^2$ sec. at most spacings. At the largest sphere-to-wall spacings, computation times increased by about a factor of three due to the slower convergence of the integrals.

II-5. Formulation for the motion of a sphere parallel to to two plane walls

In this section, the formulation will be presented for the following basic asymmetric flow problems involving a sphere of arbitrary size and position between two plane parallel boundaries:

(a) Translation without rotation of the sphere parallel to two stationary walls.

(b) Rotation without any translation of the sphere.

(c) Shear flow past a rigidly held sphere induced by the motion of one of the boundaries.

(d) Poiseuille flow past a rigidly held sphere in a channel.

Solutions for any combination of these motions may be obtained by a simple superposition of solutions. The resulting motion of the sphere when it is not rigidly held in place may also be readily obtained from these basic solutions.

The geometry of the flow configuration is shown in figure II-3. A sphere of radius a moves parallel to the two confining walls with constant velocity U. The fluid motion far removed from the sphere is unidirectional and parallel to the walls. Bretherton (1962) has shown that for such a unidirectional flow, there is no lateral force acting on the sphere in the Stokes flow limit. The equations of motion for the fluid are:

$$\mu \nabla^2 \vec{V} = \nabla p \ , \quad \nabla \cdot \vec{V} = 0 . \qquad \text{(II-5.1a,b)}$$

For the geometry of the problem at hand, it is convenient to introduce rectangular (x,y,z) and spherical (r,θ,ϕ) coordinate systems whose origins coincide at the sphere center. The velocity field V is decomposed into three parts:

$$\vec{V} = \vec{V}_\infty + \vec{V}_s + \vec{V}_w \qquad \text{(II-5.2)}$$

$\vec{V}_\infty$ represents the unidirectional velocity profile between the two plates far removed from the sphere. This profile independently satisfies (II-5.1) and the no-slip boundary conditions on the walls. For poiseuille flow

$$\vec{V}_\infty = - \frac{4 V_c (z+b)(z-c)}{(b+c)^2} \hat{i} \qquad \text{(II-5.3a)}$$

where V_c is the centerline velocity. For the shear flow resulting when the wall at z = c is in motion

$$\vec{V}_\infty = S(z+b) \hat{i} \qquad \text{(II-5.3b)}$$

where S represents the velocity gradient which is constant.

$\vec{V}_s$ represents an infinite series containing all the simply separable solutions of (II-5.1) in spherical

coordinates which have planar symmetry about the plane $y = 0$ and vanish as $r \to \infty$. This solution was obtained by Lamb (1945) and has the form given by (I-2.12) and (I-2.13). For the problem at hand, in which translational motion of the sphere occurs only along the x-axis and rotation only about the y-axis, only terms containing $m = 1$ are required to describe the spherical disturbances. Thus the spherical solution reduces to

$$\vec{V}_s = u_s \hat{i} + v_s \hat{j} + w_s \hat{k} \qquad \text{(II-5.4)}$$

where

$$u_s = \sum_{n=1}^{\infty} \left[A_n A_n' + B_n B_n' + C_n C_n' \right] \qquad \text{(II-5.5a)}$$

$$v_s = \sum_{n=1}^{\infty} \left[A_n A_n'' + B_n B_n'' + C_n C_n'' \right] \qquad \text{(II-5.5b)}$$

$$w_s = \sum_{n=1}^{\infty} \left[A_n A_n''' + B_n B_n''' + C_n C_n''' \right] \qquad \text{(II-5.5c)}$$

and

$$A_n' = \frac{1}{2r^n}\left[2n(2n-1)\sin\theta\, P_n'(\xi)\cos^2\phi + (n-2)\, P_{n-1}^2(\xi)\cos 2\phi \right.$$

$$\left. - n(n+1)(n-2)\, P_{n-1}(\xi) \right] \qquad \text{(II-5.6a)}$$

$$B_n' = -\frac{1}{2r^{n+2}}\left[P_{n+1}^2(\xi)\cos 2\phi - n(n+1)\, P_{n+1}(\xi) \right] \qquad \text{(II-5.6b)}$$

$$C_n' = \frac{1}{2r^{n+1}}\left[P_n^2(\zeta)\cos 2\phi + n(n+1)P_n(\zeta)\right] \qquad \text{(II-5.6c)}$$

$$A_n'' = \frac{1}{r^n}\left[n(2n-1)\sin\theta\, P_n'(\zeta) + (n-2)P_{n-1}^2(\zeta)\right]\cos\phi\sin\phi \qquad \text{(II-5.6d)}$$

$$B_n'' = -\frac{1}{r^{n+2}}P_{n+1}^2(\zeta)\cos\phi\sin\phi \qquad \text{(II-5.6e)}$$

$$C_n'' = \frac{1}{r^{n+1}}P_n^2(\zeta)\cos\phi\sin\phi \qquad \text{(II-5.6f)}$$

$$A_n''' = \frac{1}{r^n}\left[n(2n-1)\zeta P_n'(\zeta) - (n+1)(n-2)P_{n-1}'(\zeta)\right]\cos\phi \qquad \text{(II-5.6g)}$$

$$B_n''' = -\frac{1}{r^{n+2}}n P_{n+1}'(\zeta)\cos\phi \qquad \text{(II-5.6h)}$$

$$C_n''' = -\frac{1}{r^{n+1}}P_n'(\zeta)\cos\phi \qquad \text{(II-5.6i)}$$

Here P_n^m is the associated Legendre function of order n and degree m and $\zeta = \cos\theta$. A_n, B_n and C_n are unknown constants which will be determined by satisfying the no-slip boundary conditions on the surface of the sphere in the presence of the confining walls.

$\vec{V}_w$ represents a double integral of all separable solutions of (II-5.1) which produce finite velocities everywhere in the flow field in terms of rectangular

coordinates and is given by the double Fourier integral

$$\vec{V}_w = u_w \hat{i} + v_w \hat{j} + w_w \hat{k} \qquad \text{(II-5.7)}$$

where

$$u_w = \int_0^\infty \int_0^\infty D_1(\alpha,\beta,z) \cos\alpha x \cos\beta y \, d\alpha \, d\beta \qquad \text{(II-5.8a)}$$

$$v_w = \int_0^\infty \int_0^\infty D_2(\alpha,\beta,z) \sin\alpha x \sin\beta y \, d\alpha \, d\beta \qquad \text{(II-5.8b)}$$

$$w_w = \int_0^\infty \int_0^\infty D_3(\alpha,\beta,z) \sin\alpha x \cos\beta y \, d\alpha \, d\beta \qquad \text{(II-5.8c)}$$

$$D_1(\alpha,\beta,z) = \left[A^*\left(1+\frac{\alpha^2}{\kappa}z\right) - A^{**}\frac{\alpha\beta}{\kappa}z - A^{***}\alpha z\right] e^{\kappa z} + \left[B^*\left(1-\frac{\alpha^2}{\kappa}z\right) + B^{**}\frac{\alpha\beta}{\kappa}z - B^{***}\alpha z\right] e^{-\kappa z} \qquad \text{(II-5.9a)}$$

$$D_2(\alpha,\beta,z) = \left[-A^*\frac{\alpha\beta}{\kappa}z + A^{**}\left(1+\frac{\beta^2}{\kappa}z\right) + A^{***}\beta z\right] e^{\kappa z} + \left[B^*\frac{\alpha\beta}{\kappa}z + B^{**}\left(1-\frac{\beta^2}{\kappa}z\right) + B^{***}\beta z\right] e^{-\kappa z} \qquad \text{(II-5.9b)}$$

$$D_3(\alpha,\beta,z) = \left[A^*\alpha z - A^{**}\beta z + A^{***}(1-\kappa z)\right] e^{\kappa z} + \left[B^*\alpha z - B^{**}\beta z + B^{***}(1+\kappa z)\right] e^{-\kappa z} \qquad \text{(II-5.9c)}$$

and $k^2 = \alpha^2 + \beta^2$. Here, the starred A and B coefficients are unknown functions of separation variables α and β. By proper choice of these functions, $\vec{V}_w$ is capable of exactly cancelling the disturbances produced by the sphere along the two planar boundaries.

Equation (II-5.2) is written in mixed coordinates, the spherical coordinate system (r,θ,ϕ) and rectangular system (x,y,z). In order to apply the no-slip conditions along the two walls, it is necessary to relate the spherical coordinates to the rectangular system. The coordinate transformation is (see figure II-3)

$$r^2 = x^2 + y^2 + z^2 \qquad \text{(II-5.10a)}$$

$$\cos\theta = \frac{z}{(x^2+y^2+z^2)^{1/2}} \qquad \text{(II-5.10b)}$$

$$\tan\phi = \frac{y}{x} \qquad \text{(II-5.10c)}$$

In terms of rectangular coordinates, the primed spherical coefficients given by (II-5.6) are

$$A_n' = n(2n-1)\frac{x^2}{(x^2+y^2+z^2)^{\frac{n+1}{2}}}\frac{P_n'\left(\frac{z}{(x^2+y^2+z^2)^{1/2}}\right)}{(x^2+y^2)^{1/2}}$$
$$+\frac{1}{2}(n-2)\frac{x^2-y^2}{(x^2+y^2+z^2)^{n/2}}\frac{P_{n-1}^2\left(\frac{z}{(x^2+y^2+z^2)^{1/2}}\right)}{(x^2+y^2)}$$
$$-\frac{1}{2}n(n+1)(n-2)\frac{1}{(x^2+y^2+z^2)^{n/2}}P_{n-1}\left(\frac{z}{(x^2+y^2+z^2)^{1/2}}\right) \qquad \text{(II-5.11a)}$$

$$B_n' = -\frac{1}{2}\frac{x^2-y^2}{(x^2+y^2+z^2)^{\frac{n+2}{2}}}\frac{P_{n+1}^2\left(\frac{z}{(x^2+y^2+z^2)^{1/2}}\right)}{(x^2+y^2)}$$

$$+\frac{1}{2}n(n+1)\frac{1}{(x^2+y^2+z^2)^{\frac{n+2}{2}}}P_{n+1}\left(\frac{z}{(x^2+y^2+z^2)^{1/2}}\right) \qquad \text{(II-5.1}$$

$$C_n' = \frac{1}{2}\frac{x^2-y^2}{(x^2+y^2+z^2)^{\frac{n+1}{2}}}\frac{P_n^2\left(\frac{z}{(x^2+y^2+z^2)^{1/2}}\right)}{(x^2+y^2)}$$

$$+\frac{1}{2}n(n+1)\frac{1}{(x^2+y^2+z^2)^{\frac{n+1}{2}}}P_n\left(\frac{z}{(x^2+y^2+z^2)^{1/2}}\right) \qquad \text{(II-5.1}$$

$$A_n'' = n(2n-1)\frac{xy}{(x^2+y^2+z^2)^{\frac{n+1}{2}}}\frac{P_n'\left(\frac{z}{(x^2+y^2+z^2)^{1/2}}\right)}{(x^2+y^2)^{1/2}}$$

$$+(n-2)\frac{xy}{(x^2+y^2+z^2)^{n/2}}\frac{P_{n-1}^2\left(\frac{z}{(x^2+y^2+z^2)^{1/2}}\right)}{(x^2+y^2)} \qquad \text{(II-5.11}$$

$$B_n'' = -\frac{xy}{(x^2+y^2+z^2)^{\frac{n+2}{2}}}\frac{P_{n+1}^2\left(\frac{z}{(x^2+y^2+z^2)^{1/2}}\right)}{(x^2+y^2)} \qquad \text{(II-5.11}$$

$$C_n'' = \frac{xy}{(x^2+y^2+z^2)^{\frac{n+1}{2}}}\frac{P_n^2\left(\frac{z}{(x^2+y^2+z^2)^{1/2}}\right)}{(x^2+y^2)} \qquad \text{(II-5.11}$$

$$A_n''' = n(2n-1)\frac{xz}{(x^2+y^2+z^2)^{\frac{n+1}{2}}}\frac{P_n'\left(\frac{z}{(x^2+y^2+z^2)^{1/2}}\right)}{(x^2+y^2)^{1/2}}$$

$$-(n+1)(n-2)\frac{x}{(x^2+y^2+z^2)^{n/2}}\frac{P_{n-1}'\left(\frac{z}{(x^2+y^2+z^2)^{1/2}}\right)}{(x^2+y^2)^{1/2}} \qquad \text{(II-5.11}$$

$$B_n''' = -n \frac{x}{(x^2+y^2+z^2)^{\frac{n+2}{2}}} \frac{P_{n+1}'\left(\frac{z}{(x^2+y^2+z^2)^{1/2}}\right)}{(x^2+y^2)^{1/2}} \qquad \text{(II-5.11h)}$$

$$C_n''' = -\frac{x}{(x^2+y^2+z^2)^{\frac{n+1}{2}}} \frac{P_n'\left(\frac{z}{(x^2+y^2+z^2)^{1/2}}\right)}{(x^2+y^2)^{1/2}} \qquad \text{(II-5.11i)}$$

Application of the three boundary conditions $u = V_\infty$, $v = 0$ and $w = 0$ along the two walls yields

$$\int_0^\infty \int_0^\infty D_1(\alpha,\beta,\xi) \cos\alpha x \cos\beta y \, d\alpha \, d\beta = -\sum_{n=1}^{\infty} \left[A_n A_n'(x,y,\xi) + B_n B_n'(x,y,\xi) + C_n C_n'(x,y,\xi)\right]$$

$$\int_0^\infty \int_0^\infty D_2(\alpha,\beta,\xi) \sin\alpha x \sin\beta y \, d\alpha \, d\beta = -\sum_{n=1}^{\infty} \left[A_n A_n''(x,y,\xi) + B_n B_n''(x,y,\xi) + C_n C_n''(x,y,\xi)\right]$$

$$\int_0^\infty \int_0^\infty D_3(\alpha,\beta,\xi) \sin\alpha x \cos\beta y \, d\alpha \, d\beta = -\sum_{n=1}^{\infty} \left[A_n A_n'''(x,y,\xi) + B_n B_n'''(x,y,\xi) + C_n C_n'''(x,y,\xi)\right]$$

$$\xi = -b, \; c \qquad \text{(II-5.12)}$$

where ξ is the value of z at the two walls $z = -b, c$. The right hand sides of (II-5.12) represent the spherical disturbances as felt by the two planar boundaries. Equations (II-5.12) reveal that the unknown D_i functions

evaluated at the two walls are simply double Fourier transforms of these disturbances. These equations may be inverted to give

$$D_1(\alpha,\beta,\xi) = -\frac{4}{\pi^2}\int_0^\infty\int_0^\infty \left\{\sum_{n=1}^{\infty}\left[A_n A_n'(s,t,\xi) + B_n B_n'(s,t,\xi) + C_n C_n'(s,t,\xi)\right]\right\}\cos\alpha s\,\cos\beta t\,ds\,dt$$

$$D_2(\alpha,\beta,\xi) = -\frac{4}{\pi^2}\int_0^\infty\int_0^\infty \left\{\sum_{n=1}^{\infty}\left[A_n A_n''(s,t,\xi) + B_n B_n''(s,t,\xi) + C_n C_n''(s,t,\xi)\right]\right\}\sin\alpha s\,\sin\beta t\,ds\,dt$$

$$D_3(\alpha,\beta,\xi) = -\frac{4}{\pi^2}\int_0^\infty\int_0^\infty \left\{\sum_{n=1}^{\infty}\left[A_n A_n'''(s,t,\xi) + B_n B_n'''(s,t,\xi) + C_n C_n'''(s,t,\xi)\right]\right\}\sin\alpha s\,\cos\beta t\,ds\,dt$$

$$\xi = -b,\ c \qquad \text{(II-5.13)}$$

Analytic evaluation of the double integrals required in (II-5.13) for arbitrary n is based on expressing the associated Legendre function by its polynomial representation

$$P_n^m(\zeta) = \frac{(1-\zeta^2)^{m/2}}{2^n}\sum_{q=0}^{[\frac{n}{2}]}\frac{(-1)^q(2n-2q)!\,\zeta^{n-2q-m}}{q!\,(n-q)!\,(n-2q-m)!} \qquad \text{(II-5.14)}$$

Here the square bracket [x] represents the largest whole

integer which is less than or equal to x. Once this substitution is made, the first integration may be performed using the integral representations of the modified Bessel functions of the second kind. These representations are found in Erdelyi (1954). The second integration, now involving Fourier transforms of modified Bessel functions of the second kind may also be performed using results given in the above reference. The required results of these integrations are given below.

$$F_1(\alpha,\beta,\xi,n,m) = \int_0^\infty\int_0^\infty \frac{1}{(s^2+t^2+\xi^2)^{\frac{n+1}{2}}} \frac{P_n^m\left(\frac{\xi}{(s^2+t^2+\xi^2)^{1/2}}\right)}{(s^2+t^2)^{m/2}} \cos\alpha s \cos\beta t \, ds\,dt$$

$$= \frac{\pi}{2}|\xi| \sum_{q=0}^{[\frac{n}{2}]} S_{nmq}(\xi)(k|\xi|)^{n-q-\frac{1}{2}} K_{n-q-\frac{1}{2}}(k|\xi|) \qquad \text{(II-5.15a)}$$

$$F_2(\alpha,\beta,\xi,n,m) = \int_0^\infty\int_0^\infty \frac{s^2}{(s^2+t^2+\xi^2)^{\frac{n+1}{2}}} \frac{P_n^m\left(\frac{\xi}{(s^2+t^2+\xi^2)^{1/2}}\right)}{(s^2+t^2)^{m/2}} \cos\alpha s \cos\beta t \, ds\,dt$$

$$= \frac{\pi}{2}|\xi|^3 \sum_{q=0}^{[\frac{n}{2}]} S_{nmq}(\xi)(k|\xi|)^{n-q-\frac{3}{2}} \left[K_{n-q-\frac{3}{2}}(k|\xi|) - \alpha^2\xi^2 (k|\xi|)^{n-q-\frac{5}{2}} K_{n-q-\frac{5}{2}}(k|\xi|)\right] \qquad \text{(II-5.15b)}$$

$$F_3(\alpha,\beta,\xi,n,m) =$$

$$\int_0^\infty\int_0^\infty \frac{st}{(s^2+t^2+\xi^2)^{\frac{n+1}{2}}} \frac{P_n^m\left(\frac{\xi}{(s^2+t^2+\xi^2)^{1/2}}\right)}{(s^2+t^2)^{m/2}} \sin\alpha s \sin\beta t\, ds\, dt$$

$$= \frac{\pi}{2}\alpha\beta|\xi|^5 \sum_{q=0}^{\left[\frac{n}{2}\right]} S_{nmq}(\xi)(k|\xi|)^{n-q-\frac{5}{2}} K_{n-q-\frac{5}{2}}(k|\xi|) \qquad \text{(II-5.15c)}$$

$$F_4(\alpha,\beta,\xi,n,m) =$$

$$\int_0^\infty\int_0^\infty \frac{s}{(s^2+t^2+\xi^2)^{\frac{n+1}{2}}} P_n^m\left(\frac{\xi}{(s^2+t^2+\xi^2)^{m/2}}\right) \sin\alpha s \cos\beta t\, ds\, dt$$

$$= \frac{\pi}{2}\alpha|\xi|^3 \sum_{q=0}^{\left[\frac{n}{2}\right]} S_{nmq}(\xi)(k|\xi|)^{n-q-\frac{3}{2}} K_{n-q-\frac{3}{2}}(k|\xi|) \qquad \text{(II-5.15d)}$$

where

$$S_{nmq}(\xi) = \frac{\left(\frac{2}{\pi}\right)^{1/2}}{(-2)^q\, q!\, (n-2q-m)!\, \xi^{n+m}} \qquad \text{(II-5.16)}$$

and K_ν is the modified Bessel function of the second kind of order ν. Application of these results to (II-5.13) gives

$$D_1(\alpha,\beta,\xi) = \sum_{n=1}^{\infty}\left[A_n A_n^*(\alpha,\beta,\xi) + B_n B_n^*(\alpha,\beta,\xi) + C_n C_n^*(\alpha,\beta,\xi)\right]$$

$$D_2(\alpha,\beta,\xi) = \sum_{n=1}^{\infty}\left[A_n A_n^{**}(\alpha,\beta,\xi) + B_n B_n^{**}(\alpha,\beta,\xi) + C_n C_n^{**}(\alpha,\beta,\xi)\right]$$

$$D_3(\alpha,\beta,\xi) = \sum_{n=1}^{\infty}\left[A_n A_n^{***}(\alpha,\beta,\xi) + B_n B_n^{***}(\alpha,\beta,\xi) + C_n C_n^{***}(\alpha,\beta,\xi)\right]$$

$$\xi = -b,\ c \qquad \text{(II-5.17)}$$

where

$$A_n^*(\alpha,\beta,\xi) = -\frac{4}{\pi^2}\left\{n(2n-1)F_2(\alpha,\beta,\xi,n,1) + \frac{1}{2}(n-2)\right.$$
$$\times\left[F_2(\alpha,\beta,\xi,n-1,2) - F_2(\beta,\alpha,\xi,n-1,2)\right]$$
$$\left.-\frac{1}{2}n(n+1)(n-2)F_1(\alpha,\beta,\xi,n-1,0)\right] \qquad \text{(II-5.18a)}$$

$$B_n^*(\alpha,\beta,\xi) = -\frac{4}{\pi^2}\left\{-\frac{1}{2}\left[F_2(\alpha,\beta,\xi,n+1,2) - F_2(\beta,\alpha,\xi,n+1,2)\right]\right.$$
$$\left.+\frac{1}{2}n(n+1)F_1(\alpha,\beta,\xi,n+1,0)\right\} \qquad \text{(II-5.18b)}$$

$$C_n^*(\alpha,\beta,\xi) = -\frac{4}{\pi^2}\left\{\frac{1}{2}\left[F_2(\alpha,\beta,\xi,n,2) - F_2(\beta,\alpha,\xi,n,2)\right]\right.$$
$$\left.+\frac{1}{2}n(n+1)F_1(\alpha,\beta,\xi,n,0)\right\} \qquad \text{(II-5.18c)}$$

$$A_n^{**}(\alpha,\beta,\xi) = -\frac{4}{\pi^2}\left[n(2n-1)F_3(\alpha,\beta,\xi,n,1)\right.$$
$$\left.+(n-2)F_3(\alpha,\beta,\xi,n-1,2)\right] \qquad \text{(II-5.18d)}$$

$$B_n^{**}(\alpha,\beta,\xi) = \frac{4}{\pi^2}F_3(\alpha,\beta,\xi,n+1,2) \qquad \text{(II-5.18e)}$$

$$C_n^{**}(\alpha,\beta,\xi) = -\frac{4}{\pi^2}F_3(\alpha,\beta,\xi,n,2) \qquad \text{(II-5.18f)}$$

$$A_n^{***}(\alpha,\beta,\xi) = -\frac{4}{\pi^2}\left[n(2n-1)\,\xi\,F_4(\alpha,\beta,\xi,n,1) - (n+1)(n-2)\,F_4(\alpha,\beta,\xi,n-1,1)\right] \qquad \text{(II-5.18g)}$$

$$B_n^{***}(\alpha,\beta,\xi) = \frac{4}{\pi^2}\,n\,F_4(\alpha,\beta,\xi,n+1,1) \qquad \text{(II-5.18h)}$$

$$C_n^{***}(\alpha,\beta,\xi) = \frac{4}{\pi^2}\,F_4(\alpha,\beta,\xi,n,1) \qquad \text{(II-5.18i)}$$

Equations (II-5.17) and (II-5.18) give the D_i functions evaluated at the two walls in terms of the as yet unknown spherical coefficients A_n, B_n and C_n. These functions may be obtained for any value of z by applying (II-5.9) at the two walls z = -b,c. This procedure generates six linear algebraic equations which may be solved simultaneously to yield the six unknown functions A^*, A^{**}, A^{***}, B^*, B^{**} and B^{***} contained in (II-5.9). Once this is done, these functions are substituted back into (II-5.9) to give the D_i functions at any value of z. The process is very tedious but straightforward. The final results are

$$D_1(\alpha,\beta,z) = G_5(\eta)\,D_1(\alpha,\beta,-b) - G_5(\sigma)\,D_1(\alpha,\beta,c) + G_6(\sigma,\eta)\,\frac{\alpha}{K^2}\left[\alpha\,D_1(\alpha,\beta,-b) - \beta\,D_2(\alpha,\beta,-b)\right] - G_6(\eta,\sigma)\,\frac{\alpha}{K^2}\left[\alpha\,D_1(\alpha,\beta,c) - \beta\,D_2(\alpha,\beta,c)\right]$$

$$+G_1(\sigma,\eta)\,\frac{\alpha}{\kappa}\,D_3(\alpha,\beta,-b)$$

$$+G_1(\eta,\sigma)\,\frac{\alpha}{\kappa}\,D_3(\alpha,\beta,c) \qquad \text{(II-5.19a)}$$

$$D_2(\alpha,\beta,z) = -G_6(\sigma,\eta)\,\frac{\alpha\beta}{\kappa^2}\left[D_1(\alpha,\beta,-b)+\frac{\alpha}{\beta}\,D_2(\alpha,\beta,-b)\right]$$

$$+G_6(\eta,\sigma)\,\frac{\alpha\beta}{\kappa^2}\left[D_1(\alpha,\beta,c)+\frac{\alpha}{\beta}\,D_2(\alpha,\beta,c)\right]$$

$$+G_3(\sigma,\eta)\,D_2(\alpha,\beta,-b)-G_3(\eta,\sigma)\,D_2(\alpha,\beta,c)$$

$$-G_1(\sigma,\eta)\,\frac{\beta}{\kappa}\,D_3(\alpha,\beta,-b)$$

$$+G_1(\eta,\sigma)\,\frac{\beta}{\kappa}\,D_3(\alpha,\beta,c) \qquad \text{(II-5.19b)}$$

$$D_3(\alpha,\beta,z) = G_2(\sigma,\eta)\left[\frac{\alpha}{\kappa}\,D_1(\alpha,\beta,-b)-\frac{\beta}{\kappa}\,D_2(\alpha,\beta,-b)\right]$$

$$-G_2(\eta,\sigma)\left[\frac{\alpha}{\kappa}\,D_1(\alpha,\beta,c)-\frac{\beta}{\kappa}\,D_2(\alpha,\beta,c)\right]$$

$$+G_4(\sigma,\eta)\,D_3(\alpha,\beta,-b)$$

$$-G_4(\eta,\sigma)\,D_3(\alpha,\beta,c) \qquad \text{(II-5.19c)}$$

where

$$G_{1,2}(\mu,\nu) = 4\tau\mu\nu\left[\frac{\sinh\mu}{\mu}\pm\frac{\sinh\tau}{\tau}\,\frac{\sinh\nu}{\nu}\right]\Big/\,\delta_2 \qquad \text{(II-5.20a)}$$

$$G_{3,4}(\mu,\nu) = 4\tau\mu\nu\left\{\nu\left[\cosh\mu-\frac{\sinh\tau}{\tau}\,\frac{\sinh\nu}{\nu}\right]\right.$$

$$\left.\pm\mu\left[\frac{\sinh\mu}{\mu}-\frac{\sinh\tau}{\tau}\cosh\nu\right]\right\}\Big/\,\delta_2 \qquad \text{(II-5.20b)}$$

$$G_5(\mu) = (-2\sinh\mu)/\Delta_1 \qquad \text{(II-5.20c)}$$

$$G_6(\mu,\nu) = 8\tau^2\left\{\mu\frac{\sinh\tau}{\tau}\left[\frac{\sinh\mu}{\mu} - \frac{\sinh\tau}{\tau}\cosh\nu\right] + \nu\left[\frac{\sinh\tau}{\tau}\cosh\mu - \frac{\sinh\nu}{\nu}\right]\right\}\Big/\Delta_1\Delta_2 \qquad \text{(II-5.20d)}$$

In the above equations, the subscripts 1,3 and 2,4 refer to the plus and minus signs on the right hand sides, μ and ν are dummy variables,

$$\Delta_1 = 2\sinh\tau, \quad \Delta_2 = 4\left[\sinh^2\tau - \tau^2\right] \qquad \text{(II-5.21a,b)}$$

$$\sigma = \kappa(z+b), \quad \eta = \kappa(z-c) \qquad \text{(II-5.22a,b)}$$

and

$$\tau = \kappa(b+c) \qquad \text{(II-5.22c)}$$

The expressions for the D_i functions, which are still in terms of the unknown spherical coefficients A_n, B_n and C_n are substituted into (II-5.8) to yield $\vec{V}_w$.

The double integrals required in (II-5.8) cannot be performed analytically. However, instead of carrying out the integration for $0 \le \alpha \le \infty$, $0 \le \beta \le \infty$ the substitution

$$\alpha = \kappa\cos\gamma \qquad \beta = \kappa\sin\gamma \qquad \text{(II-5.23a,b)}$$

transforms (II-5.8) into

$$u_w = \int_0^{\infty}\int_0^{\pi/2} k\, D_1(k,\gamma,z)\cos(kx\cos\gamma)\cos(ky\sin\gamma)\,d\gamma\,dk \qquad \text{(II-5.24a)}$$

$$v_w = \int_0^{\infty}\int_0^{\pi/2} k\, D_2(k,\gamma,z)\sin(kx\cos\gamma)\sin(ky\sin\gamma)\,d\gamma\,dk \qquad \text{(II-5.24b)}$$

$$w_w = \int_0^{\infty}\int_0^{\pi/2} k\, D_3(k,\gamma,z)\sin(kx\cos\gamma)\cos(ky\sin\gamma)\,d\gamma\,dk \qquad \text{(II-5.24c)}$$

where the D_i functions are now functions of k and γ. The advantage of this form is that the inner integration with respect to γ may be performed analytically using results for Fourier transforms found in Erdelyi (1954). The required formulas are summarized in the appendix. The outer integrals with respect to k must still be performed numerically.

After performing the integration with respect to γ and substituting (II-5.5) and (II-5.24) into (II-5.2), the following expressions for the local fluid velocity are obtained:

$$\vec{V} = u\,\hat{i} + v\,\hat{j} + w\,\hat{k} \qquad \text{(II-5.25)}$$

where

$$u = V_\infty + \sum_{n=1}^{\infty}\Big\{A_n\left[A_n'(x,y,z) + \bar{A}_n'(x,y,z)\right] + B_n\left[B_n'(x,y,z) + \bar{B}_n'(x,y,z)\right] + C_n\left[C_n'(x,y,z) + \bar{C}_n'(x,y,z)\right]\Big\} \qquad \text{(II-5.26a)}$$

$$v = \sum_{n=1}^{\infty} \left\{ A_n \left[A_n''(x,y,z) + \mathcal{A}_n''(x,y,z) \right] + B_n \left[B_n''(x,y,z) + \mathcal{B}_n''(x,y,z) \right] + C_n \left[C_n''(x,y,z) + \mathcal{C}_n''(x,y,z) \right] \right\} \qquad \text{(II-5.26b)}$$

$$w = \sum_{n=1}^{\infty} \left\{ A_n \left[A_n'''(x,y,z) + \mathcal{A}_n'''(x,y,z) \right] + B_n \left[B_n'''(x,y,z) + \mathcal{B}_n'''(x,y,z) \right] + C_n \left[C_n'''(x,y,z) + \mathcal{C}_n'''(x,y,z) \right] \right\} \qquad \text{(II-5.26c)}$$

Here the primed A_n, B_n and C_n functions are given by (II-5.11). The primed $\mathcal{A}_n$, $\mathcal{B}_n$ and $\mathcal{C}_n$ functions are given by

$$\mathcal{A}_n' = \int_0^{\infty} \left\{ G_5(\eta) H_1(-b) - G_5(\sigma) H_1(c) + G_6(\sigma,\eta) H_2(-b) - G_6(\eta,\sigma) H_2(c) + G_1(\sigma,\eta) H_3(-b) - G_1(\eta,\sigma) H_3(c) \right\} dk \qquad \text{(II-5.27a)}$$

$$\mathcal{B}_n' = \int_0^{\infty} \left\{ G_5(\eta) H_4(-b) - G_5(\sigma) H_4(c) + G_6(\sigma,\eta) H_5(-b) - G_6(\eta,\sigma) H_5(c) + G_1(\sigma,\eta) H_6(-b) - G_1(\eta,\sigma) H_6(c) \right\} dk \qquad \text{(II-5.27b)}$$

$$C_n' = \int_0^\infty \{ G_5(\eta) H_7(-b) - G_5(\sigma) H_7(c) + G_6(\sigma,\eta) H_8(-b) - G_6(\eta,\sigma) H_8(c) + G_1(\sigma,\eta) H_9(-b) - G_1(\eta,\sigma) H_9(c) \} dk \qquad \text{(II-5.27c)}$$

$$A_n'' = \int_0^\infty \{ G_6(\sigma,\eta) H_{10}(-b) - G_6(\eta,\sigma) H_{10}(c) + G_3(\sigma,\eta) H_{11}(-b) - G_3(\eta,\sigma) H_{11}(c) + G_1(\sigma,\eta) H_{12}(-b) - G_1(\eta,\sigma) H_{12}(c) \} dk \qquad \text{(II-5.27d)}$$

$$B_n'' = \int_0^\infty \{ G_6(\sigma,\eta) H_{13}(-b) - G_6(\eta,\sigma) H_{13}(c) + G_3(\sigma,\eta) H_{14}(-b) - G_3(\eta,\sigma) H_{14}(c) + G_1(\sigma,\eta) H_{15}(-b) - G_1(\eta,\sigma) H_{15}(c) \} dk \qquad \text{(II-5.27e)}$$

$$C_n'' = \int_0^\infty \{ G_6(\sigma,\eta) H_{16}(-b) - G_6(\eta,\sigma) H_{16}(c) + G_3(\sigma,\eta) H_{17}(-b) - G_3(\eta,\sigma) H_{17}(c) + G_1(\sigma,\eta) H_{18}(-b) - G_1(\eta,\sigma) H_{18}(c) \} dk \qquad \text{(II-5.27f)}$$

$$A_n''' = \int_0^\infty \{ G_2(\sigma,\eta) H_{19}(-b) - G_2(\eta,\sigma) H_{19}(c) + G_4(\sigma,\eta) H_{20}(-b) - G_4(\eta,\sigma) H_{20}(c) \} dk \qquad \text{(II-5.27g)}$$

$$B_n''' = \int_0^\infty \{ G_2(\sigma,\eta) H_{21}(-b) - G_2(\eta,\sigma) H_{21}(c) + G_4(\sigma,\eta) H_{22}(-b) - G_4(\eta,\sigma) H_{22}(c) \} dk \qquad \text{(II-5.27h)}$$

$$C_n''' = \int_0^\infty \{ G_2(\sigma,\eta) H_{23}(-b) - G_2(\eta,\sigma) H_{23}(c) + G_4(\sigma,\eta) H_{24}(-b) - G_4(\eta,\sigma) H_{24}(c) \} dk \qquad \text{(II-5.27i)}$$

where

$$H_1(\xi) = -n(2n-1)\xi^2 J_0(k\rho) B_{n,1,1,0}(\xi) + n(2n-1)\frac{\xi^2}{\rho^2} B_1 B_{n,1,2,1}(\xi) - \frac{1}{2}(n-2)(y^2-x^2) B_2 B_{n-1,2,2,3}(\xi) + \frac{1}{2} n(n+1)(n-2) J_0(k\rho) B_{n-1,0,0,1}(\xi) \qquad \text{(II-5.28a)}$$

$$H_2(\xi) = \left\{-n(2n-1)\xi^2 \left[B_{n,1,1,0}(\xi) - B_{n,1,2,1}(\xi)\right] + \frac{1}{2}(n-2)\xi^2 B_{n-1,2,2,1}(\xi) + \frac{1}{2} n(n+1)(n-2) B_{n-1,0,0,1}(\xi)\right\} \frac{B_1}{\rho^2} \qquad \text{(II-5.28b)}$$

$$H_3(\xi) = \left[-n(2n-1)\xi B_{n,1,1,0}(\xi) + (n+1)(n-2) B_{n-1,1,1,0}(\xi)\right] \frac{\xi^2 B_1}{\rho^2} \qquad \text{(II-5.28c)}$$

$$H_4(\xi) = \frac{1}{2}\left[(y^2-x^2) B_2 B_{n+1,2,2,3}(\xi) - n(n+1) J_0(k\rho) B_{n+1,0,0,1}(\xi)\right] \qquad \text{(II-5.28d)}$$

$$H_5(\xi) = -\frac{1}{2}\left[\xi^2 B_{n+1,2,2,1}(\xi) + n(n+1) B_{n+1,0,0,1}(\xi)\right] \frac{B_1}{\rho^2} \qquad \text{(II-5.28e)}$$

$$H_6(\xi) = n\frac{\xi^2}{\rho^2} B_1 B_{n+1,1,1,0}(\xi) \qquad \text{(II-5.28f)}$$

$$H_7(\xi) = -\frac{1}{2}\left[(y^2-x^2)\,B_2\,B_{n,2,2,3}(\xi) + n(n+1)\,J_0(k\rho)\;B_{n,0,0,1}(\xi)\right] \qquad \text{(II-5.28g)}$$

$$H_8(\xi) = \frac{1}{2}\left[\xi^2\,B_{n,2,2,1}(\xi) - n(n+1)B_{n,0,0,1}(\xi)\right]\frac{B_1}{\rho^2} \qquad \text{(II-5.28h)}$$

$$H_9(\xi) = \xi^2\,B_{n,1,1,0}(\xi)\,\frac{B_1}{\rho^2} \qquad \text{(II-5.28i)}$$

$$H_{10}(\xi) = xy\,B_2\left[-n(2n-1)\,B_{n,1,1,2}(\xi) - \frac{1}{2}(n-2)\,B_{n-1,2,2,3}(\xi) + \frac{1}{2\xi^2}\,n(n+1)(n-2)\,B_{n-1,0,0,3}(\xi)\right] \qquad \text{(II-5.28j)}$$

$$H_{11}(\xi) = xy\,B_2\left[n(2n-1)\,B_{n,1,2,3}(\xi) + (n-2)\;B_{n-1,2,2,3}(\xi)\right] \qquad \text{(II-5.28k)}$$

$$H_{12}(\xi) = xy\,B_2\left[n(2n-1)\,\xi\,B_{n,1,1,2}(\xi) + (n+1)(n-2)\;B_{n-1,1,1,2}(\xi)\right] \qquad \text{(II-5.28l)}$$

$$H_{13}(\xi) = \frac{1}{2}\,xy\,B_2\left[B_{n+1,2,2,3}(\xi) - n(n+1)\,\frac{1}{\xi^2}\,B_{n+1,0,0,3}(\xi)\right] \qquad \text{(II-5.28m)}$$

$$H_{14}(\xi) = -\,xy\,B_2\;B_{n+1,2,2,3}(\xi) \qquad \text{(II-5.28n)}$$

$$H_{15}(\xi) = n\,xy\,B_{n+1,1,1,2}(\xi) \qquad \text{(II-5.28o)}$$

$$H_{16}(\xi) = -\frac{1}{2}\,xy\,B_2\left[B_{n,2,2,3}(\xi) + n(n+1)\,\frac{1}{\xi^2}\,B_{n,0,0,3}(\xi)\right] \qquad \text{(II-5.28p)}$$

$$H_{17}(\xi) = xy\, B_2\, B_{n,2,2,3}(\xi) \qquad \text{(II-5.28q)}$$

$$H_{18}(\xi) = xy\, B_2\, B_{n,1,1,2}(\xi) \qquad \text{(II-5.28r)}$$

$$H_{19}(\xi) = -x\,\frac{J_1(k\rho)}{k\rho}\left\{ n(2n-1)\left[B_{n,1,1,2}(\xi) - B_{n,1,2,3}(\xi)\right] - \tfrac{1}{2}(n-2)\, B_{n-1,2,2,3}(\xi) - \tfrac{1}{2} n(n+1)(n-2) \times \frac{1}{\xi^2} B_{n-1,0,0,3}(\xi)\right\} \qquad \text{(II-5.28s)}$$

$$H_{20}(\xi) = -x\,\frac{J_1(k\rho)}{k\rho}\left[n(2n-1)\,\xi\, B_{n,1,1,2}(\xi) - (n+1)(n-2)\, B_{n-1,1,1,2}(\xi)\right] \qquad \text{(II-5.28t)}$$

$$H_{21}(\xi) = -\tfrac{1}{2} x\,\frac{J_1(k\rho)}{k\rho}\left[B_{n+1,2,2,3}(\xi) + n(n+1)\frac{1}{\xi^2} B_{n+1,0,0,3}(\xi)\right] \qquad \text{(II-5.28u)}$$

$$H_{22}(\xi) = n x\,\frac{J_1(k\rho)}{k\rho}\, B_{n+1,1,1,2}(\xi) \qquad \text{(II-5.28v)}$$

$$H_{23}(\xi) = \tfrac{1}{2} x\,\frac{J_1(k\rho)}{k\rho}\left[B_{n,2,2,3}(\xi) - n(n+1)\frac{1}{\xi^2} B_{n,0,0,3}(\xi)\right] \qquad \text{(II-5.28w)}$$

$$H_{24}(\xi) = x\,\frac{J_1(k\rho)}{k\rho}\, B_{n,1,1,2}(\xi) \qquad \text{(II-5.28x)}$$

$$B_1 = x^2 J_0(k\rho) + (y^2 - x^2) \frac{J_1(k\rho)}{k\rho} \qquad \text{(II-5.29a)}$$

$$B_2 = \frac{1}{k^2\rho^2}\left[J_0(k\rho) - 2 \frac{J_1(k\rho)}{k\rho} \right] \qquad \text{(II-5.29b)}$$

$$\rho = (x^2 + y^2)^{1/2} \qquad \text{(II-5.30)}$$

and

$$B_{n,m,i,j}(\xi) = \sum_{q=0}^{[\frac{n}{2}]} S_{nmq}(\xi) (k|\xi|)^{n-q+j-\frac{1}{2}} K_{n-q-i-\frac{1}{2}}(k|\xi|) \qquad \text{(II-5.31)}$$

where J_ν is the Bessel function of the first kind and K_ν is the modiefied Bessel function of the second kind.

The solution (II-5.25) satisfies the no-slip boundary conditions all along the two walls for each value of n for any value of the constant coefficients A_n, B_n and C_n. The integrals indicated by (II-5.27) must be performed numerically. All of the precautions noted for the numerical evaluation of the integrals in the axi-symmetric case (section II-2) must also be followed for the integrals in (II-5.27).

The boundary conditions remaining to be satisfied on the sphere surface, r = a, are

$$u = U, \qquad v = 0, \qquad w = 0 \qquad \text{(II-5.32a,b,c)}$$

where U is the velocity with which the sphere is translating parallel to the walls. The collocation technique

presented in part I of the thesis may now be used for this purpose. At r = a, boundary conditions (II-5.32) are applied at M points on the surface of the sphere and the series solution (II-5.26) is truncated after M terms. This generates a system of 3M linear algebraic equations for the 3M unknown coefficients A_n, B_n and C_n of the spherical solution. The solution for the velocity field is completely known once these coefficients are determined.

The hydrodynamic force and torque acting on the sphere are found from (I-2.9) to be

$$\vec{F} = -8\pi\mu A_1 \hat{i} \qquad \vec{T} = -8\pi\mu C_1 \hat{j} \qquad \text{(II-5.33a,b)}$$

Using the notation of Goldman, Cox & Brenner (1967) for the four problems outlined at the beginning of this section, the force and torque acting on the sphere are given by

$$\vec{F} = 6\pi\mu a U F_x^t \hat{i}, \qquad \vec{T} = 8\pi\mu a^2 U T_y^t \hat{j} \qquad \text{(II-5.34a,b)}$$

for a sphere translating with velocity U in the x-direction. For a sphere rotating with angular velocity Ω about the y-axis

$$\vec{F} = 6\pi\mu a^2 \Omega F_x^r \hat{i}, \qquad \vec{T} = 8\pi\mu a^3 \Omega T_y^r \hat{j}. \qquad \text{(II-5.35a,b)}$$

For shear flow past a rigidly held sphere induced by the steady motion of the boundary at z = c

$$\vec{F} = 6\pi\mu abSF_x^s \hat{i}, \qquad \vec{T} = 4\pi\mu a^3 S T_y^s \hat{j} \qquad \text{(II-5.36a,b)}$$

while for poiseuille flow past a rigidly held sphere between two stationary walls

$$\vec{F} = 6\pi\mu a V_c F_x^p \hat{i}, \qquad \vec{T} = 8\pi\mu a^2 V_c T_y^p \hat{j}. \qquad \text{(II-5.37a,b)}$$

The non-dimensional force and torque coefficients defined by (II-5.33) - (II-5.37) are found using (II-5.33), i.e.

$$F_x^t = -\frac{4}{3}\frac{A_1^t}{aU} \qquad T_y^t = -\frac{C_1^t}{a^2 U} \qquad \text{(II-5.38a,b)}$$

$$F_x^r = -\frac{4}{3}\frac{A_1^r}{a^2\Omega} \qquad T_y^r = -\frac{C_1^r}{a^3\Omega} \qquad \text{(II-5.39a,b)}$$

$$F_x^s = -\frac{4}{3}\frac{A_1^s}{abS} \qquad T_y^s = -\frac{2C_1^s}{a^3 S} \qquad \text{(II-5.40a,b)}$$

$$F_x^p = -\frac{4}{3}\frac{A_1^p}{aV_c} \qquad T_y^p = -\frac{C_1^p}{a^2 V_c} \qquad \text{(II-5.41a,b)}$$

where the A_1 and C_1 coefficients are determined from the collocation of (II-5.26) with the appropriate boundary conditions.

II-6. Solutions for the motion of a sphere parallel to a single plane wall

In this section, the accuracy and convergence characteristics of the collocation procedure applied to (II-5.26) will be tested by comparing solutions obtained by the present method to the exact results of Goldman, Cox & Brenner (1967a) for translation without rotation of a sphere parallel to a single plane wall and for rotation about an axis parallel to the wall without any translation. The collocation solutions will also be compared against the exact solutions of Goldman, Cox & Brenner (1967b) for shear flow past a rigidly held sphere in the presence of a single planar boundary.

For the purpose of making the comparison, the effect of the second wall may be removed from the more general two-wall solution presented in the previous section by taking the limit as $c \to \infty$ as was done in section II-3 for the axisymmetric flow case. Using (II-5.20) and (II-5.28), the functions required in (II-5.27) reduce to:

$$G_{1,2}(\sigma, \eta \to -\infty) = \mp \sigma e^{-\sigma}, \quad G_{1,2}(\eta \to -\infty, \sigma) = 0 \qquad \text{(II-6.1a,b)}$$

$$G_{3,4}(\sigma, \eta \to -\infty) = (1 \mp \sigma) e^{-\sigma}, \quad G_{3,4}(\eta \to -\infty, \sigma) = 0 \qquad \text{(II-6.1c,d)}$$

$$G_5(\eta \to -\infty) = e^{-\sigma}, \quad G_5(\sigma) = 0 \qquad \text{(II-6.1e,f)}$$

$$G_6(\sigma, \eta \to -\infty) = -\sigma e^{-\sigma}, \quad G_6(\eta \to -\infty, \sigma) = 0 \qquad \text{(II-6.1g,h)}$$

$$H_i(c \to \infty) = 0, \quad i = 1, 24 \qquad \text{(II-6.2)}$$

Careful examination of (II-5.26) shows that when the no-slip boundary conditions are applied on the surface of the sphere r = a, the solution of the coefficient matrix generated becomes independent of the ϕ coordinate of the boundary points. Thus, in contrast to the more general collocation procedure presented in part I in which the no-slip boundary conditions were satisfied at discrete points on the sphere surface, for the problem at hand, when the no-slip conditions are satisfied at the point r = a, θ = const., ϕ = const., the boundary conditions are actually satisfied on the ring r = a, θ = const., $0 \leq \phi \leq 2\pi$. Thus in selecting the boundary points, any value of ϕ may be used except $\phi = 0, \pi/2$ or π since the coefficient matrix becomes singular for these values. In effect, the collocation procedure to be applied to (II-5.26) is equivalent to that used for the axisymmetric case with the exception that there are three no-slip boundary conditions to be satisfied and three sets of unknown constants instead of two.

As in the axisymmetric case, the most advantageous point to choose is $\theta = \pi/2$ since this point has the greatest control of the projected area of the sphere normal to its direction of motion and also satisfies the

no-slip boundary conditions exactly on the largest ring around the sphere. Unfortunately, as in the axisymmetric case, the coefficient matrix becomes singular if this point is used. Convergence trials for the force and torque coefficients using two adjacent points $\theta = \frac{\pi}{2} \pm \delta$ as $\delta \to 0$ are shown in table II-8 for various spacings. Convergence for all six coefficients to five significant figures is obtained for $\delta \leq 0.01^{\circ}$ at all spacings. Additional points are selected as mirror-image pairs about the plane $\theta = \pi/2$.

In the first scheme used for spacing the additional boundary points, the semi-circular arc $r = a$, $0 \leq \theta \leq \pi$, ϕ = const. was divided into equal segments (e.g. for M = 6, $\theta = 30^{\circ}$, 60°, 89.99°, 90.01°, 120°, 150°). Solutions for the force and torque coefficients with increasing M at various spacings are compared with the exact results of Goldman, Cox & Brenner (1967a,b) in table II-9. Convergence of F_x^t, T_y^r, F_x^s and T_y^s is quickly achieved to four significant digits at all spacings tested and solutions obtained are in perfect agreement with exact values. Solutions for T_y^t and F_x^r are within 0.1% of the exact solutions at the closest spacing $\alpha = 0.5$ (b/a = 1.13) for M = 14. Unfortunately, the execution time required to obtain solutions for $M \geq 16$ (approximately 30 min. on an AMDAHL 470/V6 computer) was prohibitively long. The error in the last digit of the converged value of T_y^t for $\alpha = 3$ is believed to be due to roundoff error.

At this point it would be of interest to determine how placing a boundary point near the wall $\theta = 0, \pi$ would affect the rate of convergence especially at close spacings. The singularity of the coefficient matrix at $\theta = 0, \pi$ is avoided by using the points $\theta = \delta, \frac{\pi}{2} \pm \delta, \pi - \delta$ and taking the limit as $\delta \to 0$ until convergence is achieved to the desired number of digits. The results of these convergence tests are presented in table II-10. Again, convergence to five significant digits is achieved for all spacings for $\delta \leq 0.01^{\circ}$. With additional points equally spaced along the arc $0 < \theta < \pi$ on the sphere, (e.g. for M = 6, $\theta = 0.01^{\circ}$, 45°, 89.99°, 90.01°, 135°, 179.99°) the rate of convergence with increasing M is examined in table II-11. In contrast to the axisymmetric case, comparison of table II-11 with table II-9 shows very little improvement in the rate of convergence. Apparently, significant improvement in the rate of convergence occurs only in the head-on collision of two solid bodies and not when one boundary is sliding over another.

The collocation scheme used in table II-11 converges to the exact solution to four significant figures at all spacings for $M \leq 16$ except for the last digit in F_x^r for $\alpha = 0.5$. All six force and torque coefficients converge to four significant figures with $M \geq 10$ at $\alpha = 1.0$ (b/a = 1.54), $M \geq 8$ at $\alpha = 2.0$ (b/a = 3.76) and $M \geq 6$ at $\alpha = 3.0$ (b/a = 10.1). The converged value of T_y^t for

$\alpha = 3$ is the same as that obtained using the first collocation scheme.

In light of the above numerical results, the second collocation scheme in which boundary points are placed near $\theta = 0, \pi$ is slightly more efficient and will be used in the remainder of this study.

II-7. Solutions for the motion of a sphere parallel to two plane walls

In the previous section, collocation solutions were obtained for the force and torque acting on a sphere in the presence of a single wall and compared with exact results. In this section, collocation solutions involving two walls will be presented for the four problems outlined at the beginning of section II-5. To the best of the author's knowledge, the only solutions available for these two-wall problems were obtained by the approximate method of reflections technique.

A serious practical limitation in obtaining the asymmetric bounded flow solutions contained herein is the computation time required to generate the coefficient matrix (II-5.26). Computer running times for the two-wall asymmetric configurations were found to be roughly one order of magnitude higher than for the corresponding axisymmetric case. There are three reasons for the increase in computation time. First, due to the fact that there are three no-slip boundary conditions to be satisfied at each boundary point and three sets of unknown coefficients to be determined instead of two, the number of matrix elements (and the number of numerical integrations to be performed per run) increases from $4\ M^2$ to $9\ M^2$. Second, the expressions for the integrands in the asymmetric case (II-5.27) - (II-5.31) are considerably more involved than

the corresponding expressions (II-2.23) and (II-2.17) for the axisymmetric case. Finally, since some of the force and torque coefficients in the asymmetric case are small in magnitude, the numerical integrations must be carried out at a tighter tolerance in order to compute these coefficients accurately. In view of these considerations, an upper limit of twelve points was placed to keep execution times within reasonable limits. The degree of convergence of the M = 12 solutions was determined by comparing with the corresponding results for M = 14. All solutions to be presented in this section are believed to be converged to the number of significant figures shown.

It should be noted that since the primed coefficients in (II-5.26) depend only on the geometry and not on the boundary conditions satisfied on the sphere or V_∞, the force and torque coefficients (II-5.28) may be determined in a single computer run for a given geometry for all four of the problems outlined at the beginning of section I-5 with a negligible increase in the computation time which would be required for a single problem.

Table II-12 examines the effect of the position of the wall at z = c for various sphere-to-wall spacings b/a. s = 0 corresponds to the single-wall solutions while s = 0.5 corresponds to the sphere being located midway between the two walls. It is interesting to note that the F_x^r and T_y^t coefficients change sign indicating that

there is a second position other than midway between the two planes for which a sphere translating parallel to the walls will experience no torque or a sphere rotating about an axis parallel to the walls will experience no force.

A number of formulas for the various force and torque coefficients have been obtained by method of reflections techniques for special configurations involving a sphere between two plane parallel walls and are summarized in Happel & Brenner (1973, pp. 322-329). For the purpose of comparison, the relevant formulas will now be presented.

For s = 0.25 Faxen obtained the formulas

$$F_x^t = -\frac{1}{1 - 0.6526\left(\frac{a}{b}\right) + 0.1475\left(\frac{a}{b}\right)^3 - 0.131\left(\frac{a}{b}\right)^4 - 0.0644\left(\frac{a}{b}\right)^5 + 0\left(\frac{a}{b}\right)^6} \qquad \text{(II-7.1)}$$

$$T_y^t = \frac{0.025\left(\frac{a}{b}\right)^2}{1 - 0.6526\left(\frac{a}{b}\right)} \qquad \text{(II-7.2)}$$

while for s = 0.5 he obtained

$$F_x^t = -\frac{1}{1 - 1.004\left(\frac{a}{b}\right) + 0.418\left(\frac{a}{b}\right)^3 + 0.21\left(\frac{a}{b}\right)^4 - 0.169\left(\frac{a}{b}\right)^5} \qquad \text{(II-7.3)}$$

For s = 0.25 Wakiya obtained the formulas

$$F_x^s = \frac{1}{1 - 0.6526\left(\frac{a}{b}\right) + 0.4003\left(\frac{a}{b}\right)^3 - 0.297\left(\frac{a}{b}\right)^4} \qquad \text{(II-7.4)}$$

$$T_y^s = 1 + 0.0506\left(\frac{a}{b}\right) + 0.033\left(\frac{a}{b}\right)^2 \qquad \text{(II-7.5)}$$

$$F_x^P = \frac{\frac{3}{4}\left[1 - \frac{1}{9}\left(\frac{a}{b}\right)^2\right]}{1 - 0.6526\left(\frac{a}{b}\right) + 0.3160\left(\frac{a}{b}\right)^3 - 0.242\left(\frac{a}{b}\right)^4} \qquad \text{(II-7.6)}$$

$$T_y^P = \frac{1}{4}\frac{a}{b}\left[1 + 0.0758\left(\frac{a}{b}\right) + 0.049\left(\frac{a}{b}\right)^2\right] \qquad \text{(II-7.7)}$$

The results of these formulas are compared to the collocation solutions of the present study and the method of reflections results of Ho & Leal (1974) in table II-13. At large spacings, the results of Faxen and Wakiya are in close agreement with the collocation solutions. At closer spacings, the discrepency increases but agreement is still good except for a substantial error in the results for T_y^t. The results of Ho & Leal for F_x^t are consistently low at all spacings however their solution approaches the results of Faxen and the collocation solutions of the present study at larger spacings.

For reference, converged values of the force and torque coefficients are presented in table II-14 for various wall-to-wall spacings d/a and sphere positions s.

II-8. Arbitrary motion of a sphere between two plane parallel walls

In this section, solutions for the arbitrary quasi-steady planar motion of a sphere between two plane parallel walls in the presence of a unidirectional flow will be obtained by combining the solutions for motions parallel and perpendicular to the confining walls. Due to the linearity of the governing equations for Stokes flow, the total force and torque acting on the sphere is simply the vector sum of the individual contributions, i.e.

$$\vec{F} = 6\pi\mu a \left\{ \left[U F_x^t + a\Omega F_x^r + V_c F_x^P + b S F_x^s \right] \hat{i} + W \hat{k} \right\} \qquad \text{(II-8.1)}$$

$$\vec{T} = 8\pi\mu a^2 \left[U T_y^t + a\Omega T_y^r + V_c T_y^P + \tfrac{1}{2} a S T_y^s \right] \hat{j} \qquad \text{(II-8.2)}$$

Here V_c represents the centerline velocity far from the sphere in the absence of the shear flow and $S = V_w/(b+c)$ where V_w is the velocity of the wall at $z = c$. Values of the force and torque coefficients at various wall spacings and particle positions may be obtained from tables II-6, II-7, II-12 and II-14. Some special cases of these equations will now be examined.

For a sphere settling freely under gravity in a quiescent fluid bounded by two stationary plane walls which are inclined at an angle β (see figure II-4) a force and torque balance yields

$$\frac{4}{3}\pi a^3 (\rho_s - \rho) g \left[\sin\beta\, \hat{i} + \cos\beta\, \hat{k} \right]$$

$$+ 6\pi\mu a \left\{ \left[U F_x^t + a\Omega F_x^r \right] \hat{i} + W\lambda \hat{k} \right\} = 0 \qquad \text{(II-8.3a)}$$

$$8\pi\mu a^2 \left[U T_y^t + a\Omega T_y^r \right] \hat{j} = 0 \qquad \text{(II-8.3b)}$$

Simultaneous solution of these equations for the translational and angular velocity yields

$$\frac{U}{U_t} = - \frac{T_y^r \sin\beta}{T_y^r F_x^t - F_x^r T_y^t} \qquad \text{(II-8.4a)}$$

$$\frac{W}{U_t} = - \frac{\cos\beta}{\lambda} \qquad \text{(II-8.4b)}$$

$$\frac{a\Omega}{U_t} = - \frac{T_y^t \sin\beta}{T_y^r F_x^t - F_x^r T_y^t} \qquad \text{(II-8.4c)}$$

where

$$U_t = \frac{2a^2}{9\mu} (\rho_s - \rho) g \qquad \text{(II-8.5)}$$

represents the terminal settling velocity of the sphere in an unbounded quiescent fluid.

A second case of special interest is that of a neutrally buoyant sphere being carried by two-dimensional poiseuille or simple shear flow between the two walls. The conditions of zero force and torque on the sphere require

$$U F_x^t + a\Omega F_x^r + V_c F_x^P + bS F_x^S = 0 \qquad \text{(II-8.6a)}$$

$$U T_y^t + a\Omega T_y^r + V_c T_y^P + \tfrac{1}{2} aS T_y^S = 0 \qquad \text{(II-8.6b)}$$

Simultaneous solution of these equations for pure shear flow ($V_c = 0$) yields

$$\frac{U}{bS} = \frac{\frac{1}{2}\left(\frac{a}{b}\right) F_x^r T_y^S - F_x^S T_y^r}{F_x^t T_y^r - F_x^r T_y^t} \qquad \text{(II-8.7a)}$$

$$\frac{\Omega}{\frac{1}{2}S} = \frac{2\left(\frac{b}{a}\right) F_x^S T_y^t - F_x^t T_y^S}{F_x^t T_y^r - F_x^r T_y^t} \qquad \text{(II-8.7b)}$$

while for pure two-dimensional poiseuille flow ($S = 0$)

$$\frac{U}{V_c} = \frac{F_x^r T_y^P - F_x^P T_y^r}{F_x^t T_y^r - F_x^r T_y^t} \qquad \text{(II-8.8a)}$$

$$\frac{a\Omega}{V_c} = \frac{F_x^P T_y^t - F_x^t T_y^P}{F_x^t T_y^r - F_x^r T_y^t} \qquad \text{(II-8.8b)}$$

Of particular interest is the slip velocity of a neutrally buoyant sphere

$$V_{slip} \equiv U - V_\infty \qquad \text{(II-8.9)}$$

For pure shear flow

$$\frac{V_{slip}}{bS} = \frac{\frac{1}{2}\left(\frac{a}{b}\right) F_x^r T_y^S - F_x^S T_y^r}{F_x^t T_y^r - F_x^r T_y^t} - 1 \qquad \text{(II-8.10)}$$

while for two-dimensional poiseuille flow

$$\frac{V_{slip}}{V_c} = \frac{F_x^r T_y^p - F_x^p T_y^r}{F_x^t T_y^r - F_x^r T_y^t} - 4s(1-s) \qquad \text{(II-8.11)}$$

where s appearing in (II-8.11) represents sphere position.

II-9. Concluding remarks

Part II of the thesis has demonstrated that the collocation technique presented in part I for quasi-steady unbounded multi-particle Stokes flows with planar symmetry may be extended to treat bounded flow problems with high accuracy. The success of the technique depends in large part on the ability to perform the integral transform of the disturbances felt on the confining boundaries analytically. Many of these definite integrals which are required for the more common coordinate systems may be found in the literature for Fourier and Hankel transforms. A serious limitation of the technique is the long computation time required for the evaluation of the inversion integrals for the non-axisymmetric case. Extreme care must be taken in writing the program to save repeatedly needed calculations in memory in order to keep execution time at a minimum. Since the bulk of the computation time is used in the numerical evaluation of the integrals, it is vitally important that the integrating subroutine be as efficient as possible.

In closing, it is the author's hope that the numerical solution technique presented in this study will be a valuable aid in the solution of many unsolved asymmetric bounded and unbounded Stokes flow problems.

Appendix

This appendix contains a summary of the formulas used in performing the inner set of integrals required by (II-5.23). These formulas were obtained using results and general formulas for Fourier transforms found in Erdelyi (1954).

In the formulas which follow, a and b are positive constants, $u = (a^2 + b^2)^{1/2}$ and J_0 and J_1 are Bessel functions of the first kind of order 0 and 1 respectively.

$$\int_0^{\pi/2} \cos(a\cos\gamma)\cos(b\sin\gamma)\,d\gamma = \frac{\pi}{2} J_0(u) \tag{A-1}$$

$$\int_0^{\pi/2} \cos^2\gamma \cos(a\cos\gamma)\cos(b\sin\gamma)\,d\gamma = \frac{\pi}{2u^2}\left[a^2 J_0(u) + \frac{b^2-a^2}{u} J_1(u)\right] \tag{A-2}$$

$$\int_0^{\infty} \cos^4\gamma \cos(a\cos\gamma)\cos(b\sin\gamma)\,d\gamma = \frac{\pi}{2u^6}\left[a^6 - 3a^4 + a^4b^2 + 18a^2b^2 - 3b^4\right] J_0(u) - \frac{\pi}{u^7}\left[a^6 - 3a^4 - 2a^4b^2 + 18a^2b^2 - 3a^2b^4 - 3b^4\right] \times J_1(u) \tag{A-3}$$

$$\int_0^{\pi/2} \sin^2\gamma \cos(a\cos\gamma)\cos(b\sin\gamma)\,d\gamma = \frac{\pi}{2u^2}\left[b^2 J_0(u) - \frac{b^2-a^2}{u} J_1(u)\right] \tag{A-4}$$

$$\int_0^{\pi/2} \sin^2\gamma \cos^2\gamma \cos(a\cos\gamma)\cos(b\sin\gamma)\,d\gamma$$
$$= \frac{\pi}{2u^6}\left[3a^4 + a^4b^2 - 18a^2b^2 + a^2b^4 + 3b^4\right] J_0(u)$$
$$+ \frac{\pi}{2u^7}\left[a^6 - 5a^4b^2 - 6a^4 + 36a^2b^2 - 6b^4 - 5b^4a^2 + b^6\right] J_1(u) \qquad \text{(A-5)}$$

$$\int_0^{\pi/2} \cos\gamma \sin\gamma \sin(a\cos\gamma)\sin(b\sin\gamma)\,d\gamma$$
$$= -\frac{\pi}{2}\frac{ab}{u^2}\left[J_0(u) - \frac{2}{u}J_1(u)\right] \qquad \text{(A-6)}$$

$$\int_0^{\pi/2} \cos^3\gamma \sin\gamma \sin(a\cos\gamma)\sin(b\sin\gamma)\,d\gamma$$
$$= \frac{\pi}{2}\frac{ab}{u^6}\left[\left(-a^4 + 12a^2 - a^2b^2 - 12b^2\right) J_0(u) + \left(5a^4 - 24a^2 + 2a^2b^2 + 24b^2 - 3b^4\right)\frac{J_1(u)}{u}\right] \qquad \text{(A-7)}$$

$$\int_0^{\pi/2} \sin^3\gamma \cos\gamma \sin(a\cos\gamma)\sin(b\sin\gamma)\,d\gamma$$
$$= \frac{\pi}{2}\frac{ab}{u^6}\left[\left(-b^4 + 12b^2 - a^2b^2 - 12a^2\right) J_0(u) + \left(5b^4 - 24b^2 + 2a^2b^2 + 24a^2 - 3a^4\right)\frac{J_1(u)}{u}\right] \qquad \text{(A-8)}$$

$$\int_0^{\pi/2} \cos\gamma \sin(a\cos\gamma)\cos(b\sin\gamma)\,d\gamma$$
$$= \frac{\pi}{2}\frac{a}{u}J_1(u) \qquad \text{(A-9)}$$

$$\int_0^{\pi/2} \cos^3\gamma \sin(a\cos\gamma)\cos(b\sin\gamma)\,d\gamma$$

$$= \frac{\pi}{2}\frac{a}{u^4}\left[(a^2-3b^2)J_0(u) + (a^4-2a^2+a^2b^2+6b^2)\frac{J_1(u)}{u}\right] \qquad \text{(A-10)}$$

$$\int_0^{\pi/2} \sin^2\gamma \cos\gamma \sin(a\cos\gamma)\cos(b\sin\gamma)\,d\gamma$$

$$= -\frac{\pi}{2}\frac{a}{u^4}\left[(a^2-3b^2)J_0(u) - (b^4-6b^2+a^2b^2+2a^2)\frac{J_1(u)}{u}\right] \qquad \text{(A-11)}$$

Table II-1. Drag correction factor for a sphere translating perpendicular to a single plane wall, M = 2. Convergence tests for optimum δ.

δ	$\alpha = 0.5$ $\frac{b}{a} = 1.13$	$\alpha = 1.0$ $\frac{b}{a} = 1.54$	$\alpha = 2.0$ $\frac{b}{a} = 3.76$	$\alpha = 3.0$ $\frac{b}{a} = 10.1$
10°	-3.5674	-2.5251	-1.4039	-1.1249
1°	-3.4885	-2.5000	-1.4030	-1.1249
0.1°	-3.4877	-2.4998	-1.4030	-1.1249
0.01°	-3.4877	-2.4997	-1.4030	-1.1249
0.001°	-3.4877	-2.4997	-1.4030	-1.1249

Table II-2. Convergence of λ for single wall at various sphere-to-wall spacings. Sphere translating perpendicular to wall.

	$\alpha = 0.5$	$\alpha = 1.0$	$\alpha = 1.5$	$\alpha = 2.0$	$\alpha = 2.5$	$\alpha = 3.0$
M	$\frac{b}{a} = 1.13$	$\frac{b}{a} = 1.54$	$\frac{b}{a} = 2.35$	$\frac{b}{a} = 3.76$	$\frac{b}{a} = 6.13$	$\frac{b}{a} = 10.1$
2	-3.4877	-2.4997	-1.7728	-1.4030	-1.2202	-1.1249
4	-6.3569	-2.9842	-1.8359	-1.4128	-1.2220	-1.1252
6	-7.8347	-3.0309	-1.8374	-1.4129	-1.2220	-1.1252
8	-8.6423	-3.0356	-1.8375	-1.4129		
10	-9.0189	-3.0360	-1.8375			
12	-9.1693	-3.0361				
14	-9.2237	-3.0361				
16	-9.2424					
18	-9.2486					
20	-9.2507					
22	-9.2514					
24	-9.2516					
26	-9.2517					
28	-9.2518					
30	-9.2518					
EXACT	-9.2518	-3.0361	-1.8375	-1.1429	-1.2220	-1.1252

Table II-3. Drag correction factor for a sphere translating perpendicular to a single plane wall, M = 4. Convergence tests for optimum δ.

δ	$\alpha = 0.5$ $\frac{b}{a} = 1.13$	$\alpha = 1.0$ $\frac{b}{a} = 1.54$	$\alpha = 2.0$ $\frac{b}{a} = 3.76$	$\alpha = 3.0$ $\frac{b}{a} = 10.1$
10°	-20.434	-3.1592	-1.4131	-1.1252
1°	-33.195	-3.1948	-1.4132	-1.1252
0.1°	-33.407	-3.1952	-1.4132	-1.1252
0.01°	-33.409	-3.1952	-1.4132	-1.1252
0.001°	-33.409	-3.1952	-1.4132	-1.1252

Table II-4. Convergence of λ for single wall at various sphere-to-wall spacings with boundary points placed near $\theta = 0, \pi$. Sphere translating perpendicular to wall.

M	$\alpha = 0.5$ $\frac{b}{a} = 1.13$	$\alpha = 1.0$ $\frac{b}{a} = 1.54$	$\alpha = 1.5$ $\frac{b}{a} = 2.35$	$\alpha = 2.0$ $\frac{b}{a} = 3.76$	$\alpha = 2.5$ $\frac{b}{a} = 6.13$	$\alpha = 3.0$ $\frac{b}{a} = 10.1$
4	-33.409	-3.1952	-1.8428	-1.4132	-1.2220	-1.1252
6	-14.902	-3.0399	-1.8374	-1.4129	-1.2220	-1.1252
8	-9.8323	-3.0360	-1.8375	-1.4129		
10	-9.3260	-3.0361	-1.8375			
12	-9.2603	-3.0361				
14	-9.2513					
16	-9.2511					
18	-9.2515					
20	-9.2517					
22	-9.2517					
24	-9.2518					
26	-9.2518					
EXACT	-9.2518	-3.0361	-1.8375	-1.4129	-1.2220	-1.1252

Table II-5. Convergence of two-wall solutions at various sphere positions s and sphere-to-wall spacings b/a.

b/a	M	s=0.1	s=0.2	s=0.25	s=0.3	s=0.4	s=0.5
1.1	16	-11.46	-11.50	-11.56	-11.69	-12.48	-21.00
	18	-11.46	-11.50	-11.56	-11.69	-12.48	-21.02
	20	-11.46	-11.50	-11.56	-11.69	-12.48	-21.03
	22	-11.46	-11.50	-11.56	-11.69	-12.48	-21.03
1.5	8	-3.206	-3.223	-3.253	-3.313	-3.619	-4.779
	10	-3.206	-3.223	-3.253	-3.313	-3.619	-4.780
	12	-3.206	-3.223	-3.253	-3.313	-3.619	-4.780
2.0	6	-2.126	-2.135	-2.151	-2.182	-2.335	-2.789
	8	-2.126	-2.135	-2.151	-2.182	-2.335	-2.789
5.0	4	-1.285	-1.287	-1.290	-1.296	-1.325	-1.397
	6	-1.285	-1.287	-1.290	-1.296	-1.325	-1.397

Table II-6. Drag correction factors for a sphere translating perpendicular to two plane parallel walls for various sphere-to-wall spacings b/a and particle positions s. (s = 0 corresponds to single-wall solution).

b/a	s=0	s=0.1	s=0.2	s=0.25	s=0.3	s=0.4	s=0.5
1.1	-11.46	-11.46	-11.50	-11.56	-11.69	-12.48	-21.03
1.25	-5.305	-5.306	-5.333	-5.379	-5.473	-5.988	-8.840
1.5	-3.205	-3.206	-3.223	-3.253	-3.313	-3.619	-4.780
2.0	-2.126	-2.126	-2.135	-2.151	-2.182	-2.335	-2.789
3.0	-1.569	-1.569	-1.573	-1.581	-1.595	-1.663	-1.840
4.0	-1.380	-1.380	-1.383	-1.387	-1.396	-1.437	-1.541
5.0	-1.285	-1.285	-1.287	-1.290	-1.296	-1.325	-1.397
6.0	-1.228	-1.228	-1.229	-1.232	-1.236	-1.259	-1.313
8.0	-1.163	-1.163	-1.163	-1.165	-1.168	-1.183	-1.219
10.0	-1.126	-1.126	-1.127	-1.128	-1.131	-1.142	-1.169

Table II-7. Drag correction factors for a sphere translating perpendicular to two plane parallel walls for various wall-to-wall spacings d/a and particle positions s.

d/a	s=0.1	s=0.2	s=0.25	s=0.3	s=0.4	s=0.5
3.0	-	-	-	-	-	-4.780
4.0	-	-	-	-6.527	-3.201	-2.789
5.0	-	-	-5.379	-3.313	-2.335	-2.149
6.0	-	-6.371	-3.253	-2.470	-1.953	-1.840
8.0	-	-2.864	-2.151	-1.849	-1.601	-1.541
10.0	-	-2.135	-1.772	-1.595	-1.437	-1.397
12.0	-6.342	-1.816	-1.581	-1.457	-1.343	-1.313
15.0	-3.206	-1.573	-1.422	-1.339	-1.259	-1.237
20.0	-2.126	-1.383	-1.290	-1.236	-1.183	-1.169

Table II-8. Force and torque coefficients for translation or rotation of a sphere parallel to a single plane wall or in the presence of a shear flow parallel to the wall, M = 2. Convergence tests for optimum λ.

	α = 0.5		α = 1.0		α = 2.0		α = 3.0	
λ	$\frac{b}{a}$ = 1.13		$\frac{b}{a}$ = 1.54		$\frac{b}{a}$ = 3.76		$\frac{b}{a}$ = 10.1	
	$\underline{F}_x^t$	$\underline{T}_y^t$	$\underline{F}_x^t$	$\underline{T}_y^t$	$\underline{F}_x^t$	$\underline{T}_y^t$	$\underline{F}_x^t$	$\underline{T}_y^t$
10^0	-1.7214	0.044701	-1.4716	0.011423	-1.1692	3.7911×10^{-4}	-1.0586	8.1918×10^{-6}
1^0	-1.7055	0.045281	-1.4651	0.011991	-1.1688	4.0466×10^{-4}	-1.0588	8.7167×10^{-6}
0.1^0	-1.7053	0.045286	-1.4651	0.011996	-1.1688	4.0491×10^{-4}	-1.0588	8.7220×10^{-6}
0.01^0	-1.7053	0.045287	-1.4651	0.011996	-1.1688	4.0492×10^{-4}	-1.0588	8.7220×10^{-6}
0.001^0	-1.7053	0.045287	-1.4651	0.011996	-1.1688	4.0492×10^{-4}	-1.0588	8.7220×10^{-6}
	$\underline{F}_x^r$	$\underline{T}_y^r$	$\underline{F}_x^r$	$\underline{T}_y^r$	$\underline{F}_x^r$	$\underline{T}_y^r$	$\underline{F}_x^r$	$\underline{T}_y^r$
10^0	0.19835	-1.2123	0.053319	-1.0802	1.4895×10^{-3}	-1.0057	2.9061×10^{-5}	-1.0003
1^0	0.20409	-1.2048	0.055851	-1.0785	1.5777×10^{-3}	-1.0057	3.0762×10^{-5}	-1.0003
0.1^0	0.20415	-1.2047	0.055876	-1.0785	1.5786×10^{-3}	-1.0057	3.0779×10^{-5}	-1.0003
0.01^0	0.20415	-1.2047	0.055876	-1.0785	1.5786×10^{-3}	-1.0057	3.0779×10^{-5}	-1.0003
0.001^0	0.20415	-1.2047	0.055877	-1.0785	1.5786×10^{-3}	-1.0057	3.0779×10^{-5}	-1.0003
	$\underline{F}_x^s$	$\underline{T}_y^s$	$\underline{F}_x^s$	$\underline{T}_y^s$	$\underline{F}_x^s$	$\underline{T}_y^s$	$\underline{F}_x^s$	$\underline{T}_y^s$
10^0	1.5649	0.98883	1.5208	0.97955	1.3953	0.98141	1.0585	0.99984
1^0	1.5142	0.97986	1.3919	0.98110	1.1628	0.99725	1.0585	0.99983
0.1^0	1.5141	0.97986	1.3918	0.98110	1.1628	0.99725	1.0585	0.99983
0.01^0	1.5141	0.97986	1.3918	0.98110	1.1628	0.99725	1.0585	0.99983
0.001^0	1.5141	0.97986	1.3918	0.98110	1.1628	0.99725	1.0585	0.99983

Table II-9a. Convergence of F_x^t for single wall at various sphere-to-wall spacings.

	α=0.5	α=1.0	α=1.5	α=2.0	α=3.0
M	$\frac{b}{a}$=1.13	$\frac{b}{a}$=1.54	$\frac{b}{a}$=2.35	$\frac{b}{a}$=3.76	$\frac{b}{a}$=10.1
2	-1.705	-1.465	-1.285	-1.169	-1.059
4	-2.031	-1.560	-1.307	-1.174	-1.059
6	-2.121	-1.567	-1.308	-1.174	
8	-2.144	-1.567	-1.308		
10	-2.149				
12	-2.151				
14	-2.151				
EXACT	-2.151	-1.567	-1.308	-1.174	-1.059

Table II-9b. Convergence of T_y^t for single wall at various sphere-to-wall spacings.

	α=0.5	α=1.0	α=1.5	α=2.0	α=3.0
M	$\frac{b}{a}$=1.13	$\frac{b}{a}$=1.54	$\frac{b}{a}$=2.35	$\frac{b}{a}$=3.76	$\frac{b}{a}$=10.1
2	0.04529	0.01200	0.002402	0.0004049	8.722×10^{-6}
4	0.06357	0.01336	0.002554	0.0004165	8.761×10^{-6}
6	0.07073	0.01455	0.002641	0.0004216	8.775×10^{-6}
8	0.07235	0.01464	0.002642	0.0004216	8.775×10^{-6}
10	0.07315	0.01465	0.002642		
12	0.07352	0.01465			
14	0.07365				
EXACT	0.07372	0.01465	0.002642	0.0004216	8.774×10^{-6}

Table II-9c. Convergence of F_x^r for single wall at various sphere-to-wall spacings.

	α=0.5	α=1.0	α=1.5	α=2.0	α=3.0
M	$\frac{b}{a}$=1.13	$\frac{b}{a}$=1.54	$\frac{b}{a}$=2.35	$\frac{b}{a}$=3.76	$\frac{b}{a}$=10.1
2	0.2041	0.05588	0.01027	0.0001579	$3.078 \times 10^{-}$
4	0.1232	0.02229	0.003705	0.0005726	$1.173 \times 10^{-}$
6	0.1041	0.01978	0.003530	0.0005623	$1.170 \times 10^{-}$
8	0.09961	0.01956	0.003523	0.0005621	$1.170 \times 10^{-}$
10	0.09868	0.01954	0.003523	0.0005621	
12	0.09844				
14	0.09836				
EXACT	0.09829	0.01953	0.003523	0.0005621	$1.170 \times 10^{-}$

Table II-9d. Convergence of F_y^r for single wall at various sphere-to-wall spacings.

	α=0.5	α=1.0	α=1.5	α=2.0	α=3.0
M	$\frac{b}{a}$=1.13	$\frac{b}{a}$=1.54	$\frac{b}{a}$=2.35	$\frac{b}{a}$=3.76	$\frac{b}{a}$=10.1
2	-1.205	-1.079	-1.023	-1.006	-1.000
4	-1.346	-1.099	-1.025	-1.006	-1.000
6	-1.380	-1.100	-1.025		
8	-1.387	-1.100			
10	-1.388				
12	-1.388				
EXACT	-1.388	-1.100	-1.025	-1.006	-1.000

Table II-9e. Convergence of F_x^s for single wall at various sphere-to-wall spacings.

	α=0.5	α=1.0	α=1.5	α=2.0	α=3.0
M	$\frac{b}{a}$=1.13	$\frac{b}{a}$=1.54	$\frac{b}{a}$=2.35	$\frac{b}{a}$=3.76	$\frac{b}{a}$=10.1
2	1.514	1.392	1.262	1.163	1.059
4	1.614	1.438	1.278	1.167	1.059
6	1.616	1.439	1.278	1.167	
8	1.616	1.439			
EXACT	1.616	1.439	1.278	1.167	1.059

Table II-9f. Convergence of T_y^s for single wall at various sphere-to-wall spacings.

	α=0.5	α=1.0	α=1.5	α=2.0	α=3.0
M	$\frac{b}{a}$=1.13	$\frac{b}{a}$=1.54	$\frac{b}{a}$=2.35	$\frac{b}{a}$=3.76	$\frac{b}{a}$=10.1
2	0.9799	0.9811	0.9913	0.9972	0.9998
4	0.9548	0.9748	0.9903	0.9971	0.9998
6	0.9535	0.9742	0.9901	0.9971	
8	0.9537	0.9742	0.9901		
10	0.9537				
EXACT	0.9537	0.9742	0.9901	0.9971	0.9998

Table II-10. Force and torque coefficients for translation or rotation of a sphere parallel to a single plane wall or in the presence of a shear flow parallel to the wall, M = 4. Convergence tests for optimum δ.

	α = 0.5		α = 1.0		α = 2.0		α = 3.0	
δ	$\frac{b}{a}$ = 1.13		$\frac{b}{a}$ = 1.54		$\frac{b}{a}$ = 3.76		$\frac{b}{a}$ = 10.1	
	F_x^t	T_y^t	F_x^t	T_y^t	F_x^t	T_y^t	F_x^t	T_y^t
10°	-3.1125	-0.13301	-1.5911	1.2147×10^{-2}	-1.1739	4.1464×10^{-4}	-1.0591	8.7552×10^{-6}
1°	-4.0681	-0.37644	-1.5979	1.1188×10^{-2}	-1.1740	4.1180×10^{-4}	-1.0591	8.7472×10^{-6}
0.1°	-4.0841	-0.38062	-1.5980	1.1177×10^{-2}	-1.1740	4.1177×10^{-4}	-1.0591	8.7471×10^{-6}
0.01°	-4.0842	-0.38067	-1.5980	1.1177×10^{-2}	-1.1740	4.1177×10^{-4}	-1.0591	8.7471×10^{-6}
0.001°	-4.0842	-0.38067	-1.5980	1.1177×10^{-2}	-1.1740	4.1177×10^{-4}	-1.0591	8.7471×10^{-6}
	F_x^r	T_y^r	F_x^r	T_y^r	F_x^r	T_y^r	F_x^r	T_y^r
10°	-1.1104	-1.8281	5.2442×10^{-3}	-1.1057	5.2778×10^{-4}	-1.0059	1.1613×10^{-5}	-1.0003
1°	-2.5220	-2.2574	9.5982×10^{-4}	-1.1074	5.1811×10^{-4}	-1.0059	1.1589×10^{-5}	-1.0003
0.1°	-2.5463	-2.2646	9.1413×10^{-4}	-1.1074	5.1811×10^{-4}	-1.0059	1.1589×10^{-5}	-1.0003
0.01°	-2.5466	-2.2647	9.1368×10^{-4}	-1.1074	5.1811×10^{-4}	-1.0059	1.1589×10^{-5}	-1.0003
0.001°	-2.5466	-2.2647	9.1368×10^{-4}	-1.1074	5.1811×10^{-4}	-1.0059	1.1589×10^{-5}	-1.0003
	F_x^s	T_y^s	F_x^s	T_y^s	F_x^s	T_y^s	F_x^s	T_y^s
10°	1.6231	0.95360	1.4414	0.97322	1.1672	0.99713	1.0587	0.99983
1°	1.6317	0.95790	1.4420	0.97298	1.1672	0.99715	1.0587	0.99983
0.1°	1.6318	0.95799	1.4420	0.97298	1.1672	0.99715	1.0587	0.99983
0.01°	1.6319	0.95799	1.4420	0.97298	1.1672	0.99715	1.0587	0.99983
0.001°	1.6319	0.95799	1.4420	0.97298	1.1672	0.99715	1.0587	0.99983

Table II-11a. Convergence of F_x^t for single wall at various sphere-to-wall spacings.

	α=0.5	α=1.0	α=1.5	α=2.0	α=3.0
M	$\frac{b}{a}$=1.13	$\frac{b}{a}$=1.54	$\frac{b}{a}$=2.35	$\frac{b}{a}$=3.76	$\frac{b}{a}$=10.1
4	-4.084	-1.598	-1.310	-1.174	-1.059
6	-2.176	-1.567	-1.308	-1.174	-1.059
8	-2.140	-1.567	-1.308		
10	-2.148				
12	-2.151				
14	-2.151				
EXACT	-2.151	-1.567	-1.308	-1.174	-1.059

Table II-11b. Convergence of T_y^t for single wall at various sphere-to-wall spacings.

	α=0.5	α=1.0	α=1.5	α=2.0	α=3.0
M	$\frac{b}{a}$=1.13	$\frac{b}{a}$=1.54	$\frac{b}{a}$=2.35	$\frac{b}{a}$=3.76	$\frac{b}{a}$=10.1
4	-0.3807	0.01118	0.002478	0.0004118	8.747×10^{-6}
6	0.08567	0.01504	0.002651	0.0004218	8.775×10^{-6}
8	0.07882	0.01465	0.002642	0.0004216	8.775×10^{-6}
10	0.07518	0.01465	0.002642	0.0004216	
12	0.07398				
14	0.07375				
16	0.07372				
EXACT	0.07372	0.01465	0.002642	0.0004216	8.774×10^{-6}

Table II-11c. Convergence of F_x^r for single wall at various sphere-to-wall spacings.

	$\alpha=0.5$	$\alpha=1.0$	$\alpha=1.5$	$\alpha=2.0$	$\alpha=3.0$
M	$\frac{b}{a}=1.13$	$\frac{b}{a}=1.54$	$\frac{b}{a}=2.35$	$\frac{b}{a}=3.76$	$\frac{b}{a}=10.1$
4	-2.547	0.0009137	0.002677	0.0005181	1.159×10^{-5}
6	0.09606	0.02017	0.003536	0.0005624	1.170×10^{-5}
8	0.1116	0.01956	0.003523	0.0005621	1.170×10^{-5}
10	0.1017	0.01953	0.003523	0.0005621	
12	0.09893	0.01953			
14	0.09839				
16	0.09830				
EXACT	0.09829	0.01953	0.003523	0.0005621	1.170×10^{-5}

Table II-11d. Convergence of F_y^r for single wall at various sphere-to-wall spacings.

	$\alpha=0.5$	$\alpha=1.0$	$\alpha=1.5$	$\alpha=2.0$	$\alpha=3.0$
M	$\frac{b}{a}=1.13$	$\frac{b}{a}=1.54$	$\frac{b}{a}=2.35$	$\frac{b}{a}=3.76$	$\frac{b}{a}=10.1$
4	-2.265	-1.107	-1.025	-1.006	-1.000
6	-1.378	-1.099	-1.025	-1.006	-1.000
8	-1.381	-1.100			
10	-1.386	-1.100			
12	-1.387				
14	-1.388				
16	-1.388				
EXACT	-1.388	-1.100	-1.025	-1.006	-1.000

Table II-11e. Convergence of F_x^s for single wall at various sphere-to-wall spacings.

	$\alpha=0.5$	$\alpha=1.0$	$\alpha=1.5$	$\alpha=2.0$	$\alpha=3.0$
M	$\frac{b}{a}=1.13$	$\frac{b}{a}=1.54$	$\frac{b}{a}=2.35$	$\frac{b}{a}=3.76$	$\frac{b}{a}=10.1$
4	1.632	1.442	1.279	1.167	1.059
6	1.616	1.439	1.278	1.167	1.059
8	1.616	1.439	1.278		
EXACT	1.616	1.439	1.278	1.167	1.059

Table II-11f. Convergence of T_y^s for single wall at various sphere-to-wall spacings.

	$\alpha=0.5$	$\alpha=1.0$	$\alpha=1.5$	$\alpha=2.0$	$\alpha=3.0$
M	$\frac{b}{a}=1.13$	$\frac{b}{a}=1.54$	$\frac{b}{a}=2.35$	$\frac{b}{a}=3.76$	$\frac{b}{a}=10.1$
4	0.9580	0.9730	0.9903	0.9971	0.9998
6	0.9539	0.9743	0.9901	0.9971	0.9998
8	0.9535	0.9742	0.9901		
10	0.9537	0.9742			
12	0.9537				
EXACT	0.9537	0.9742	0.9901	0.9971	0.9998

Table II-12a. Force coefficient F_x^t for sphere translating parallel to two plane walls with no rotation at various sphere-to-wall spacings b/a and positions s.

b/a	s=0	s=0.1	s=0.2	s=0.25	s=0.3	s=0.4	s=0.5
1.1	-2.26	-2.28	-2.39	-2.48	-2.61	-2.99	-3.94
1.25	-1.859	-1.875	-1.957	-2.032	-2.133	-2.433	-3.019
1.5	-1.596	-1.607	-1.668	-1.723	-1.797	-2.011	-2.377
2.0	-1.383	-1.390	-1.429	-1.463	-1.510	-1.641	-1.846
3.0	-1.227	-1.231	-1.253	-1.272	-1.297	-1.367	-1.471
4.0	-1.162	-1.165	-1.179	-1.192	-1.210	-1.256	-1.324
8.0	-1.075	-1.077	-1.083	-1.089	-1.096	-1.115	-1.142

Table II-12b. Torque coefficient T_y^t for sphere translating parallel to two plane walls with no rotation at various sphere-to-wall spacings b/a and positions s.

b/a	s=0	s=0.1	s=0.2	s=0.25	s=0.3	s=0.4	s=0.5
1.1	0.089	0.085	0.069	0.058	0.049	0.040	0
1.25	0.03956	0.03626	0.02352	0.01564	0.00881	0.00387	0
1.5	0.01657	0.01439	0.00588	0.000594	-0.003964	-0.00653	0
2.0	0.005025	0.00387	-0.0006245	-0.003417	-0.005802	-0.006750	0
3.0	0.001020	0.000547	-0.001301	-0.002439	-0.003393	-0.003613	0
4.0	0.0003318	0.000077	-0.0009157	-0.001523	-0.002026	-0.002097	0
8.0	0.00002178	-0.000038	-0.0002679	-0.0004069	-0.0005196	-0.0005204	0

Table II-12c. Force coefficient F_x^r for sphere rotating about the y-axis with no translation at various sphere-to-wall spacings b/a and positions s.

b/a	s=0	s=0.1	s=0.2	s=0.25	s=0.3	s=0.4	s=0.5
1.1	0.12	0.11	0.092	0.079	0.066	0.054	0
1.25	0.0528	0.0483	0.0314	0.0209	0.0118	0.00516	0
1.5	0.02210	0.01918	0.00784	0.00079	-0.00529	-0.00871	0
2.0	0.006700	0.005165	-0.0008326	-0.004556	-0.007735	-0.009000	0
3.0	0.001360	0.0007295	-0.001734	-0.003251	-0.004524	-0.004818	0
4.0	0.0004424	0.0001028	-0.001221	-0.002031	-0.002701	-0.002797	0
8.0	0.00002904	-0.000050	-0.0003571	-0.0005426	-0.0006928	-0.0006939	0

Table II-12d. Torque coefficient T_y^r for sphere rotating about the y-axis with no translation at various sphere-to-wall spacings b/a and position s.

b/a	s=0	s=0.1	s=0.2	s=0.25	s=0.3	s=0.4	s=0.5
1.1	-1.46	-1.46	-1.46	-1.46	-1.47	-1.51	-1.85
1.25	-1.228	-1.229	-1.232	-1.234	-1.238	-1.262	-1.419
1.5	-1.110	-1.111	-1.113	-1.114	-1.116	-1.129	-1.198
2.0	-1.042	-1.042	-1.043	-1.043	-1.044	-1.049	-1.073
3.0	-1.012	-1.012	-1.012	-1.012	-1.012	-1.014	-1.020
4.0	-1.005	-1.005	-1.005	-1.005	-1.005	-1.006	-1.008
8.0	-1.001	-1.001	-1.001	-1.001	-1.001	-1.001	-1.001

Table II-12e. Force coefficient F_x^s for rigidly held sphere in shear flow between two plane parallel walls at various sphere-to-wall spacings b/a and positions s.

b/a	s=0	s=0.1	s=0.2	s=0.25	s=0.3	s=0.4	s=0.5
1.1	1.633	1.658	1.785	1.900	2.054	2.539	3.940
1.25	1.551	1.571	1.670	1.758	1.877	2.238	3.019
1.5	1.453	1.467	1.537	1.599	1.683	1.929	2.377
2.0	1.332	1.340	1.382	1.420	1.470	1.614	1.846
3.0	1.213	1.218	1.240	1.261	1.287	1.361	1.471
4.0	1.156	1.159	1.174	1.188	1.205	1.254	1.324
8.0	1.075	1.076	1.082	1.088	1.095	1.115	1.142

Table II-12f. Torque coefficient T_y^s for rigidly held sphere in shear flow between two plane parallel walls at various sphere-to-wall spacings b/a and positions s.

b/a	s=0	s=0.1	s=0.2	s=0.25	s=0.3	s=0.4	s=0.5
1.1	0.9518	0.9642	1.011	1.039	1.065	1.101	1.336
1.25	0.9613	0.9715	1.010	1.034	1.055	1.079	1.149
1.5	0.9727	0.9805	1.010	1.028	1.045	1.059	1.064
2.0	0.9854	0.9906	1.010	1.023	1.034	1.040	1.021
3.0	0.9947	0.9977	1.009	1.017	1.023	1.025	1.005
4.0	0.9975	0.9997	1.008	1.013	1.017	1.018	1.002
8.0	0.9997	1.001	1.004	1.007	1.008	1.008	1.000

Table II-12g. Force coefficient F_x^p for rigidly held sphere in two-dimensional poiseuille flow between two stationary plane parallel walls at various sphere-to-wall spacings b/a and positions s.

b/a	s=0.1	s=0.2	s=0.25	s=0.3	s=0.4	s=0.5
1.1	0.5882	1.100	1.347	1.590	2.060	2.481
1.25	0.5587	1.036	1.261	1.479	1.892	2.253
1.5	0.5232	0.9614	1.161	1.351	1.698	1.989
2.0	0.4795	0.8723	1.044	1.202	1.476	1.685
3.0	0.4371	0.7884	0.9364	1.067	1.278	1.416
4.0	0.4166	0.7485	0.8853	1.005	1.188	1.296
8.0	0.3872	0.6919	0.8147	0.9182	1.067	1.137

Table II-12h. Torque coefficient T_y^p for rigidly held sphere in two dimensional poiseuille flow between two stationary plane parallel walls at various sphere-to-wall spacings b/a and positions s.

b/a	s=0.1	s=0.2	s=0.25	s=0.3	s=0.4	s=0.5
1.1	0.1390	0.2174	0.2333	0.2306	0.1599	0
1.25	0.1235	0.1923	0.2058	0.2031	0.1413	0
1.5	0.1042	0.1611	0.1718	0.1691	0.1177	0
2.0	0.07911	0.1214	0.1287	0.1260	0.08729	0
3.0	0.05319	0.08095	0.08531	0.08300	0.05689	0
4.0	0.03998	0.06062	0.06368	0.06174	0.04204	0
8.0	0.02001	0.03017	0.03156	0.03044	0.02050	0

Table II-13. Comparison of values for force and torque coefficients obtained by the present collocation technique to values obtained by method of reflections theories at special values of s.

(a) F_x^t (s = 0.25)

b/a	collocation theory	Faxen eq. (II-7.1)	Ho & Leal
1.1	-2.48	-2.58	-1.59
1.25	-2.032	-2.089	-1.522
1.5	-1.723	-1.741	-1.435
2.0	-1.463	-1.466	-1.326
3.0	-1.272	-1.272	-1.218
4.0	-1.192	-1.192	-1.163
8.0	-1.089	-1.089	-1.082

(b) T_y^t (s = 0.25)

b/a	collocation theory	Faxen eq. (II-7.2)	Ho & Leal
1.1	0.058	0.051	-0.021
1.25	0.01564	0.03348	-0.0162
1.5	0.000594	-0.01967	-0.0113
2.0	-0.03417	-0.009277	-0.00633
3.0	-0.002439	-0.003550	-0.00281
4.0	-0.001523	-0.001867	-0.00158
8.0	-0.0004069	-0.0004253	-0.000396

(c) F_x^t (s = 0.5)

b/a	collocation theory	Faxen eq. (II-7.3)	Ho & Leal
1.1	-3.94	-2.27	-1.91
1.25	-3.019	-2.265	-1.803
1.5	-2.377	-2.111	-1.669
2.0	-1.846	-1.792	-1.502
3.0	-1.471	-1.465	-1.335
4.0	-1.324	-1.322	-1.251
8.0	-1.142	-1.142	-1.126

(continued)

Table II-13. (continued)

(d) F_x^s (s = 0.25)

b/a	collocation theory	Wakiya eq. (II-7.4)
1.1	1.900	1.982
1.25	1.758	1.782
1.5	1.599	1.600
2.0	1.420	1.418
3.0	1.261	1.260
4.0	1.188	1.188
8.0	1.088	1.088

(e) T_y^s (s = 0.25)

b/a	collocation theory	Wakiya eq. (II-7.5)
1.1	1.039	1.073
1.25	1.034	1.061
1.5	1.028	1.048
2.0	1.023	1.034
3.0	1.017	1.021
4.0	1.013	1.015
8.0	1.007	1.007

(f) F_x^p (s = 0.25)

b/a	collocation theory	Wakiya eq. (II-7.6)
1.1	1.347	1.422
1.25	1.261	1.289
1.5	1.161	1.167
2.0	1.044	1.045
3.0	0.9364	0.9362
4.0	0.8858	0.8858
8.0	0.8147	0.8147

(continued)

Table II-13. (continued)

(g) T_y^p (s = 0.25)

b/a	collocation theory	Wakiya eq. (II-7.7)
1.1	0.2333	0.2521
1.25	0.2058	0.2184
1.5	0.1718	0.1787
2.0	0.1287	0.1313
3.0	0.08531	0.08589
4.0	0.06368	0.06388
8.0	0.03156	0.03157

Table II-14. Force and torque coefficients at various wall-to-wall spacings d/a and sphere positions s.

	d/a	s=0.2	s=0.25	s=0.3	s=0.4	s=0.5
F_x^t	10.0	-1.429	-1.343	-1.297	-1.256	-1.246
	15.0	-1.253	-1.208	-1.183	-1.159	-1.153
	20.0	-1.179	-1.145	-1.132	-1.115	-1.111
T_y^t	10.0	-0.0006245	-0.003076	-0.003393	-0.002097	0
	15.0	-0.001301	-0.001704	-0.001620	-0.0009339	0
	20.0	-0.0009157	-0.001013	-0.0009233	-0.0005204	0
F_x^r	10.0	-0.0008326	-0.004102	-0.004524	-0.002797	0
	15.0	-0.001734	-0.002273	-0.002160	-0.001245	0
	20.0	-0.001221	-0.001351	-0.001231	-0.0006939	0
T_y^r	10.0	-1.043	-1.021	-1.012	-1.006	-1.004
	15.0	-1.012	-1.006	-1.004	-1.002	-1.001
	20.0	-1.005	-1.003	-1.002	-1.001	-1.000
F_x^s	10.0	1.382	1.322	1.287	1.254	1.246
	15.0	1.240	1.202	1.180	1.158	1.153
	20.0	1.174	1.147	1.130	1.115	1.111
T_y^s	10.0	1.010	1.019	1.023	1.018	1.001
	15.0	1.009	1.014	1.015	1.012	1.000
	20.0	1.008	1.010	1.011	1.008	1.000
F_x^p	10.0	0.8723	0.9785	1.067	1.188	1.230
	15.0	0.7884	0.8957	0.9849	1.106	1.146
	20.0	0.7485	0.8567	0.9461	1.067	1.107
T_y^p	10.0	0.1214	0.1027	0.08300	0.04204	0
	15.0	0.08095	0.06799	0.05472	0.02757	0
	20.0	0.06062	0.05077	0.04078	0.02050	0

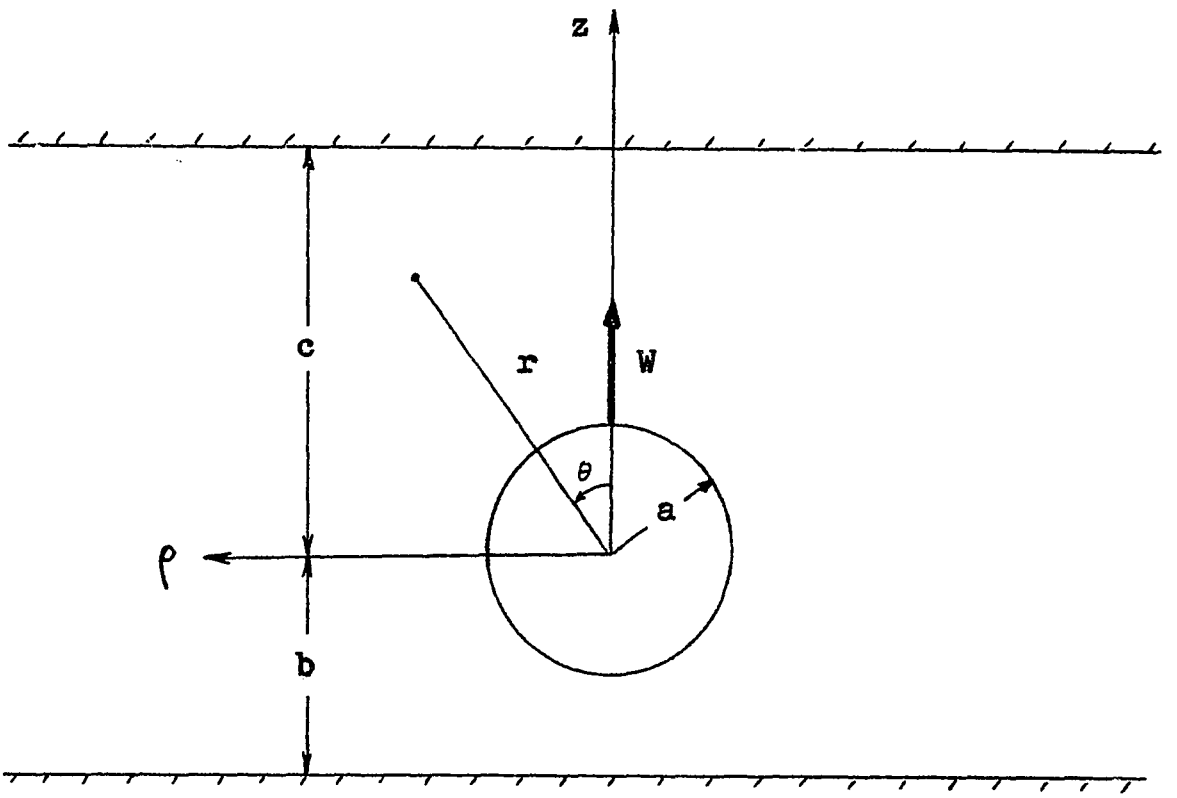

Figure II-1. Geometry for the axisymmetric flow configuration.

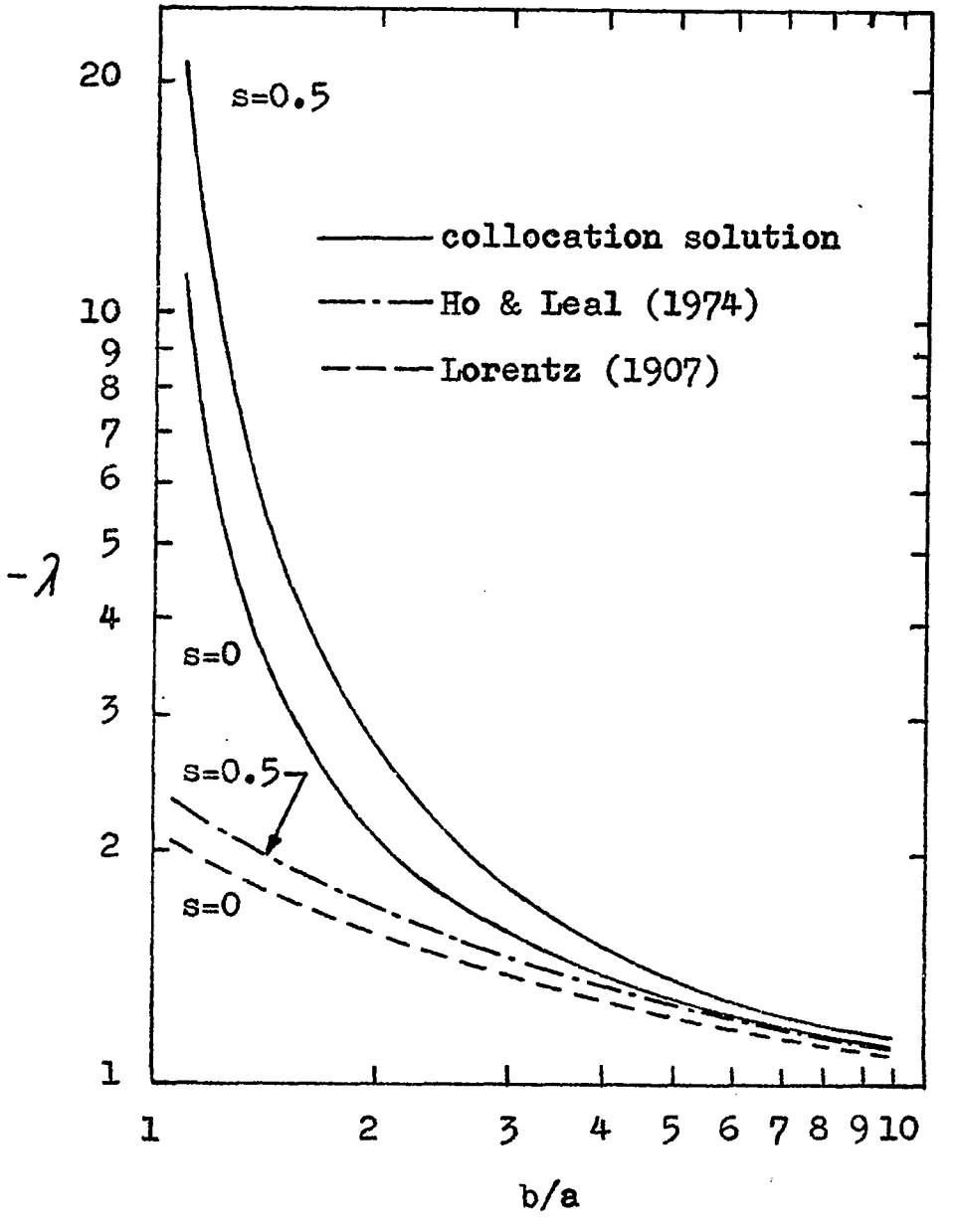

Figure II-2. Comparison between solutions for λ obtained by the collocation technique and the method of reflections. (Solid line for s = 0 also corresponds to the exact solution for a single wall, Brenner 1961).

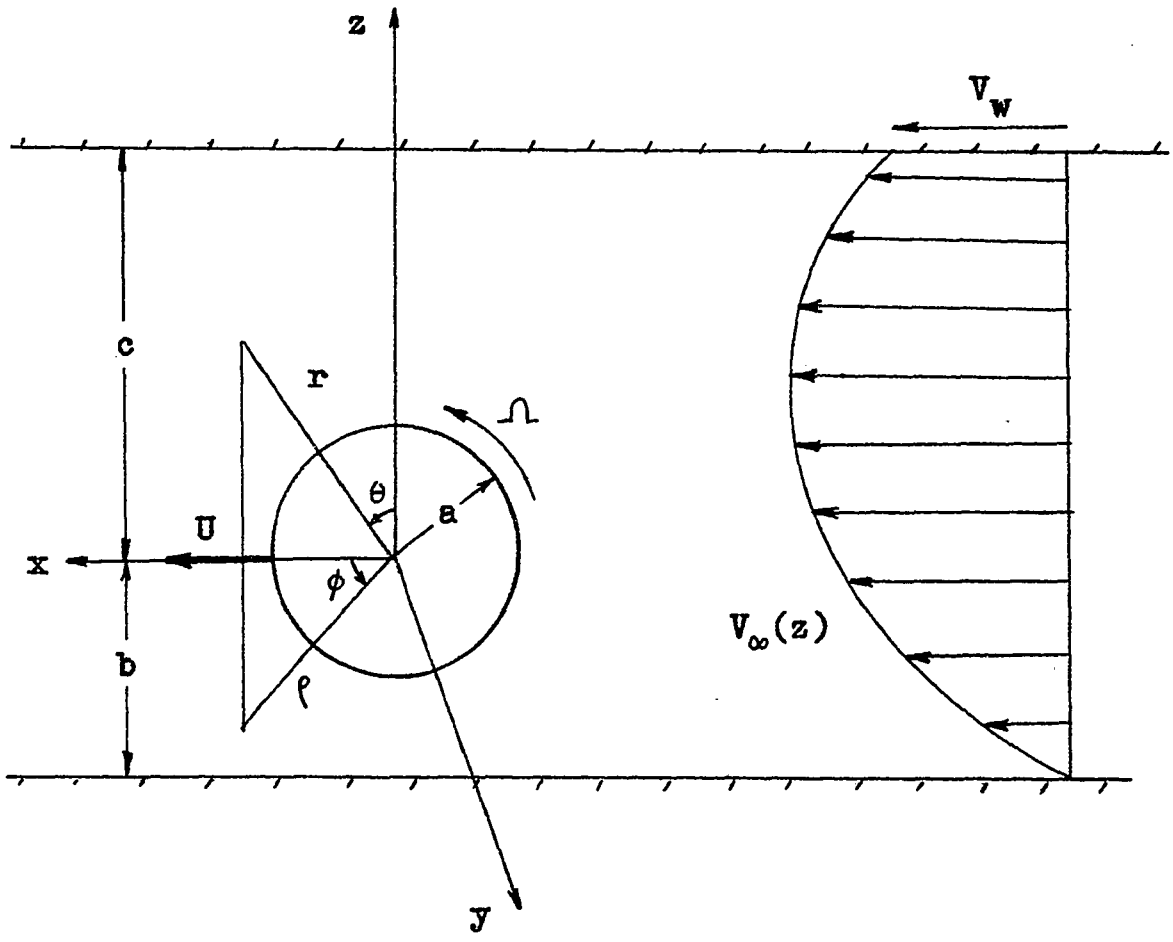

Figure II-3. Geometry for the asymmetric flow configuration.

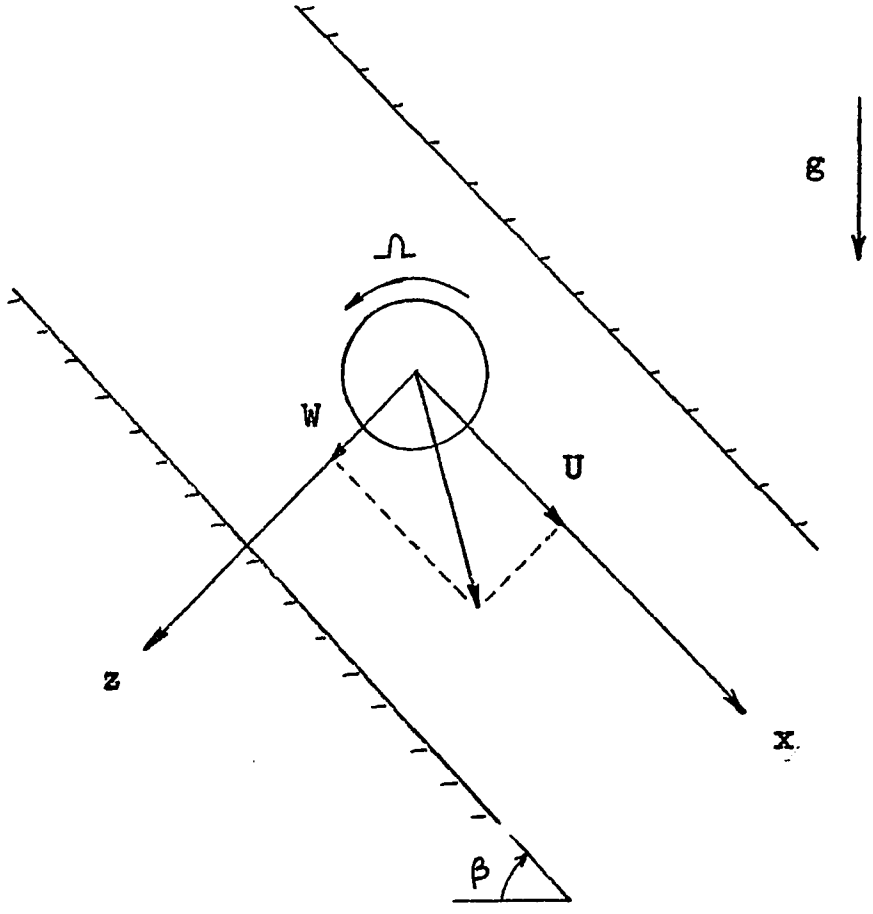

Figure II-4. Sphere settling freely under gravity in a quiescent fluid between two plane parallel walls inclined at an angle β.

REFERENCES

Arminski, L., Weinbaum, S. & Pfeffer, R. 1979 (in preparation).

Brenner, H. 1961 Chem. Eng. Sci. 16, 242.

Bretherton, F.P. 1962 J. Fluid Mech. 14, 284.

Chen, T.C. & Skalak, R. 1970 Appl. Sci. Res. 22, 403.

Curry, F.E. 1974 Microvascular Res. 8, 236.

Davis, A.M.J., O'Neill, M.E., Dorrepaal, J.M. & Ranger, K.B. 1976 J. Fluid Mech. 77, 625.

Erdelyi, A. et al. 1954 Tables of Integral Transforms, vols. 1,2, McGraw-Hill.

Faxen, H., 1923 Arkiv. Mat. Astron. Fys. 17, No. 27.

Ganatos, P., Pfeffer, R. & Weinbaum, S. 1978 J. Fluid Mech. 84, 79.

Gluckman, M.J., Pfeffer, R. & Weinbaum, S. 1971 J. Fluid Mech. 50, 705.

Gluckman, M.J., Weinbaum, S. & Pfeffer, R. 1972 J. Fluid Mech. 55, 677.

Goldman, A.J., Cox, R.G. & Brenner, H. 1966 Chem. Eng. Sci. 21, 1151.

Goldman, A.J., Cox, R.G. & Brenner, H. 1967a Chem. Eng. Sci. 22, 637.

Goldman, A.J., Cox, R.G. & Brenner, H. 1967b Chem. Eng. Sci. 22, 653.

Halow, J.S. & Wills, G.B. 1970 A.I.Ch.E. J. 16, 281.

Happel, J. & Brenner, H. 1973 Low Reynolds Number Hydrodynamics, 2nd ed. Noordhoff.

Ho, B.P. & Leal, L.G. 1974 J. Fluid Mech. 65, 365.

Hocking, L.M. 1964 J. Fluid Mech. 20, 129.

Hyman, W.A. & Skalak, R. 1972 Appl. Sci. Res. 26, 27.

Jayaweera, K.O.L.F., Mason, B.J. & Slack, H.W. 1964 J. Fluid Mech. 20, 121.

Jeffery, G.B. 1922 Proc. Roy. Soc. A 102, 161.

Kynch, G.J. 1959 J. Fluid Mech. 5, 193.

Lamb, H. 1945 Hydrodynamics, 6th edn. Dover.

Leichtberg, S., Pfeffer, R. & Weinbaum, S. 1976 Int. J. Multiphase Flow 3, 147.

Leichtberg, S., Weinbaum, S. & Pfeffer, R. 1976 Biorheol. 13, 165.

Leichtberg, S., Weinbaum, S., Pfeffer, R. & Gluckman, M.J. 1976 Phil. Trans. Roy. Soc. A 282, 585.

Lorentz, H.A. 1907 Abhand. theor. Phys. 1, 23.

O'Brien, V. 1968 A.I.Ch.E. J. 14, 870.

O'Neill, M.E. 1964 Mathematika 11, 67.

Skalak, R., Chen, P.H. & Chien, S. 1972 Biorheol. 9, 67.

Stimson, M. & Jeffery, G.B. 1926 Proc. Roy. Soc. A 111, 110.

Wakiya, S. 1956 Res. Rep. Fac. Engng, Niigata University (Japan), 5, 1.

Wang, H. & Skalak, R. 1969 J. Fluid Mech. 38, 75.

Weinbaum, S. & Caro, C.C. 1976 J. Fluid Mech. 74, 611.

Youngren, G.K. & Acrivos, A. 1975 J. Fluid Mech. 69, 377.